NTNU – Trondheim
Norwegian University of
Science and Technology

Non-linear Response in Reinforced Concrete related to Cryogenic Conditions

Fredrik Jenseg Eriksen

Civil and Environmental Engineering (2 year)
Submission date: June 2014
Supervisor: Jan Arve Øverli, KT

Norwegian University of Science and Technology
Department of Structural Engineering

NTNU

Non-linear Response in Reinforced Concrete related to Cryogenic Conditions

Fredrik Jenseg Eriksen

Civil and Environmental Engineering

Submission date: June 2014

Principal Supervisor: Jeovan Freitas, DNV GL

Principal Supervisor: Bente Skovseth Nyhus, Dr. Techn. Olav Olsen AS

Assistant Supervisor: Jan Arve Øverli, NTNU

Norwegian University of Science and Technology

Department of Structural Engineering

Department of Structural Engineering
Faculty of Engineering Science and Technology
NTNU- Norwegian University of Science and Technology

ACCESSIBILITY

OPEN

MASTER THESIS 2014

SUBJECT AREA:	DATE:	NO. OF PAGES:
NON-LINEAR FINITE ELEMENT ANALYSIS	10.06.14	

"NON-LINEAR RESPONSE IN REINFORCED CONCRETE RELATED TO CRYOGENIC CONDITIONS"

"IKKE-LINEÆR RESPONS FOR ARMERT BETONG UTSATT FOR KRYOGENISKE TEMPERATURLASTER"

BY:

FREDRIK JENSEG ERIKSEN

RESPONSIBLE TEACHER: JAN ARVE ØVERLI

PRINCIPAL SUPERVISOR: JEOVAN FRITAS

PRINCIPAL SUPERVISOR: BENTE SKOVSETH NYHUS

CARRIED OUT AT: NTNU

SUMMARY:

A reinforced outer concrete containment tank exposed for liquefied natural gas was the basis for this study. The containment tank was analysed both linearly and non-linearly by use of two different finite element programs; Abaqus and Sestra/ShellDesign.

The main goal for this study was to examine whether a given concrete containment tank would fulfil the formal rules and regulations regarding, the residual compressive zone and the crack width limitation, without a thermal corner protection.

Non-linear analyses were carried out by use of temperature dependent material properties. The results showed an acceptable residual compressive zone for both the wall and the slab, but the required limit crack width was exceeded by 100 % (0.5 mm). The residual compressive zone will ensure impermeability and the outer containment tank will withstand a major leak event. Abaqus proved itself to be a good tool for non-linear analysis due to a cryogenic condition.

The results from Abaqus were compared to a similar model created and analysed with Sestra/ShellDesign. Some unfavourable peak values was found at the edges of the thermal load. The non-linear reinforcement stresses were however reliable for the tests ran without any concrete tensile capacity, and should be considered a solid basis for further studies for Sestra/ ShellDesign due to a cryogenic liquid spill condition.

MASTER THESIS, SPRING 2014

for

FREDRIK JENSEG ERIKSEN

Non-linear Response in Reinforced Concrete related to Cryogenic Conditions

The storage of liquefied natural gas at low temperatures is a relevant and challenging scenario. It is feasible to cool gas into a liquid form, and then store it in a steel inner tank with a concrete containment tank as a surrounding load carrier. In case of a leakage from the steel inner tank, the outer containment tank needs to be liquid proof and serve as a catch basin. Therefore, it is crucial to determine the thermal properties of the materials involved, and how they interact with each other.

In cryogenic conditions, the difference in material behavior between concrete and reinforcement with resulting internal forces have to be considered as well as the more external non-linear redistribution of stress resultants.

The assignment will be to analyze a representative storage tank by use of finite element method. Non-linear temperature dependent materials will be used and analyzed by Abaqus and Sestra/ShellDesign. The non-linear results achieved from these applications should be compared and important parameters that affect the results should be identified. The advantages and disadvantages using Abaqus vs. ShellDesign should be addressed.

The proposed thesis should be developed based on the following assumptions:

1. The geometry of the tank and the loads should be the same as defined in reference (1). An alternative geometry could also be used, defined in (2). DNV GL shall approve the final geometry.
2. Shell based elements should be used for all finite element models. Additional solid elements model could be considered in Abaqus, if shell elements are insufficient.
3. A steady-state temperature flow scenario with linear gradient variation over thickness should be assumed.
4. All material properties (concrete and steel) shall be defined by DNV GL.

The thesis should be delivered by existing guidelines. Deadline June 10.2014

Supervisors

Jeovan Freitas	(DNV GL)
Bente Skovseth Nyhus	(Dr. Techn. Olav Olsen AS)
Jan Arve Øverli	(NTNU)

Preface

This Master's thesis was written at the Department of Structural Engineering at the Norwegian University of Science and Technology in Trondheim, during the spring 2014. The assignment was provided by Ph.d. Jeovan Freitas at DNV GL, who also has been of great assistance with Abaqus modelling and general guidance. M.Sc. Bente Skovseth Nyhus at Dr. Techn. Olav Olsen has been at great help in all matters regarding Sestra and ShellDesign. I would also like to thank M.Sc. Hege Berg Thurman, the Head of Concrete Sections at DNV GL, for making this interesting master thesis available for me, including the Patran model I acquired for the Sestra/ShellDesign analyses.

Creating the Abaqus model has been essential for this thesis, and very time consuming. A literature study was done in the Abaqus Analysis User's Manual, and a great number of analyses were run in order to evolve a dependable model. Some software issues were met regarding the analyses in Sestra/ShellDesign. These issues were solved by great assistance from Bente Skovseth Nyhus, and I am very grateful for her time invested in these issues.

I would also like to thank my fellow students at 2-46D, Bendik, Tor Jørgen, Olav and Kenth. Together, we have created a great environment that has overcome all errors and perplexities.

Summary

A reinforced outer concrete containment tank exposed for liquefied natural gas was the basis for this study. The containment tank was analysed both linearly and non-linearly by use of two different finite element programs; Abaqus and Sestra/ShellDesign. Hand calculations were performed to substantiate the finite element programs, by verifying the different load effects.

Both finite element programs should analyse full-scale models, based on a 360° revolved shell element. The obtained results should be compared, and important parameters should be identified. Far as known, prior to this study, no prestressed outer containment tank made of a revolved shell element has been analysed due to a cryogenic liquid spill condition.

The main goal for this study was to examine whether a given concrete containment tank would fulfil the formal rules and regulations regarding, the residual compressive zone and the crack width limitation, without a thermal corner protection.

This report contains a detailed description of how to create a finite element model in Abaqus for this issue, including brief discussions of important properties. Relevant load cases in Abaqus were controlled by hand calculations in order to verify the revolved shell section's behaviour and create a solid basis for comparison due to ShellDesign.

Non-linear analyses were carried out by use of temperature dependent material properties. The results showed an acceptable residual compressive zone for both the wall and the slab, but the required limit crack width was exceeded by 100 % (0.5 mm). The residual compressive zone will ensure impermeability and the outer containment tank will withstand a major leak event. Abaqus proved itself to be a good tool for non-linear analysis due to a cryogenic liquid spill condition.

The results from Abaqus were compared to a similar model created and analysed with Sestra/ShellDesign. Some unfavourable peak values was found at the edges of the thermal load. The non-linear reinforcement stresses were however reliable for the tests ran without any concrete tensile capacity, and should be considered a solid basis for further studies for Sestra/ ShellDesign due to a cryogenic liquid spill condition.

Sammendrag

En armert betongtank utsatt for en større lekkasje av flytende, kryogenisk gass var utgangspunktet for den oppgaven. Betongtanken skulle analysers både lineært og ikke-lineært ved å bruke to forskjellige analyseprogrammer, basert på elementmetoden. Håndberegninger ble utført for å underbygge elementmetodeprogrammene, ved å kontrollere ulike effekter fra påsatte laster.

Begge programpakkene skulle analysere fullskalamodeller lagd av et skallelement omdreiet 360° om egen akse. Resultatene skulle sammenliknes, og viktige parametere skulle gjøres rede for. Ved oppstart av oppgaven var det ikke kjent om et slikt forspent element tidligere har blitt analysert for en så stor temperaturlast.

Hensikten med studien var å undersøke om en gitt betongtank kunne oppfylle gjeldende regelverk uten bruk av beskyttelse mot temperaturlasten. Regelverket regulerer gjenværende trykktykkelse i betongen og maksimal størrelse på rissvidde.

Rapporten inneholder en detaljert beskrivelse av hvordan en modell i Abaqus bygges opp for problemstillingen, inkludert raske avveininger for valg av egenskaper. Aktuelle laster fra Abaqus ble kontrollert av håndberegninger fra etablert aksesymmetrisk teori, for å dokumentere at elementmodellen fungerte etter hensikten. Verifiseringen av resultatene fra Abaqus dannet grunnlaget for sammenlikningen av resultater fra ShellDesign.

Ikke-lineære analyser ble utført ved å bruke temperaturavhengige materialegenskaper. Resultatene viste at påkrevd trykktykkelse i betongen ble oppfylt, og at maksimal rissvidde ble overskredet med 100 % (0.5 mm). Konklusjonen er at betongtanken vil motstå en større kryogenisk gasslekkasje, selv om rissviddeanbefalingen ikke ble oppfylt. Abaqus har vist seg å være et godt egent verktøy for ikke-lineære analyser for betong utsatt for flytende kryogenisk gass.

Resultatene fra Abaqus ble kontrollert opp mot en tilsvarende modell lagd og analysert av Sestra/ShellDesign. Her ble det funnet noen uheldige maksimalverdier rundt temperaturlastene. Resultatene for de ikke-lineære armeringsspenningene viste seg å være gode og pålitelige for beregningene hvor betongen ikke hadde strekkapasitet. De resultatene bør anses som et godt utgangspunkt for videre studier av store temperaturlaster i Sestra/ShellDesign.

Contents

List of Figures

List of Tables

Chapter 1

1 General Description

1.1 Abstract

Liquefied natural gas (LNG) is natural gas condensed into a liquid form by cooling it to approximately -165 °C, before stored in a specially designed containment tank. By this phase transition from gas to liquid, the volume reduction is 600 to 1 (1). Storage and transportation becomes manageable, but causes some technical challenges. A major leak event from either storage or transportation would potentially do huge damage to the environment, life and assets.

A containment tank is mainly made of an inner steel tank, an insulation layer and a concrete tank. The sensitive steel tank shall ideally handle the cryogenic (very low) temperature and the internal hydrostatic pressure by itself. The concrete tank shall also protect due to external loads and accidents, and serve as a catch basin in case of failure of the inner tank.

Figure 1-1 shows a typical full containment tank, used by the industry. In this study, it will be in focus how the cryogenic temperature affect the concrete under a major leak event. It is essential that the concrete tank will contain a LNG leakage to prevent damage. Therefore, the thickness of the residual compressive zone, the reinforcement steel stresses and the characteristic crack width must be verified.

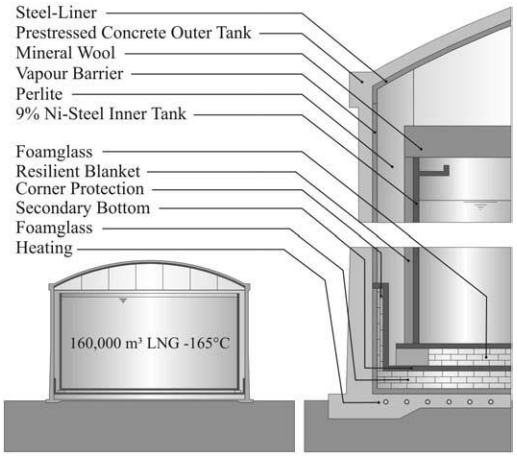

Figure 1-1: Typical components of a LNG tank (1)

1.2 Design

The supervisor at DNV GL decided that the full containment tank should be modelled as one shell element, drawn as an axis symmetric section before revolved 360° into a full global model. Model a tank with shell elements would be a good choice because of the shell's high membrane capacity and well tested bending properties. A shell element would also be applicable for this structure because of its low ratio between thickness and cylindrical radius.

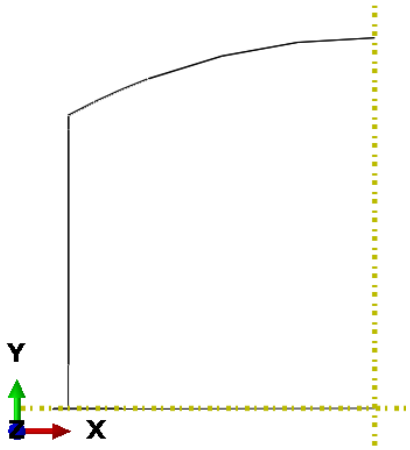

Figure 1-2: Axis symmetric section

By modelling the whole structure instead of an axis symmetric section would ease constraints simulations significantly. An overall deformation pattern would also be present for actual verification of the global behaviour of the cylinder.

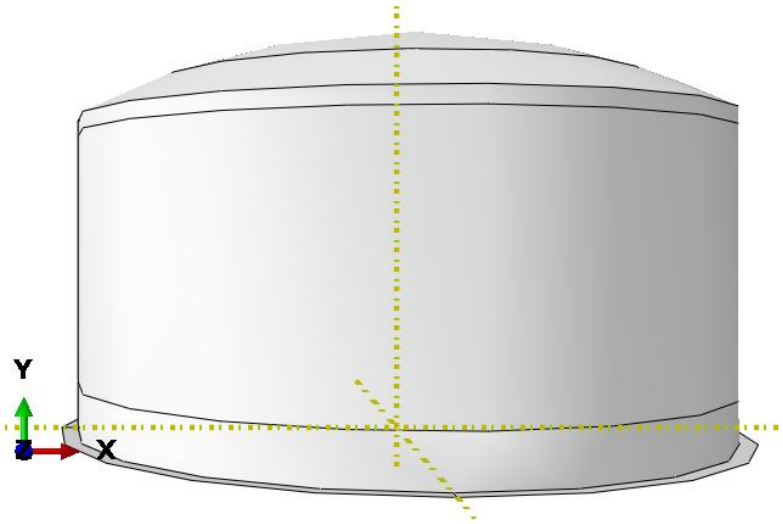

Figure 1-3: Axis symmetric section revolved 360°

1.3 Sections and dimensions

The shell element shown in Figure 1-3 was divided into four different sections, where different shell thickness, material properties and rebar layers were applied. The dimensions listed in Table 1-1 are in accordance to reference (2). Some dimensions are shown in Figure 1-4.

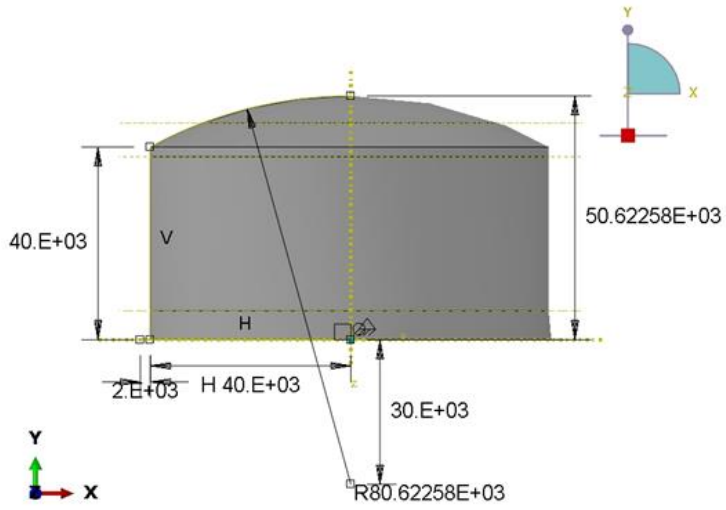

Figure 1-4: Dimensions of full containment tank

Table 1-1: Dimensions of full containment tank

Section	Dimensions
Radius midside of wall	40 400 mm
Wall height	38 000 mm
Thickness of wall	800 mm
Radius midside ring beam	40 600 mm
Thickness ring beam	1 200 mm
Height ring beam	2 000 mm
Radius slab	42 000 mm
Thickness slab	1 000 mm
Coordinate top surface and centroid of slab	(0, 0, 0)
Radius of spherical roof	80 623 mm
Coordinate top point at roof	(0, 50 623, 0)

1.4 Loads

For this study, it was important to simulate loads according to design codes giving formal regulations. Reference (1) and (2) are both discussing formal regulations given by BS 7777 and EN 14620. BS 7777 requires in case of liquid spill the verification of an average concrete stress of 1 MPa in the residual compressive zone to ensure impermeability. EN 14620 additionally define the minimum compressive zone to 100 mm or 10 % of the cross sectional height. Since the liquid spill is considered as a short duration accident, crack widths up to 0.5 mm should be accepted, because of the short duration of the accidental load will not cause corrosion in the reinforcement.

The liquid spill height in load case 10 and 11 was designed as a worst-case scenario. This was because of the combination between edge disturbance from the bottom slab and the LNG leakage with its cryogenic condition and thermal moments are predicted to induce high tensile stresses in this area.

The internal gas pressure is introduced in the tank for shifting the vapour point of natural gas. The hydrostatic load is due the accidental liquid spill height.

Figure 1-5 graphically shows load case 10. The LNG leakage was modelled at the inside of the tank.

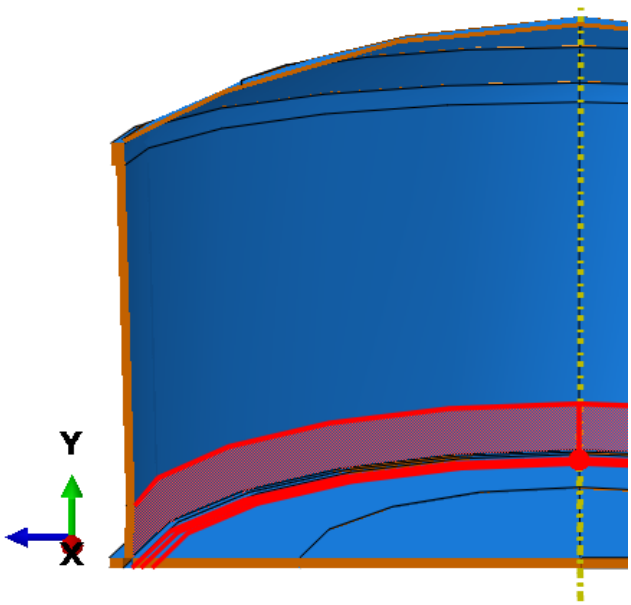

Figure 1-5: LNG leakage in load case 10

Table 1-2: Load cases

Load case	Section	Location	Surface	Magnitude
1	Wall-pressure	0 – 40000	Internal surface	0.029 MPa
2	Wall-liquid-6	0 – 6000	Internal surface	5E-6*(6000-Z) MPa
3	Wall-liquid-10	0 – 10000	Internal surface	5E-6*(10000-Z) MPa
8	Roof-gravity	Entire section	Internal surface	-0.010 MPa
9	Roof-pressure	Entire section	Internal surface	0.029 MPa
10	Slab	0 – 38200	Inside	0 °C
	Slab	38200 – 40000	Inside	-165 °C
	Slab	40000 – 42000	Inside	0 °C
	Slab	0 – 42000	Outside	35 °C
	Wall	0 – 6000	Inside	-165 °C
	Wall	6000 – 38000	Inside	0 °C
	Wall	0 – 38000	Outside	35 °C
	Ring beam	38000 – 40000	Inside	0 °C
	Ring beam	38000 – 40000	Outside	25 °C
	Roof	Entire section	Inside	0 °C
	Roof	Entire section	Outside	35 °C
11	Slab	0 – 38200	Inside	0 °C
	Slab	38200 – 40000	Inside	-165 °C
	Slab	40000 – 42000	Inside	0 °C
	Slab	0 – 42000	Outside	35 °C
	Wall	0 – 10000	Inside	-165 °C
	Wall	10000 – 38000	Inside	0 °C
	Wall	0 – 38000	Outside	35 °C
	Ring beam	38000 – 40000	Inside	0 °C
	Ring beam	38000 – 40000	Outside	25 °C
	Roof	Entire section	Inside	0 °C
	Roof	Entire section	Outside	35 °C

1.5 Boundary conditions

The literature regarding big storage tanks is based on the assumption that the slab is fixed to the ground, which means that the wall connection should be considered as fixed. This would be appropriate for this structure, since the slab is 1 meter thick.

The slab, however, should be able to deflect and respond to the boundary constraints and shrink in accordance with the thermal load. In contrast to most literature about cylindrical tanks, the slab should not be fixed to the ground. If the shrinkage cooling causes would be restrained, infinite stresses would occur at the thermal load area at the slab. This would mislead the results dramatically.

To remedy this undesirable effect, the slab was modelled restrained in the Y –direction nearby the LNG leakage. The area close to the origin, where there was no change in temperature, was modelled pinned.

Table 1-3: Boundary conditions for slab

Boundary condition	Restraint	Area (by radius)	Dimensions
Pinned	U1 = U2 = U3 = 0	25 000	mm
Y- constrained	U2 = 0	25000 – 42 000	mm

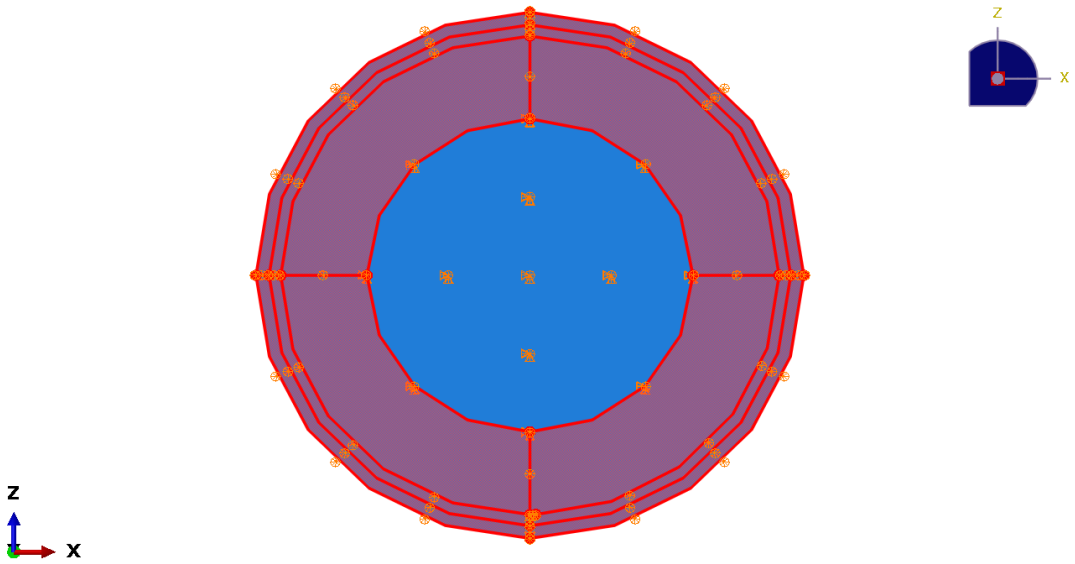

Figure 1-6: Boundary condition, y-constrained area

The best solution would however be to model the boundary conditions as springs, because it would also let the slab-wall connection rotate. That is not included in this thesis, and the difference between current boundary conditions and springs are considered negligible.

1.6 Rebar layers and prestressing

In reference (1), the size of the reinforcement layer for the wall section was specified, along with the prestressing tendons. The reinforcement in the other sections was in cooperation with DNV GL, designed for this thesis.

Table 1-4: Rebar layers in slab section

Layer name	Material	Area per bar	Spacing	Orientation angle	Position*
Slabx+	Steel460	491	150	0	400
Slabz+	Steel460	491	150	90	-375
Slabx-	Steel460	491	150	0	-400
Slabz-	Steel460	491	150	90	-375

*from middle of section

Table 1-5: Rebar layers in wall section

Layer Name	Material	Area per bar	Spacing	Orientation angle	Position*
Hoop+	Steel460	491	150	0	340
Hoop-	Steel460	491	150	0	-340
Vertical+	Steel460	491	300	90	315
Vertical-	Steel460	491	300	90	-315
Prestress_H	Tendon	4200	600	0	0
Prestress_V	Tendon	4200	1000	90	0

*from middle of section

Table 1-6: Rebar layers in ring beam section

Layer name	Material	Area per bar	Spacing	Orientation angle	Position*
RingHoop+	Steel460	491	150	0	540
RingHoop-	Steel460	491	150	90	-540
RingVertical+	Steel460	491	150	0	515
RingVertical-	Steel460	491	150	90	-515
Prestress_H	Tendon	4200	300	0	0
Prestress_V	Tendon	4200	1000	90	0

*from middle of section

Table 1-7: Rebar layers in roof section

Layer name	Material	Area per bar	Spacing angle	Orientation angle	Position*
Roofx+	Steel460	491	150	0	150
Roofz+	Steel460	491	150	90	125
Roofx-	Steel460	491	150	0	-150
Roofz-	Steel460	491	150	90	-125

*from middle of section

1.7 Mesh

A medium fine mesh was made for the tank. It was important that the mesh replicated bending appropriate, but not increased the calculation cost unnecessary. A too coarse mesh would on the other hand hardened convergence in the analysis.

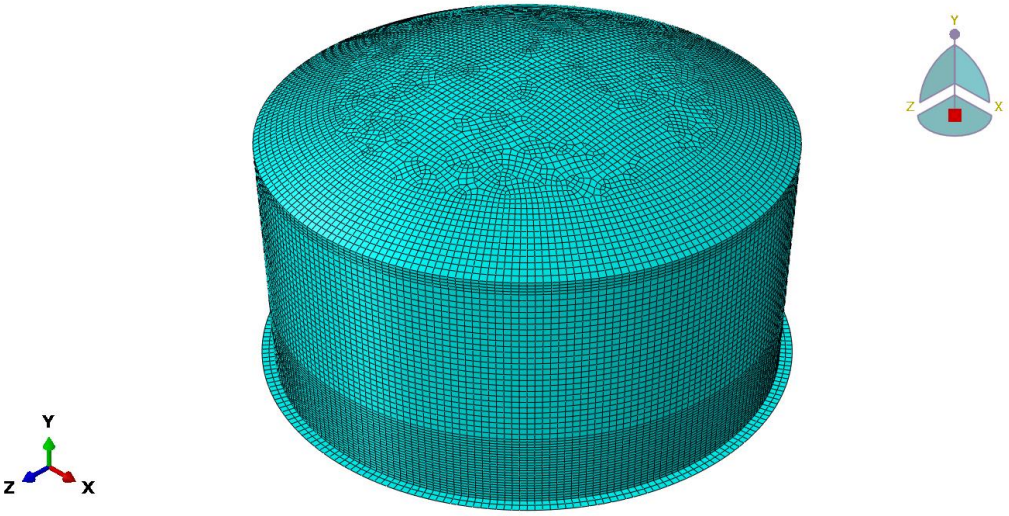

Figure 1-7: Full scale mesh

A number of 240 elements was decided to be suitable in the circumferential direction. This means that each element has a length of 1.0 meter and got an initial curvature of 1,5° for the wall. A more coarse mesh was made at the pined area for the slab, and at the top of the roof in order to decrease calculation cost.

For the wall, two different shell height was assigned. For the first 12 meters, a finer mesh was chosen to simulate bending more appropriate with an element height of 0.5 meter. For the rest of the wall, the element height was assigned 1.0 meter.

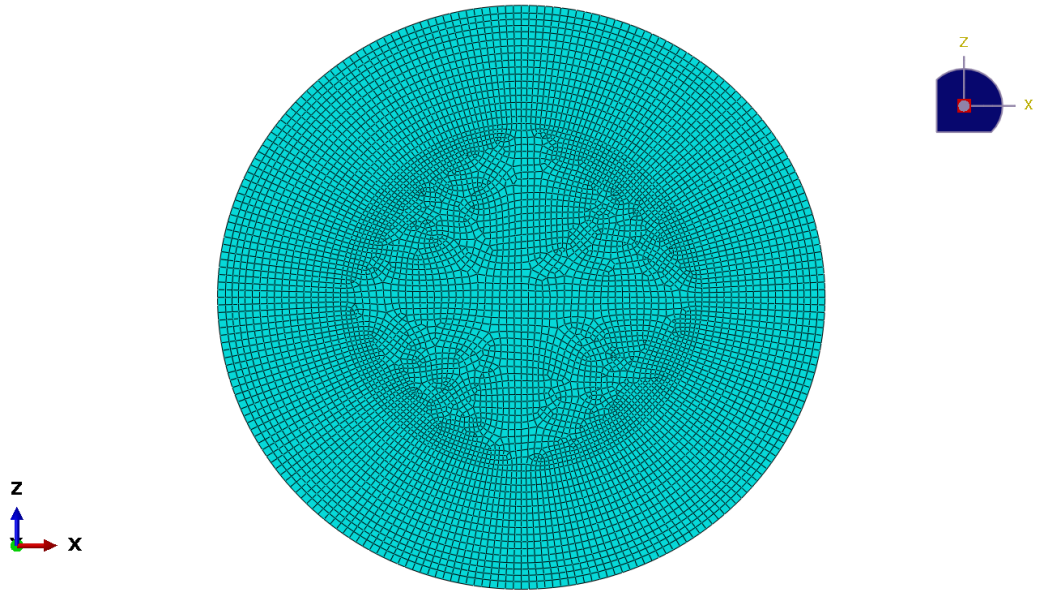

Figure 1-8: Mesh at slab

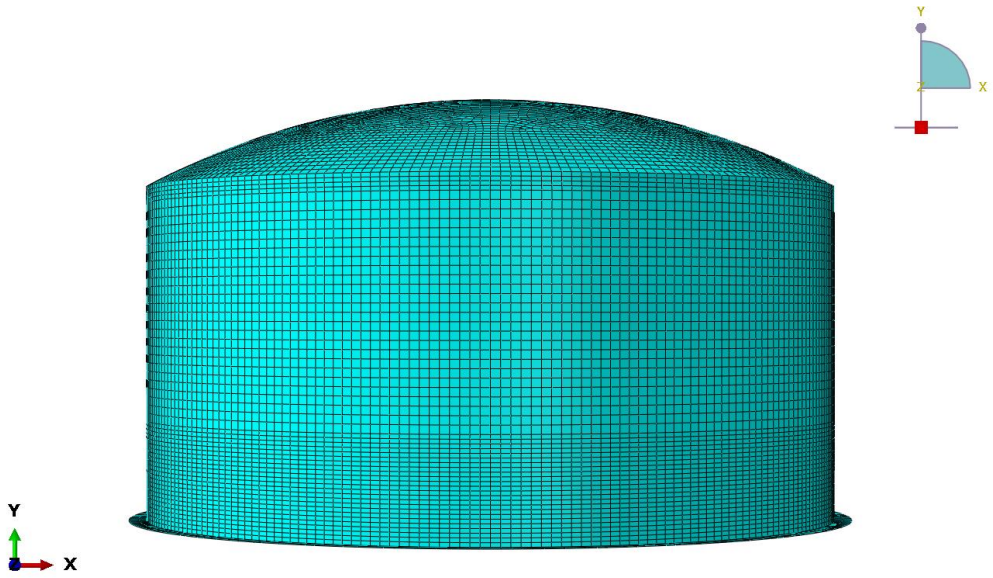

Figure 1-9: Mesh at wall

The ring beam located between the wall and the intersection got a finer mesh. This connection got a geometry change, and the initial thought was to employ more integration points in order to give a better distribution of forces.

1.8 Material properties

The material properties have been decided in cooperation with DNV GL, based on NS-EN-1992-1-1 (3). The chosen concrete strength class was F_{ck} = 55 MPa, and the reinforcement yield stress was F_{yk} = 460 MPa. Yield stress for the tendons was 1400 MPa. The initial prestress in the tendons was 1000 MPa.

Material factors for accidental load was defined by (3), table 2.1. The succeeding accidental load factors in Table 1-8 were used.

Table 1-8: Material factors for accidental loads

Load	γ_c	γ_s	γ_p
Accidental load	1.2	1.0	1.0

Table 1-9: Material Properties for Concrete

Material Property	**Value**	**Unit**
Density	2.4E-9	Ton/mm^3
Young's modulus	35000	MPa
Poisson's ratio	0.2	-
Specific heat	850000	mm^2/(kg K)

Expansion	**Expansion coefficient**	**Unit**	**Temperature**	**Unit**
	1E-5	K^{-1}	-180	°C
	1E-5	K^{-1}	50	°C

Conductivity	**Conductivity**		**Temperature**	**Unit**
	3.33	-	-180	°C
	3.2	-	-160	°C
	2	-	25	°C

	1.77	-	60 °C

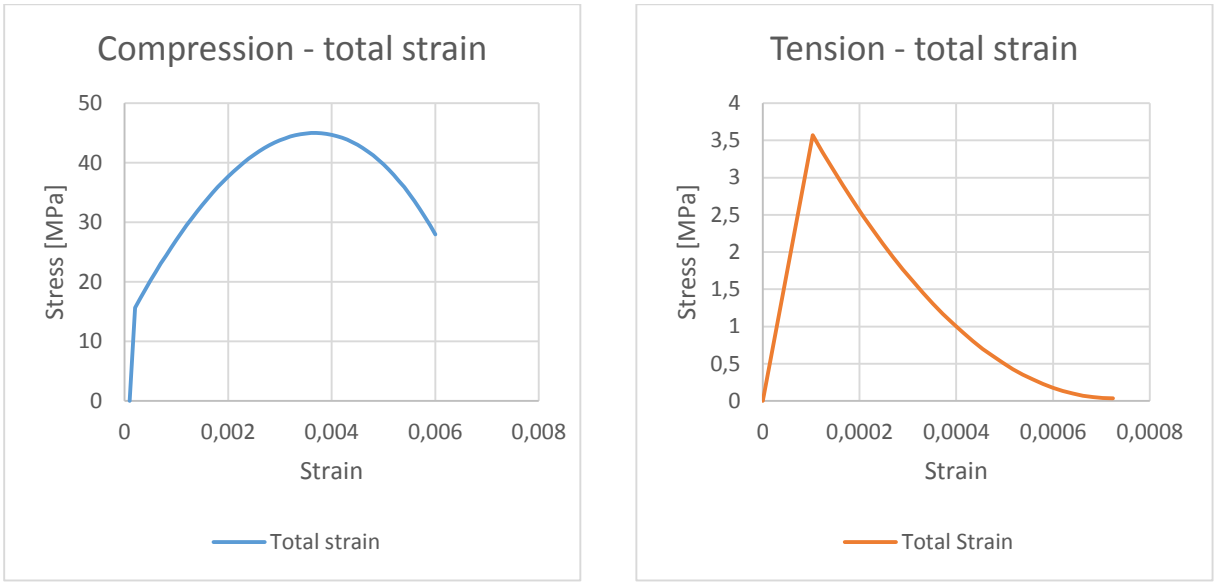

Figure 1-10: Compressive (L) and tensile (R) behaviour, concrete

Table 1-10: Reinforcement properties

Material property	Value	Unit
Density	7.85E-9	Ton/mm^3
Young's Modulus	200000	MPa
Poisson's Ratio	0.3	-
Expansion	1E-5	K^{-1}

Plastic material property	Yield stress	Unit	Plastic strain
	460	MPa	0
	460	MPa	0.0027

Table 1-11: Tendon properties

Material property	Value	Unit
Density	7.85E-9	Ton/mm^3
Young's Modulus	200000	MPa
Poisson's Ratio	0.3	-
Expansion	1E-5	K^{-1}

Plastic material property	Yield stress	Unit	Plastic strain
	1400	MPa	0
	1590	MPa	0.000199
	1750	MPa	0.00104
	1840	MPa	0.0107
	1900	MPa	0.0206
	1900	MPa	0.0904

Chapter 2

2 Elastic Theory for Concrete Shell Elements

2.1 Deriving the differential equation

Different types of concrete structures for containment often consist of axisymmetric shells. The symmetry in the shell elements refers to the geometry, material behaviour and boundary conditions. Additionally, some load cases as internal pressure, hydrostatic pressure and self-weight have good compatibility for axisymmetric cases, since there is independency between axis direction r and rotational direction φ. A cylindrical coordinate system is therefore appropriate.

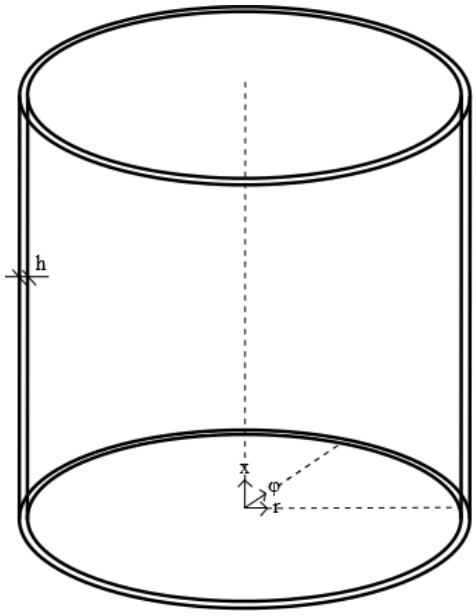

Figure 2-1: An axisymmetric shell structure

Because of the independency between axis direction and rotational direction, axisymmetric structures can be simplified from a three dimensional structure into a two dimensional plate. A part of the cylindrical wall in Figure 2-1 is shown in Figure 2-2, with differential amendment

for present forces. Due to the axisymmetric condition, the membrane shear force $N_{\varphi x}$, the torsional moment $M_{\varphi x}$ and the shear force V_{φ} are zero.

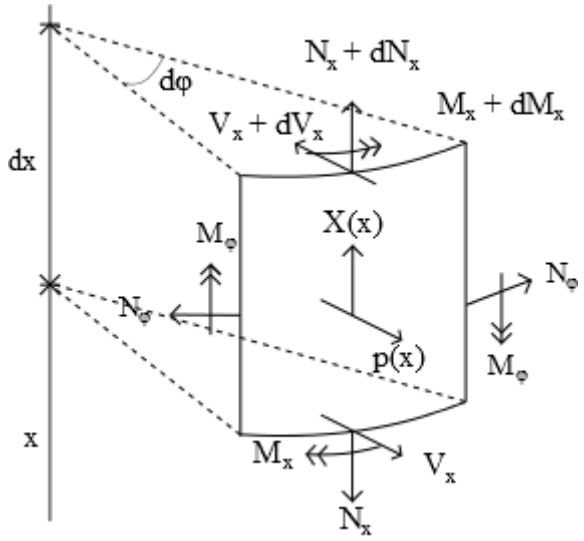

Figure 2-2: Forces in a cylindrical shell element

The following equations of equilibrium are obtained by summation of forces and moments in Figure 2-2.

$$\sum F_{radial} \qquad \frac{dV_x}{dx} + \frac{1}{r} N_{\varphi} = p(x) \qquad \textit{Eq. 2-1}$$

$$\sum M_{tangenti} \qquad \frac{dM_x}{dx} - v_x = 0 \qquad \textit{Eq. 2-2}$$

$$\sum F_x \qquad \frac{dN_x}{dx} + X(x) = 0 \qquad \textit{Eq. 2-3}$$

Forces in the x direction of the shell can be solved individually since Eq. 2-3 is uncoupled from Eq. 2-1 and Eq. 2-2. By inserting Eq. 2-2 in Eq. 2-1, the equilibrium equation for the shell section is

$$\frac{d^2M_x}{dx^2} + \frac{1}{r}\,N_\varphi = p(x) \qquad \textit{Eq. 2-4}$$

Strains in the containers longitudinal direction, ε_x, and hoop direction, ε_φ, is given by Hook's law for a plane stress situation. E is defined as Young's modulus.

$$\varepsilon_x = \frac{1}{E}(\sigma_x - \upsilon\sigma_\varphi) \qquad \textit{Eq. 2-5}$$

$$\varepsilon_\varphi = \frac{1}{E}(\sigma_\varphi - \upsilon\sigma_x) \qquad \textit{Eq. 2-6}$$

To simplify the derivation of forces, N_x is assumed to be zero. ν is defined as Poisson's ratio. The strains will then be

$$\varepsilon_x = -\frac{1}{E}\upsilon\sigma_\varphi = -\frac{\upsilon N_\varphi}{Eh} \qquad \textit{Eq. 2-7}$$

$$\varepsilon_\varphi = \frac{1}{E}\sigma_\varphi = \frac{N_\varphi}{Eh} \qquad \textit{Eq. 2-8}$$

A radial displacement, w, is defined positive from centre. This displacement yields the arc length by r ∗ dφ in Figure 2-3, which the hoop strain is derived from.

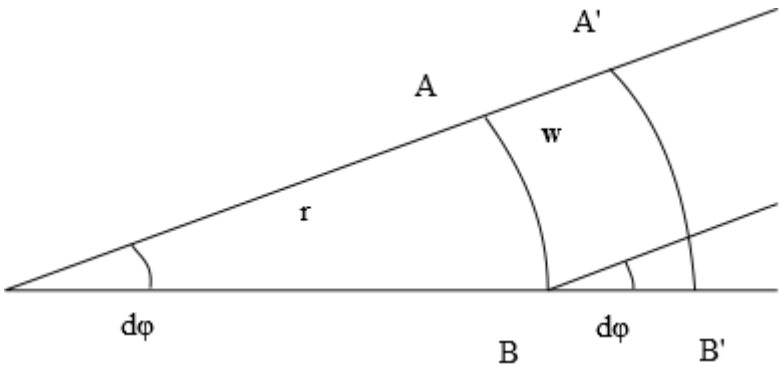

Figure 2-3: Radial displacement w in hoop direction

Strain in the hoop direction becomes

$$\varepsilon_\varphi = \frac{A'B' - AB}{AB} = \frac{(r+w)d\varphi}{rd\varphi} = \frac{w}{r} \qquad \textit{Eq. 2-9}$$

➔ $$N_\varphi = Eh\varepsilon_\varphi = \frac{Eh}{r}\mathrm{w} \qquad \textit{Eq. 2-10}$$

From the theory for plate structures, the relationship between moment and curvature is known as

$$M_x = D\left(\kappa_x - \upsilon\kappa_\varphi\right) \qquad \textit{Eq. 2-11}$$

$$D = \frac{Eh^3}{12(1-\upsilon^2)} \qquad \textit{Eq. 2-12}$$

$$\kappa_x = \frac{d^2w}{dx^2} \qquad \textit{Eq. 2-13}$$

$$\kappa_\varphi = \frac{1}{r+w} - \frac{1}{r} = -\frac{w}{r(r+w)} \approx 0 \qquad \textit{Eq. 2-14}$$

➔ $$M_x = D\frac{d^2w}{dx^2} \qquad \textit{Eq. 2-15}$$

Eq. 2-10 and Eq. 2-15 are inserted in the differential Eq. 2-4. The differential equation becomes

$$\frac{d^4w}{dx^4} + \frac{Eh}{Dr^2}w = \frac{p(x)}{D} \qquad \textit{Eq. 2-16}$$

2.2 Solving the differential equation

The solution of the differential equation may be split into a homogenous and a particular part. The particular solution, w_p, represents a membrane effect, like the uniform radial displacement, while the homogenous solution, w_h, represents the effect from the boundary constraints.

P(x) is assumed to be a polynomial of third degree or less.

$$w_p = \frac{r^2}{Eh} p(x) \qquad \textit{Eq. 2-17}$$

P(x) will therefore not be a part of the homogenous solution.

$$\frac{d^4 w}{dx^4} + \frac{Eh}{Dr^2} w = 0 \qquad \textit{Eq. 2-18}$$

By defining

$$4\beta^4 = \frac{Eh}{4Dr^2}$$

$$\beta = \frac{1}{L_e}$$

the elastic length L_e is found as

$$\beta^4 = \frac{Eh}{4r^2 \frac{Eh^3}{12(1-v^2)}}$$

$$\beta^4 = \frac{3(1-v^2)}{h^2 r^2}$$

$$L_e^4 = \frac{h^2 r^2}{3(1-\upsilon^2)}$$

$$L_e = \frac{\sqrt{hr}}{\sqrt[4]{3(1-\upsilon^2)}} \qquad \textit{Eq. 2-19}$$

By defining a dimensionless constant $\xi = x/L_e$, the homogenous equation becomes

$$\frac{d^4 w}{dx^4 L_e^4} + \frac{4}{L_e^4} w = 0$$

$$\frac{d^4 w}{dx^4} + 4w = 0 \qquad \textit{Eq. 2-20}$$

Eq. 2-20 was an ordinary differential equation with constant coefficients. The homogenous solution represents the flexural rigidity as the impact from moments, shear force, displacement and strains.

$$w_h = C_1 e^{m1} + C_2 e^{m2} + C_3 e^{m3} + C_4 e^{m4} \qquad \textit{Eq. 2-21}$$

where c_i are constants and m^i are roots of Eq. 2-20. The general homogenous solution is alertly written as

$$w_h = e^{-\xi}(C_1 \cos\xi + C_2 \cos\xi) + e^{\xi}(C_3 \sin\xi + C_4 \sin\xi) \qquad \textit{Eq. 2-22}$$

For the cylindrical tank considered in this thesis, it was assumed that the wall exceeded the elastic length. Only boundary constraints from one edge is considered at once.

The first term of the homogenous solution is multiplied with $e^{-\xi}$, and $e^{-\xi} \rightarrow 0$ when $\xi \rightarrow \infty$, so this part will be damped when ξ grows. The second term is multiplied with e^{ξ}, and e^{ξ} tends to infinite when $\xi \rightarrow \infty$, which is impossible.

The homogenous constants C_1 and C_2 may differ from zero, while C_3 and C_4 must be zero. The homogenous part becomes

$$w_h = e^{-\xi}(C_1 \cos\xi + C_2 \sin\xi) \qquad \textit{Eq. 2-23}$$

The hoop force will then be

Hoop force (Eq. 2-10)

$$N_{\varphi h} = \frac{Eh}{r} e^{-\xi}(C_1 \cos\xi + C_2 \sin\xi) \qquad \textit{Eq. 2-24}$$

For simplification, the following functions are introduced on behalf of Eq. 2-23

Table 2-1: G-functions

$$g_1 = e^{-\xi}\cos\xi$$

$$g_2 = e^{-\xi}\sin\xi$$

$$g_3 = g_1(\xi) + g_2(\xi)$$

$$g_4 = g_1(\xi) - g_2(\xi)$$

Eq. 2-23 can be rewritten as

$$w_h = C_1 g_1(\xi) + C_2 g_2(\xi) \qquad \textit{Eq. 2-25}$$

In order to find the longitudinal moment, and the shear force from the boundary constraints, Eq. 2-25 is differentiated.

Angular deflection
$$\frac{dw_h}{dx} = \frac{1}{L_e}\left(C_1\frac{dg_1}{d\xi} + C_2\frac{dg_2}{d\xi}\right)$$

Curvature
$$\frac{d^2w_h}{dx^2} = \frac{1}{L_e{}^2}\left(C_1\frac{d^2g_1}{d\xi^2} + C_2\frac{d^2g_2}{d\xi^2}\right) \qquad \textit{Eq. 2-26}$$

Shear force
$$\frac{d^3w_h}{dx^3} = \frac{1}{L_e{}^3}\left(C_1\frac{d^3g_1}{d\xi^3} + C_2\frac{d^3g_2}{d\xi^3}\right)$$

Differentiation of the formulas above are carried out to obtain the angular deflection and curvature.

1.1
$$\frac{dg_1}{d\xi} = -e^{-\xi}\cos\xi - e^{-\xi}\sin\xi = -(g_1 + g_2) = -g_3(\xi)$$

1.2
$$\frac{d^2g_1}{d\xi^2} = -e^{-\xi}\cos\xi - e^{-\xi}\sin\xi - e^{-\xi}\sin\xi + e^{-\xi}\cos\xi$$
$$\frac{d^2g_1}{d\xi^2} = -2e^{-\xi}\sin\xi = -2g_2$$

1.3
$$\frac{d^3g_1}{d\xi^3} = 2\left(e^{-\xi}\cos\xi - e^{-\xi}\sin\xi\right) = 2g_4$$

2.1
$$\frac{dg_2}{d\xi} = -e^{-\xi}\sin\xi + e^{-\xi}\cos\xi = -g_2 + g_1 = g_4(\xi)$$

2.2
$$\frac{d^2g_2}{d\xi^2} = e^{-\xi}\sin\xi - e^{-\xi}\cos\xi - e^{-\xi}\cos\xi - e^{-\xi}\sin\xi$$
$$\frac{d^2g_1}{d\xi^2} = -2e^{-\xi}\cos\xi = -2g_1$$

2.3
$$\frac{d^3g_2}{d\xi^3} = -2\left(-e^{-\xi}\cos\xi - e^{-\xi}\sin\xi\right) = 2g_3$$

Angular deflection

$$\frac{dw_h}{dx} = \frac{1}{L_e}(C_1(-g_3(\xi)) + C_2 g_4(\xi)) \qquad \textit{Eq. 2-27}$$

Curvature

$$\frac{d^2 w_h}{dx^2} = \frac{1}{L_e{}^2}\left(C_1(-2g_2) + C_2(-2g_1)\right) \qquad \textit{Eq. 2-28}$$

Shear force

$$\frac{d^3 w_h}{dx^3} = \frac{1}{L_e{}^3}(C_1 2g_4 + C_2 2g_3) \qquad \textit{Eq. 2-29}$$

Since the edge is clamped, and no displacement or rotation is allowed, C_1 and C_2 can be redefined as M_0 and V_0. See Figure 2-4.

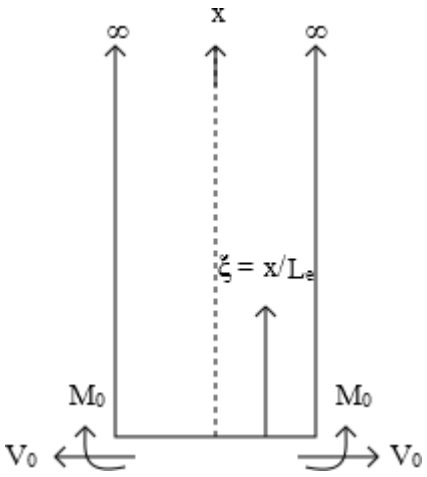

Figure 2-4: Infinite cylinder wall

For $\xi = 0$, the g-functions are

Table 2-2: G-functions for $\xi = 0$

$$g_1 = e^{-\xi}\cos\xi = 1$$

$$g_2 = e^{-\xi}\sin\xi = 0$$

$$g_3 = g_1(\xi) + g_2(\xi) = 1$$

$$g_4 = g_1(\xi) - g_2(\xi) = 1$$

M(x) and V(x) are found by inserting Eq. 2-15 into Eq. 2-28 and Eq. 2-29.

$$M(x) = -D\frac{1}{L_e{}^2}\left(C_1(-2g_2) + C_2(-2g_1)\right) \qquad \textit{Eq. 2-30}$$

$$V(x) = D\frac{1}{L_e{}^3}(C_1 2g_4 + C_2 2g_3) \qquad \textit{Eq. 2-31}$$

M(0) and V(0) are obtained by inserting the g-function's values from Table 2-2. M(0) and V(0) are rewritten on matrix form as

$$\begin{bmatrix} M_0 \\ V_0 \end{bmatrix} = \frac{2D}{L_e^2}\begin{bmatrix} 0 & -1 \\ \frac{1}{L_e} & \frac{1}{L_e} \end{bmatrix}\begin{bmatrix} C_1 \\ C_2 \end{bmatrix} \qquad \textit{Eq. 2-32}$$

Inverted, C_1 and C_2 are defined as:

$$\begin{bmatrix} C_1 \\ C_2 \end{bmatrix} = \frac{L_e^2}{2D}\begin{bmatrix} 1 & 1 \\ -1 & 0 \end{bmatrix}\begin{bmatrix} M_0 \\ V_0 L_e \end{bmatrix} \qquad \textit{Eq. 2-33}$$

By replacing C_1 and C_2 in Eq. 2-23, Eq. 2-24, Eq. 2-27, Eq. 2-30 and Eq. 2-31, the following relation between shell effects and clamping forces is found in reference (4).

$$\begin{bmatrix} w_h \frac{2D}{L_e^2} \\ N_\varphi \frac{L_e^2}{2r} \\ \frac{dw}{dx}\frac{2D}{L_e} \\ M_x \\ V_x L_e \end{bmatrix} = \begin{bmatrix} g_4(\xi) & g_1(\xi) \\ g_4(\xi) & g_1(\xi) \\ -2g_1(\xi) & -g_3(\xi) \\ g_3(\xi) & g_2(\xi) \\ -2g_2(\xi) & g_4(\xi) \end{bmatrix}\begin{bmatrix} M_0 \\ V_0 L_e \end{bmatrix} \qquad \textit{Eq. 2-34}$$

M_0 and V_0 in Eq. 2-34 are solved by use of the initial conditions for displacement and angular deflection at $\xi = 0$.

$\xi = 0$

$$w_h = (g_4 M_0 + g_1 V_0 L_e)\frac{{L_e}^2}{2D}$$

$$w_h = (M_0 + V_0 L_e)\frac{{L_e}^2}{2D}$$

$\xi = 0$

$$\frac{dw_h}{dx} = (-2g_1 M_0 - g_3 V_0 L_e)\frac{L_e}{2D}$$

$$\frac{dw_h}{dx} = (-2M_0 - V_0 L_e)\frac{L_e}{2D}$$

The particular solution for the displacement was given in Eq. 2-17, and must be considered in the calculation for the integration constants.

$$w_p(x) = \frac{r^2}{Eh}p(x) \qquad \textit{Eq. 2-35}$$

Furthermore, in this derivation, p(x) is defined as a constant (for instant a uniform pressure load), which made

$$\frac{dw_p(x)}{dx} = 0 \qquad \textit{Eq. 2-36}$$

By summation, the total displacement and rotation are stated as two equations with two unknowns.

$$w_{tot} = \frac{pr^2}{Eh} + (M_0 + V_0 L_e)\frac{{L_e}^2}{2D} = 0 \qquad \textit{Eq. 2-37}$$

$$\frac{dw_{tot}}{dx} = (-2M_0 - V_0 L_e)\frac{L_e}{2D} = 0 \qquad \textit{Eq. 2-38}$$

This set of equation is solved, and the integration constants are

$$M_0 = \frac{2Dr^2p}{{L_e}^2Eh} \qquad \textit{Eq. 2-39}$$

$$V_0L_e = -p{L_e}^2 \qquad \textit{Eq. 2-40}$$

By inserting M_0 and V_0 in Eq. 2-34, the following moment and shear force are

$$M_x(\xi) = \frac{p{L_e}^2}{2}g_3(\xi) - p{L_e}^2g_2(\xi) = \frac{p{L_e}^2}{2}g_4(\xi) \qquad \textit{Eq. 2-41}$$

$$V_x(\xi) = -pL_eg_2(\xi) = -pL_eg_4(\xi) = -pL_eg_1(\xi) \qquad \textit{Eq. 2-42}$$

The hoop force is combined by the particular part and the homogenous part into the total hoop force.

$$N_{\varphi p} = \frac{Eh}{r}w_p = \frac{Eh}{r}\frac{pr^2}{Eh} = pr$$

$$N_{\varphi h}(\xi) = (g_4(\xi)M_0 + g_1(\xi)V_0L_e)\frac{2r}{L_e^2}$$

$$N_{\varphi}(\xi) = pr + (g_4(\xi)M_0 + g_1(\xi)V_0L_e)\frac{2r}{L_e^2} \qquad \textit{Eq. 2-43}$$

The g functions has proven itself to be a great tool for solving the boundary effects for a cylindrical tank. In Figure 2-5, the g-functions are plotted for visualization of the damping length. Every g-function has been damped out between 3 and 4. A universal damping length has therefore been defined in Eq. 2-44 as.

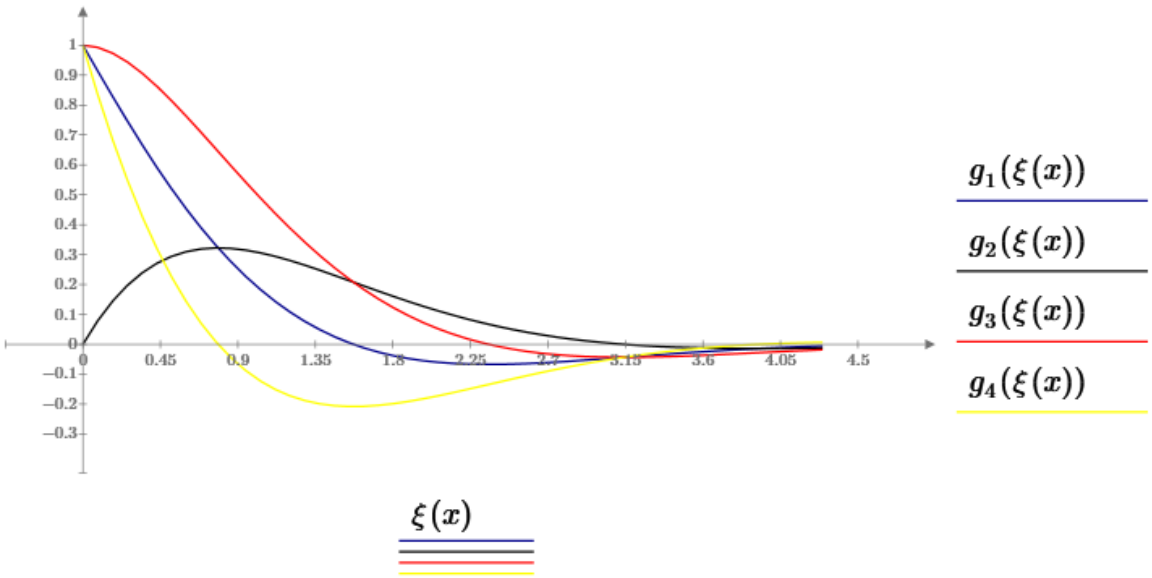

Figure 2-5: G-functions

$$L_c = \pi L_e \qquad \textit{Eq. 2-44}$$

Considering the damping length L_c at an early stage would be smart, in order to verify interfering boundary constraints. In this thesis, it was assumed that height of the wall exceeded L_c.

For a hydrostatic pressure load, the load is defined as a linear polynomial instead of a constant, where γ_s is the density of the liquid.

$$p(x) = \gamma_s(H - x) \qquad \textit{Eq. 2-45}$$

The equations for displacement and angular deflection are changed into:

$$w_p(x) = \frac{r^2\gamma_s}{Eh}(H - x) \qquad \textit{Eq. 2-46}$$

$$w_h(x) = \frac{{L_e}^2}{2D}(g_4M_0 + g_1V_0L_e) \qquad \textit{Eq. 2-47}$$

$$w_{tot}(x) = \frac{{L_e}^2}{2D}(g_4M_0 + g_1V_0L_e) + \frac{r^2\gamma_s}{Eh}(H - x) \qquad \textit{Eq. 2-48}$$

$$\frac{dw_p}{dx} = -\frac{r^2\gamma_s}{Eh} \qquad \textit{Eq. 2-49}$$

$$\frac{dw_h}{dx} = \frac{L_e}{2D}(-2g_1M_0 - g_3V_0L_e) \qquad \textit{Eq. 2-50}$$

$$\frac{dw_{tot}}{dx} = \frac{L_e}{2D}(-2g_1M_0 - g_3V_0L_e) - \frac{r^2\gamma_s}{Eh} \qquad \textit{Eq. 2-51}$$

At the wall-slab connection, both the displacement and rotation equal 0 when $\xi = 0$ (x = 0).

$\xi = 0$ $$w_{tot} = \frac{{L_e}^2}{2D}(M_0 + V_0L_e) + \frac{r^2\gamma_s}{Eh}H = 0 \qquad \textit{Eq. 2-52}$$

$\xi = 0$ $$\frac{dw_{tot}}{dx} = \frac{L_e}{2D}(-2M_0 - V_0L_e) - \frac{r^2\gamma_s}{Eh} = 0 \qquad \textit{Eq. 2-53}$$

The set of two equations with two unknowns is solved, and the constants of integration are:

$$M_0 = (\frac{H}{L_e} - 1)\frac{r^2\gamma_s}{Eh}\frac{2D}{L_e} \quad \textit{Eq. 2-54}$$

$$V_0 L_e = (1 - \frac{2H}{L_e})\frac{r^2\gamma_s}{Eh}\frac{2D}{L_e} \quad \textit{Eq. 2-55}$$

The constants derived in Eq. 2-54 and Eq. 2-55 can be inserted in Eq. 2-34 to obtain the behaviour of the wall.

M_0 and V_0 are identical as for the universal pressure, while the hoop force will differ because of $w_p(x)$

$$M_x(\xi) = g_3(\xi)M_0 + g_2(\xi)V_0 L_e \quad \textit{Eq. 2-56}$$

$$V_x(\xi)L_e = -2g_2(\xi)M_0 + g_4(\xi)V_0 L_e \quad \textit{Eq. 2-57}$$

$$N_{\varphi p} = \frac{Eh}{r}w_p(x) = \frac{Eh}{r}\frac{r^2\gamma_s}{Eh}(H - x) = r\gamma_s(H - x) \quad \textit{Eq. 2-58}$$

$$N_{\varphi h}(\xi) = (g_4(\xi)M_0 + g_1(\xi)V_0 L_e)\frac{2r}{L_e^2} \quad \textit{Eq. 2-59}$$

$$N_\varphi(\xi) = r\gamma_s(H - x) + (g_4(\xi)M_0 + g_1(\xi)V_0 L_e)\frac{2r}{L_e^2} \quad \textit{Eq. 2-60}$$

2.3 Thermal stresses in cylinders

A temperature change in a material render a volume change. It is normal that a material enlarges when heated, and shrinks when cooled down. The extent of variation is decided by the material's thermal expansion coefficient.

For an unconstrained beam element, the change in length would be

$$\Delta L = L\Delta T\alpha \qquad \textit{Eq. 2-61}$$

Where L is the initial length, ΔT is the temperature change (assumed positive), and α is the thermal expansion coefficient. For a constrained beam, the deformation will not be permitted, and stress would occur by

$$\sigma = -E\Delta T\alpha \qquad \textit{Eq. 2-62}$$

For a radial temperature variation across the thickness, stress will occur on behalf of the change in the temperature. Since one edge will be heated, and the other edge cooled down, both compression and tension would be initiated, and a resulting moment would appear. The moment is found by combining section modulus and the stress.

$$M = -E\Delta T\alpha \qquad \textit{Eq. 2-63}$$

For a cylindrical tank, Poisson's ratio must be considered, so the stress and moment would be in accordiance with (5), where T = +T = -T.

$$\sigma_x = \sigma_\theta = \frac{E\alpha T}{1-\nu} \qquad \textit{Eq. 2-64}$$

$$M_0 = \frac{2\sigma_x h^2}{12} = \frac{E\alpha T h^2}{6(1-\nu)} \qquad \textit{Eq. 2-65}$$

For the special temperature issue in this thesis, T_i would be the applicable temperature load, creating the moment M_0.

$$a := \frac{|T_i|}{|T_i| + |T_o|} = 0.825$$

$$b := \frac{|T_o|}{|T_i| + |T_o|} = 0.175$$

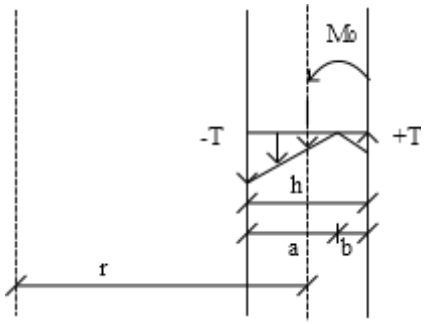

Figure 2-6: Temperature load

Where M_0 is given by:

$$\sigma_i = \frac{E\alpha T_i}{1-\nu} \qquad \textit{Eq. 2-66}$$

$$\sigma_u = \frac{E\alpha T_u}{1-\nu} \qquad \textit{Eq. 2-67}$$

$$M_0 = \frac{\sigma_i h^2}{12} = \frac{E\alpha T_i h^2}{12(1-\nu)} \qquad \textit{Eq. 2-68}$$

M_0 would be the moment for any unconstrained cylindrical wall section, and be the clamped moment for a slab-wall connection. For a thermal load facing a free edge, a constraint moment must be induced in the opposite direction. In addition to M_0, flare stress is added by $\sigma_{\theta e}$ and contraction stress is subtracted by $\sigma_{\theta.}$ (5).

$$\sigma_{\theta e} = \frac{2M_0\lambda^2 R}{\mathrm{h}} \qquad \textit{Eq. 2-69}$$

Where

$$\lambda = \left(\frac{3(1-\upsilon^2)}{r^2 t^2}\right)^{\frac{1}{4}} \qquad \textit{Eq. 2-70}$$

$$\sigma_\theta = \frac{6M_0}{\mathrm{h}^2} \qquad \textit{Eq. 2-71}$$

$\sigma_{\theta net}$ is given by Eq. 2-72 and the corresponding moment is given by Eq. 2-73

$$\sigma_{\theta net} = \frac{E\alpha T_i}{1-\upsilon} + \frac{2M_0\lambda^2 R}{h} - \upsilon\frac{6M_0}{t^2} \qquad \textit{Eq. 2-72}$$

$$M_{\theta net} = \frac{\sigma_{\theta net} t^2}{12(1-\upsilon)} \qquad \textit{Eq. 2-73}$$

Chapter 3

3 Abaqus

3.1 Abaqus

Abaqus is a software platform for finite element analysis, known for its high performance and ability to simulate a wide range of challenging simulations. The Abaqus platform consist of three products: Abaqus/Standard, Abaqus/Explicit and Abaqus/CAE (6).

Abaqus/Standard utilizes the traditional implicit finite element analysis method. This method uses the basis from the backward Euler method by solving an equation of involving both current state of the system and a predicted one. For each time increment, an equation must be solved and the analysis may therefore be computational expensive. Abaqus/Standard is well arranged for solving static, dynamic and thermal problems.

Abaqus/Explicit employ the explicit finite element analysis method, which uses the principles of the forward Euler method. The forward Euler method calculates the state of a system at a later time from the state of the system at current time. This method often claim a huge amount of small, inexpensive time increments and are well equipped for short period analyses, such as a regular quasi-static problem. (7)

Abaqus/CAE provide a complete modelling and visualization system for Abaqus/Implicit and Abaqus/Explicit, where the abbreviation stands for “Complete Abaqus Environment”. Most functionalities for Abaqus/Implicit and Abaqus/Explicit are supported in Abaqus/CAE. Excluded functionalities for Abaqus may on the other hand be defined in the input file (such as initial prestressing stress for tendons).

3.2 Creation of Abaqus model

In this thesis, the creation of the Abaqus model has been essential. It was time consuming, and sometimes experimental, to evolve a complete model representing all current effects. This sub chapter will go through the main issues and important details experienced in the process of creating the Abaqus model.

1. Create the part:
   A 3D deformable shell element revolved 360°.
2. Verify the element normal. Be certain of which surfaces facing inside and outside.
   Module: Property, Assign Element Normal.
3. Create materials. Add the materials described in 1.8.
4. Create sections and assign shell thickness, thickness integration points, thickness integration rule and temperature variation.

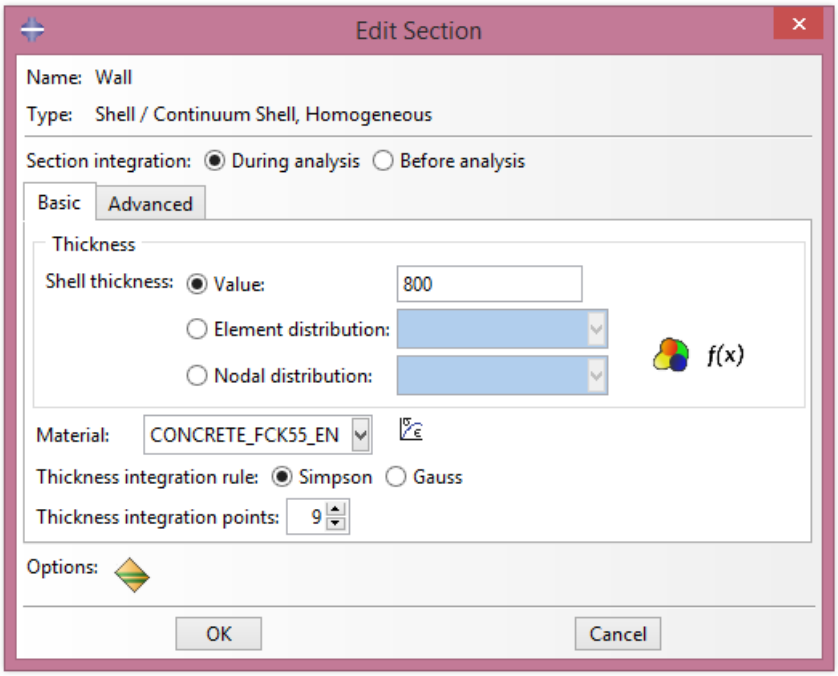

Figure 3-1: Edit section, basic

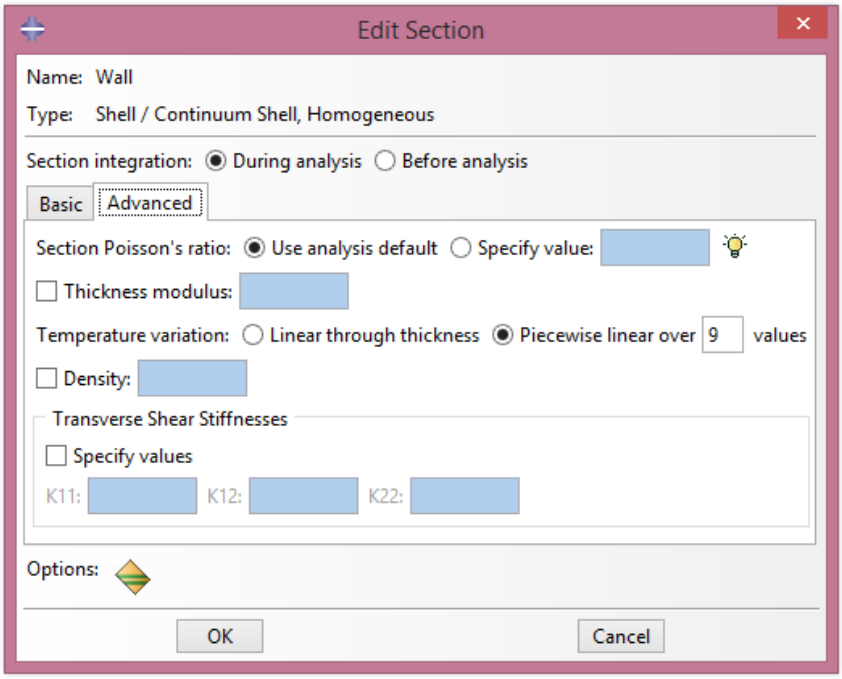

Figure 3-2: Edit section, advanced.

Due to chapter 29.6.5: "Using a shell section integrated during the analysis to define the section behaviour" in the Abaqus Analysis User's Manual, there is specified that for all heat transfer or sequentially coupled temperature-displacement shell elements, Simpsons rule must be assigned (6).

5. Create partitions considering sections, loads and mesh.
6. Create instances.
7. Check section thickness and verify thickness positions.
8. Create Datum axis: Principal axis in origin for datum.
9. Create datum:

   Module: Assembly/Tools/Datum/2 lines/Cylindrical.

   Use the two principal axis for the cylindrical datum.
10. Mesh the tank.
11. Create structural boundary conditions.
12. Create appropriate local orientation system for each section.

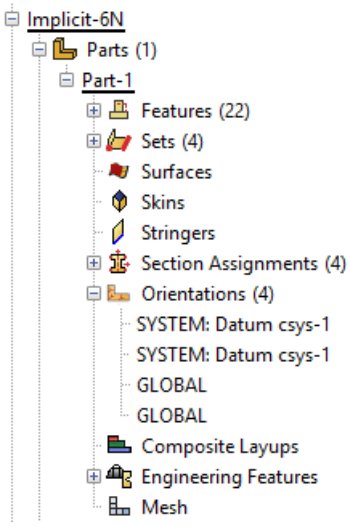

Figure 3-3: Orientation assignments

13. Assign material orientation for each section:
    Module: Property, Assign Material Orientation.

The mentioned points above was the foundation of the model. None of the selected properties should be modified in later models. It was essential that the coordinate system and mesh remained identical. Otherwise, the results would be useless.

The heat transfer analysis has been described in the points below.

14. Assign element type for heat transfer
    Module: Mesh, Family: Heat Transfer, Element Type: DS4

A 4-node quadrilateral shell element have the advantage of transferring heat transfer results to a stress analysis. By first analysing a heat transfer through a structure, before assigning the heat transfer effects to another model, gives the possibility of analysing non-linear effects due to temperature dependent materials (7).

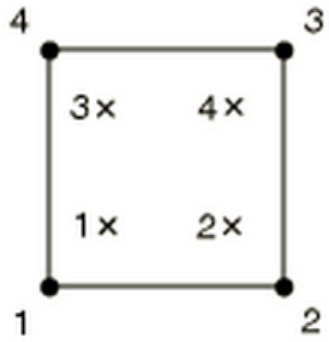

Figure 3-4: DS4 element with integration points

15. Create Step

    Type: Heat Transfer with a steady-state respond.

Uncoupled heat transfer analysis was used to model heat transfer conduction with general, temperature-dependent conductivity. Heat transfer problems can be nonlinear because the material properties are temperature dependent. In the assignment text, the heat transfer analysis was specified to be a steady state response. Different types of heat transfer has been discussed in (2). The consequence of a steady-state analysis it that the internal energy term in the governing heat transfer equation is omitted. There will be no meaningful time scale for heat transfer with steady state response (8).

16. Create thermal loads as boundary condition.

Assign the temperature at a chosen degree of freedom. Since there was 9 thickness integration points specified, and the thermal degrees of freedom in a DS4 element starts at 11, the inside thermal load must be assigned to the degree of freedom number 11. The thermal load at the outside would then be assigned to degree of freedom number 19 (6). The inner and outer surface is defined by the element normal direction.

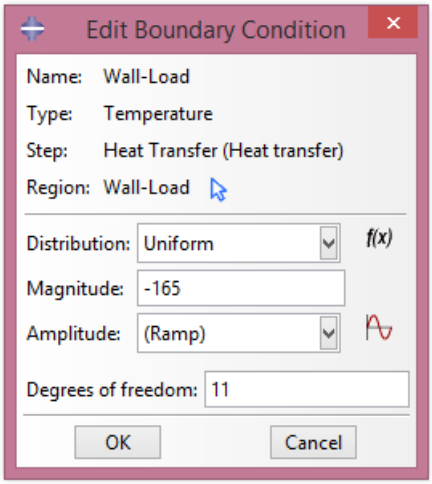

Figure 3-5: Edit boundary condition, temperature assignment

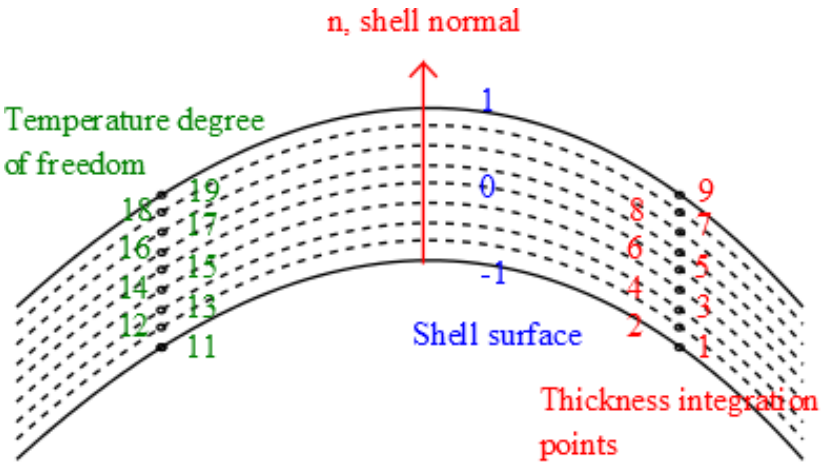

Figure 3-6: Overview section integration definitions

17. Create Field Output Request and select nodal temperature and element temperature. Specify shell layered section points.

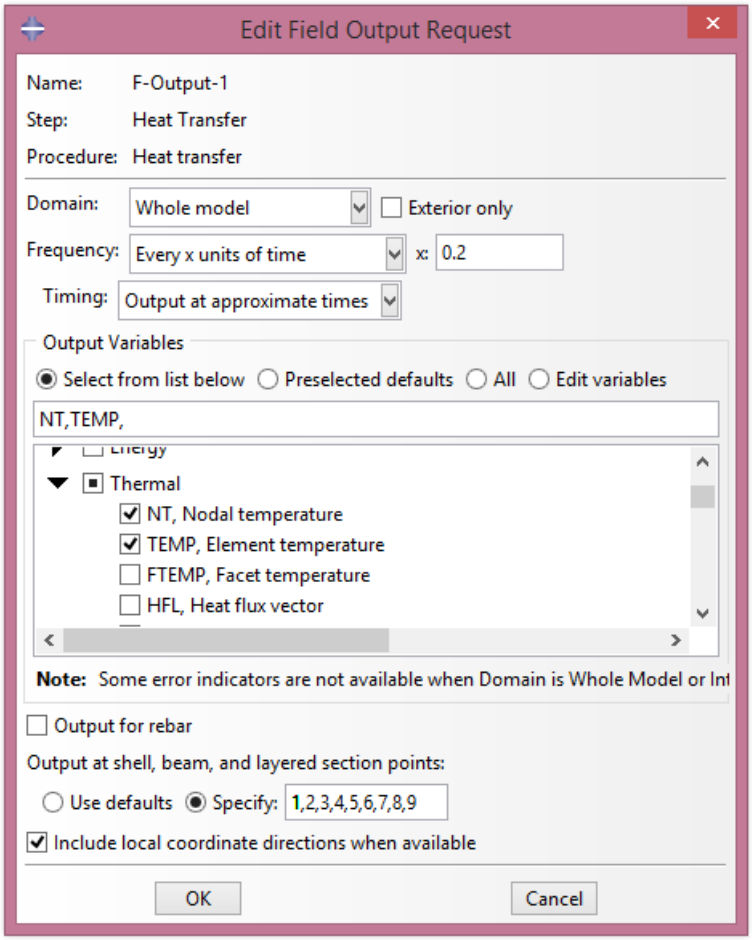

Figure 3-7: Edit field output request

For the second part of the sequentially coupled thermal stress analysis, the following points should be considered. In general, the type of element and the step should be changed and regular rebar layers should be defined.

18. Assign element type for stress analysis

    Module: Mesh, Family: Shell, Element type: S4R

This element is a 4-node general-purpose shell, with a reduced integration formula and hourglass control.

19. Create Steps

    Type: Static general for static loads (pressure and prestressing loads)

    Type: Dynamic implicit for thermal impact

A step for each loading effect should be put in sequence in order to simulate the assigned loads.

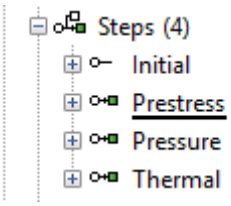

Figure 3-8: Steps

The step dynamic implicit has been chosen since it uses implicit time integration to calculate the quasi-static response of a system. Quasi-static applications are primarily interested in determining a final static response, while ensuring convergence by using small time increments when necessary. A dynamic implicit step also allows nonlinearities in material due to temperature properties by including a thermal expansion coefficient (9).

The description above fits well for concrete problems involving cracking.

20. Create Rebar Layers

Sections, Rebar Layers

Rebar layers are defined by clicking the yellow option button in Figure 3-1.

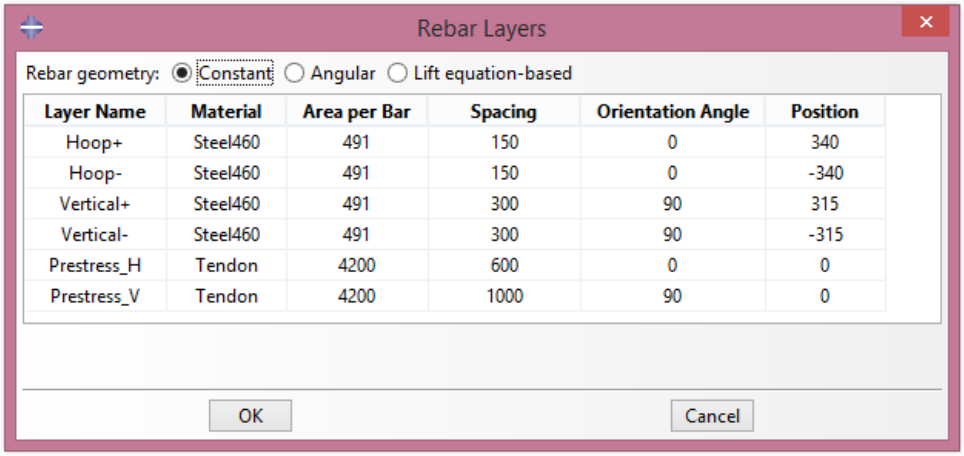

Figure 3-9: Rebar layers for wall section

The rebar layers need to be designed by a local orientation system for all three-dimensional elements (12). Orientation angle zero will then be assigned in the local 1-direction for the

element. A positive angle defines a rotation from local direction 1 to local direction 2 around the element's user-defined normal direction. In this case, orientation angle 0 will be the hoop direction for the wall, meanwhile orientation angle 90 will be in the vertical direction (11). The element's normal direction has been shown in Figure 3-6.

This procedure is also applicable for the slab and the roof. Common construction practise for roof is to apply spherical and circumferential reinforcement, which is rather complicated to control graphically in Abaqus, and assign in ShellDesign. A global coordinate system was therefore assigned for the roof and the slab, where the local direction 1 are the x direction. See Figure 3-10 for the coordinate system and Table 1-7 for the reinforcement in the roof.

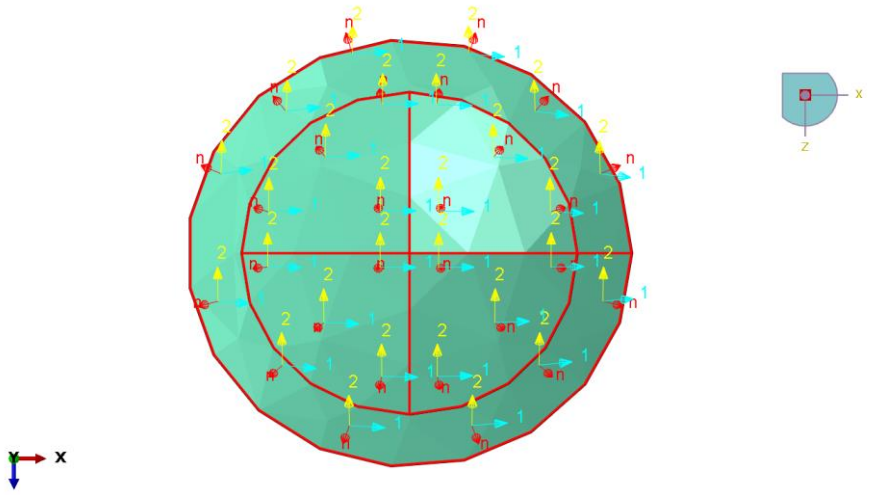

Figure 3-10: Local coordinate system for the roof section

Assigning a prestressing condition is not possible in Abaqus/CAE, but can be done directly in the input file as an initial condition (12).

```
55704  ** Section: Wall
55705  *Shell Section, elset=Wall, material=CONCRETE_FCK55_EN, orientation=Ori-1, temperature=9, offset=SNEG
55706  800., 9
55707  *Rebar Layer
55708  Hoop+, 491., 150., 340., Steel460, 0., 1
55709  Hoop-, 491., 150., -340., Steel460, 0., 1
55710  Vertical+, 491., 300., 315., Steel460, 90., 1
55711  Vertical-, 491., 300., -315., Steel460, 90., 1
55712  Prestress_H, 4200., 600., 0., Tendon, 0., 1
55713  Prestress_V, 4200., 1000., 0., Tendon, 90., 1
```

Figure 3-11: Prestressing input file

21. Create loads

    The hydrostatic spill loads need to be described by use of an analytical field

22. Assign the predefined temperature field from the heat transfer analysis.

The heat transfer must be created in the initial step and be modified in the thermal step (12). The number of thickness integration points and the mesh number must also be the same as in the heat transfer analysis.

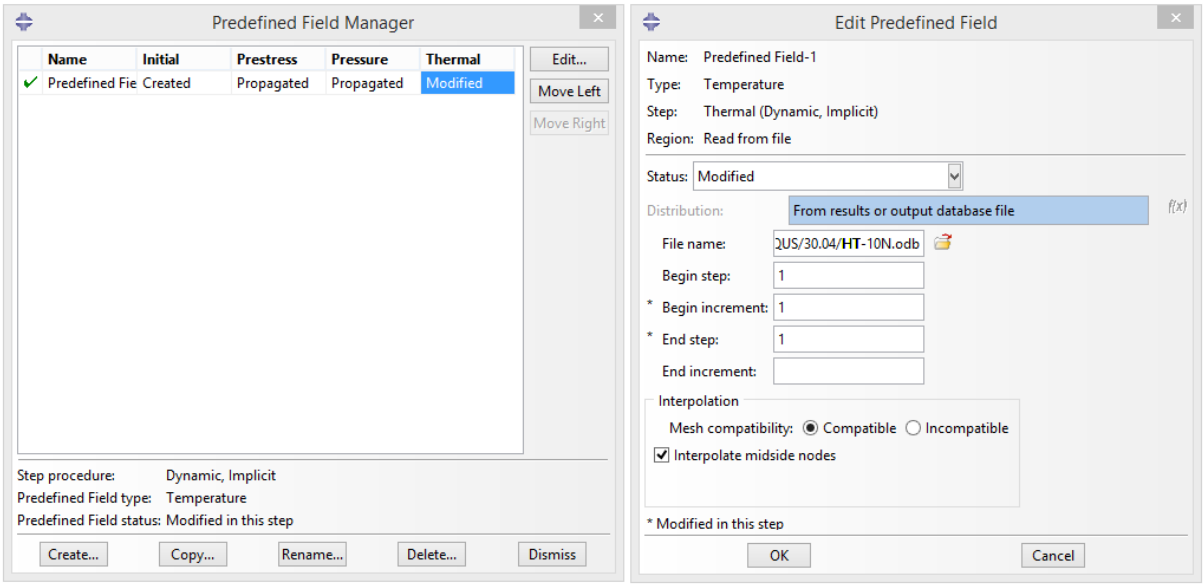

Figure 3-12: Predefined field manager

The interpolated midside notes is turned on in the analysis. This is required because the change in the order of interpolation varies between the first order heat transfer element and the (selectable) second order stress element. The advantage of using a second order stress element is to obtain a more realistic deformation pattern, and avoid discontinuity for the strains. See Figure 3-13

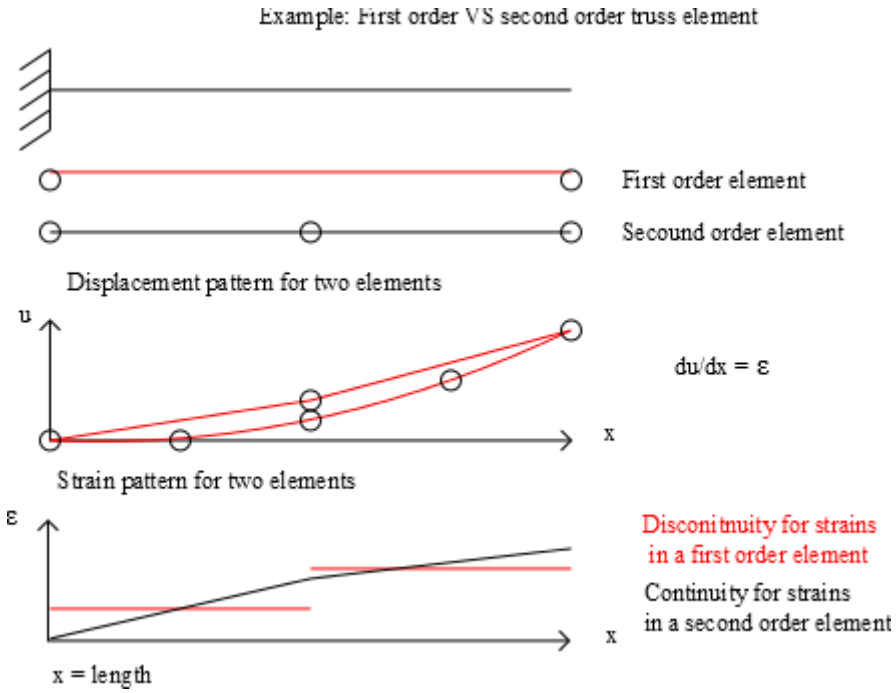

Figure 3-13: Interpolation order

3.3 Verification of heat transfer analysis

The initial temperature in the concrete containment tank was set to 0 °C. Thermal loads were applied to the structure as noted in load case 10 and 11 in Table 1-2. As the assignment text states, a steady-state, linear gradient variation should be assumed. Reference (2) discusses the different outcomes of linear and transient temperature gradients, and recommend that linear temperature gradients should be considered, since it would cause deeper cracks.

A test with solid elements was done in order to visualize a linear heat transfer. The section displayed in Figure 3-14 below is a part of the wall in the temperature loading area. Solid elements was used since Abaqus is only capable of giving value for one thickness integration point at the time. Figure 3-14 shows the initial temperature, while Figure 3-15 shows the final, linear temperature distribution.

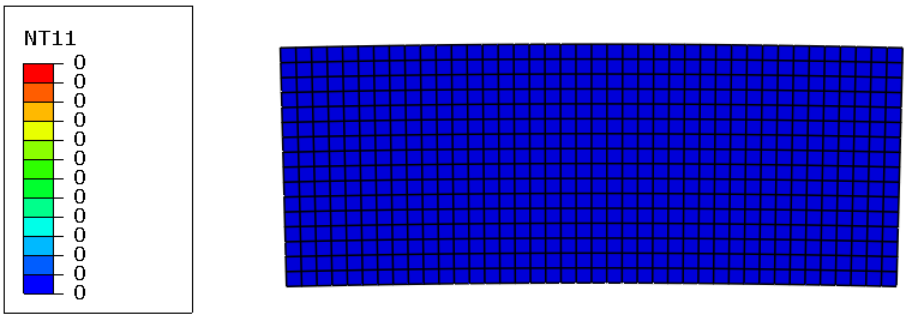

Figure 3-14: Initial temperature

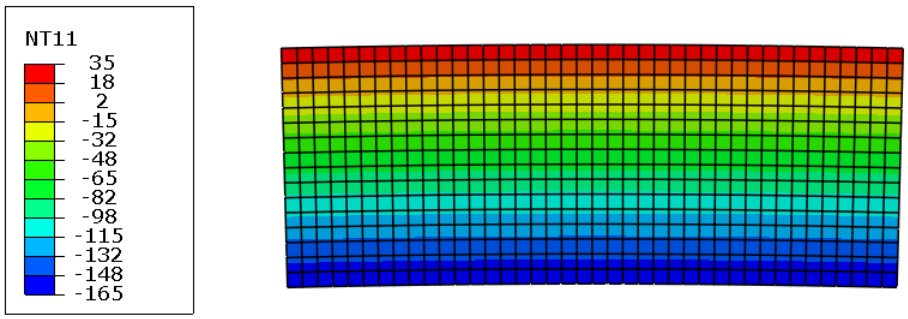

Figure 3-15: Final temperature

Temperature data from thickness integration points may however be plotted. Figure 3-16 and Figure 3-17 show the temperature in the thickness integration points through the wall. HT6NT11 is the node at the inside of the wall, while HT6NT19 is the node at the outside. The thickness integration points have constant spacing, which implies a linear heat distribution.

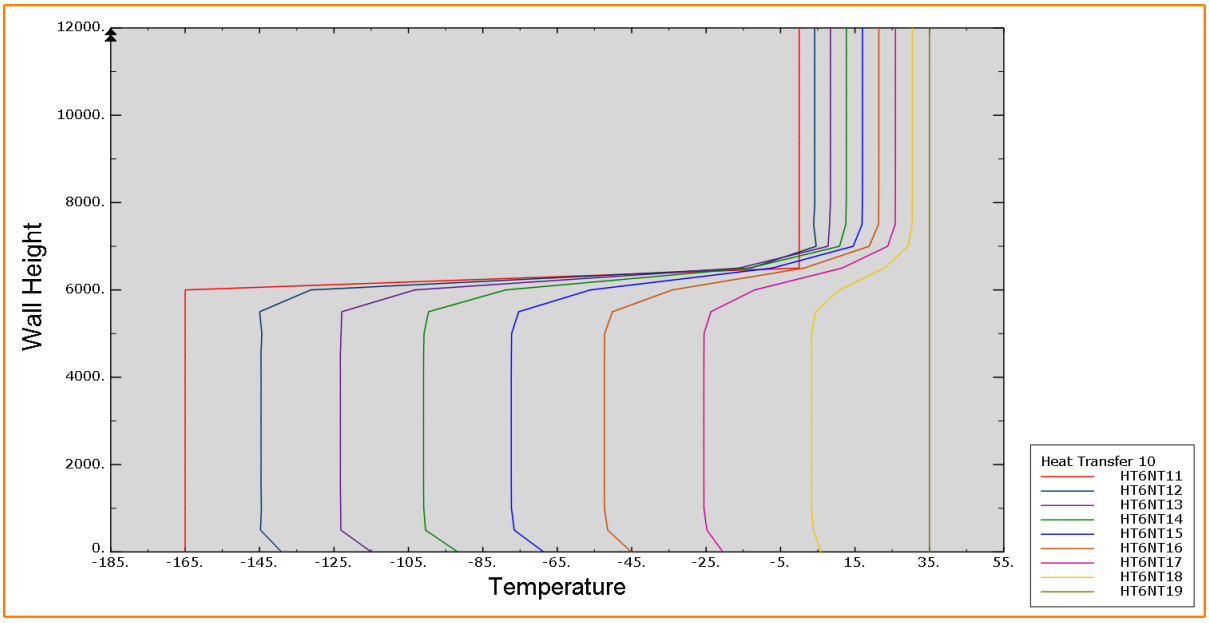

Figure 3-16: Temperature distribution for load case 10

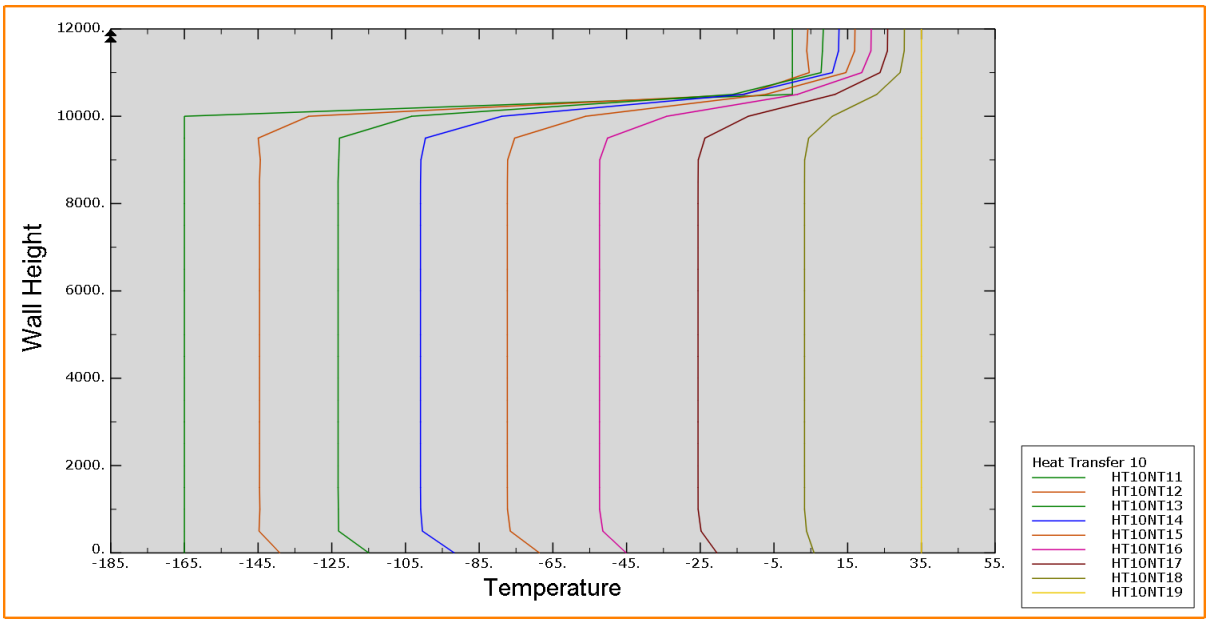

Figure 3-17: Temperature distribution for load case 11

The transition between the thermal loading and air at the inside of the tank, is modelled as similar boundary conditions, with different values. This causes the sharp temperature change at the inside of the wall. A temperature variation of 165 °C over an infinitesimal is not realistic, but may be considered as conservative. A large temperature difference vertically will cause high stresses and result in greater surface cracks.

The final temperature distribution for the inner and outer face is shown in Figure 3-18.

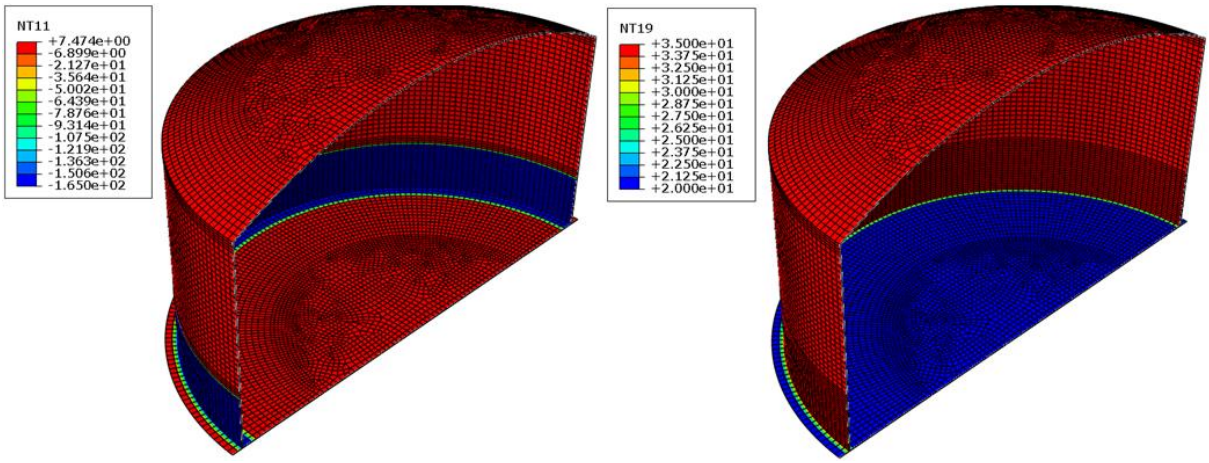

Figure 3-18: Temperature at inner surface (L) and outer surface (R)

3.4 Verification of pressure forces and boundary effects

On behalf of deviation in chapter 2.2, the wall behavouir for a cylindrical tank may be calculated. This therory should be used to verify the finite element model, in order to make sure that the FEM model functions as intended.

One of the load cases for this tank was the internal gas pressure. In order to verify the wall behaviour and the boundary effects in the FEM model, hand calculations were carried out. The main matrix was given in Eq. 2-34:

$$\begin{bmatrix} w_h \frac{2D}{L_e^2} \\ N_\varphi \frac{L_e^2}{2r} \\ \frac{dw}{dx}\frac{2D}{L_e} \\ M_x \\ V_x L_e \end{bmatrix} = \begin{bmatrix} g_4(\xi) & g_1(\xi) \\ g_4(\xi) & g_1(\xi) \\ -2g_1(\xi) & -g_3(\xi) \\ g_3(\xi) & g_2(\xi) \\ -2g_2(\xi) & g_4(\xi) \end{bmatrix} \begin{bmatrix} M_0 \\ V_0 L_e \end{bmatrix} \qquad \textit{Eq. 2-34}$$

The constants for integration were given by:

$$M_0 = \frac{2Dr^2p}{{L_e}^2 Eh} = 280.8\ kNm\frac{1}{m} \qquad \textit{Eq. 2-39}$$

$$V_0 L_e = -p{L_e}^2 = -127.6\ kN\frac{1}{m} \qquad \textit{Eq. 2-40}$$

Where the cylindrical constants was given as:

$$r = 40\ m, p = 0.029\ MPa, E = 35000\ MPa$$

$$D = \frac{Eh^3}{12(1-v^2)} = 1.641 * 10^6\ kNm \qquad \textit{Eq. 2-12}$$

$$L_e = \frac{\sqrt{hr}}{\sqrt[4]{3(1-v^2)}} = 4.40\ m \qquad \textit{Eq. 2-19}$$

The hand calculation was plotted and controlled by its initial definition, which gives that U(x=0) and Nφ(x=0) must be zero. The FEM model results was then compared to the hand calculation.

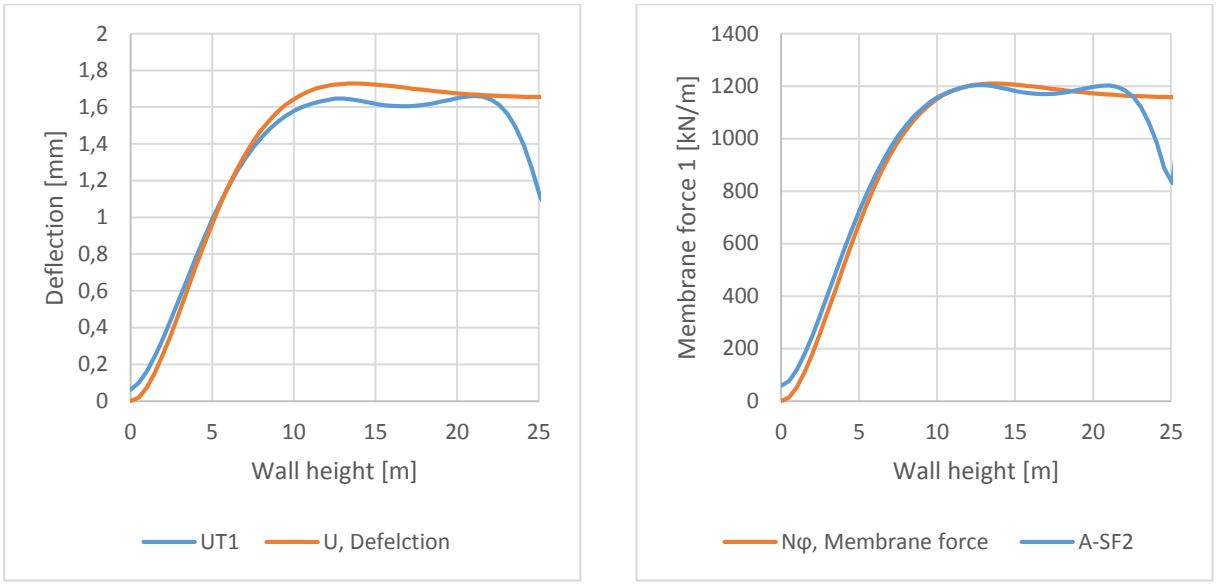

Figure 3-19: Deflection (L) and membrane force (R) by internal gas pressure

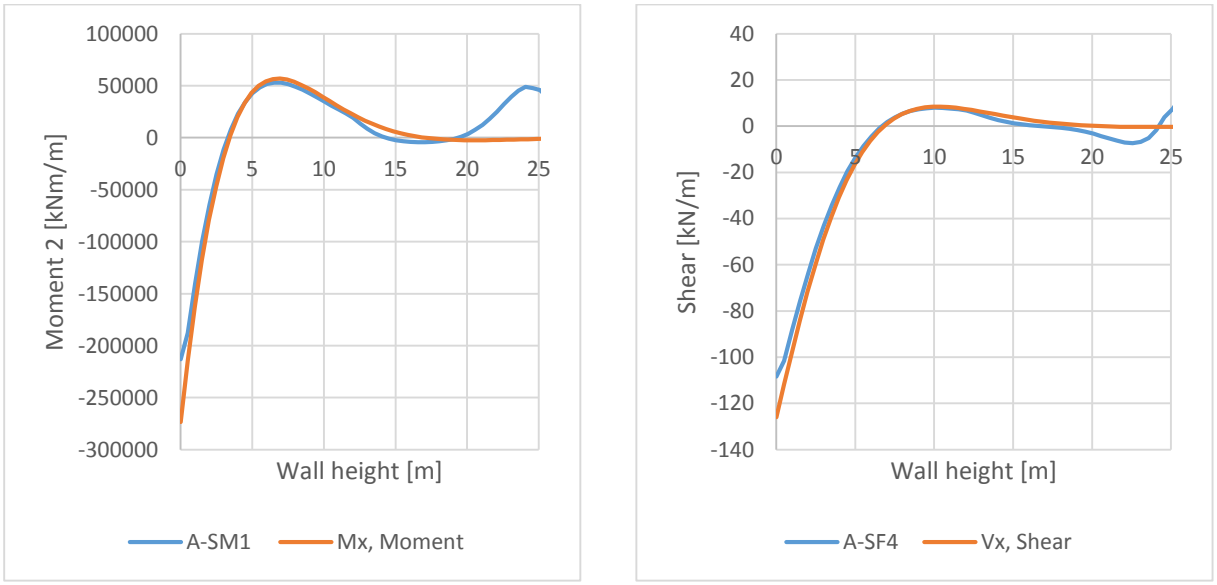

Figure 3-20: Longitudinal moment (L) and shear force (R) by internal gas pressure

As seen in the figures above, the FEM model does not replicate the hand calculation exactly. There are small differences, mainly because of a small boundary deflection that appeared at the wall-slab connection. This deformation was considered realistic, since the pressure load would deform the slab in radial direction. The boundary constraints defined for the hand calculation, where w_h and dw_h/dx was stated 0, cause no deformation or angular deflection, which again result in the mathematical correct solution for the longitudinal moment and shear force. The plots stop at wall height 25 m. From this height, the constraints from the ring beam would take action. Constraints from two edges was not considered in this thesis.

A second verification of the FEM model was done in order to verify a hydrostatic load. For simplification, a hydrostatic load for the entire wall was assigned, instead of one of the liquid loads. This is a simplification since a new boundary effect would be created if the hydrostatic load did not cover the entire wall height (4). The constants for integration were given in Eq. 2-54 and Eq. 2-55.

$$M_0 = \left(\frac{H}{L_e} - 1\right)\frac{r^2\gamma_s}{Eh}\frac{2D}{L_e} = 3173\ kNm\frac{1}{m} \qquad \textit{Eq. 2-54}$$

$$V_0 L_e = \left(1 - \frac{2H}{L_e}\right)\frac{r^2\gamma_s}{Eh}\frac{2D}{L_e} = \ 1556\ kN\frac{1}{m} \qquad \textit{Eq. 2-55}$$

$$r\ =\ 40\ m, \gamma_s = 10\frac{kN}{m^3}, E\ =\ 35000\ MPa, H\ =\ 38\ m$$

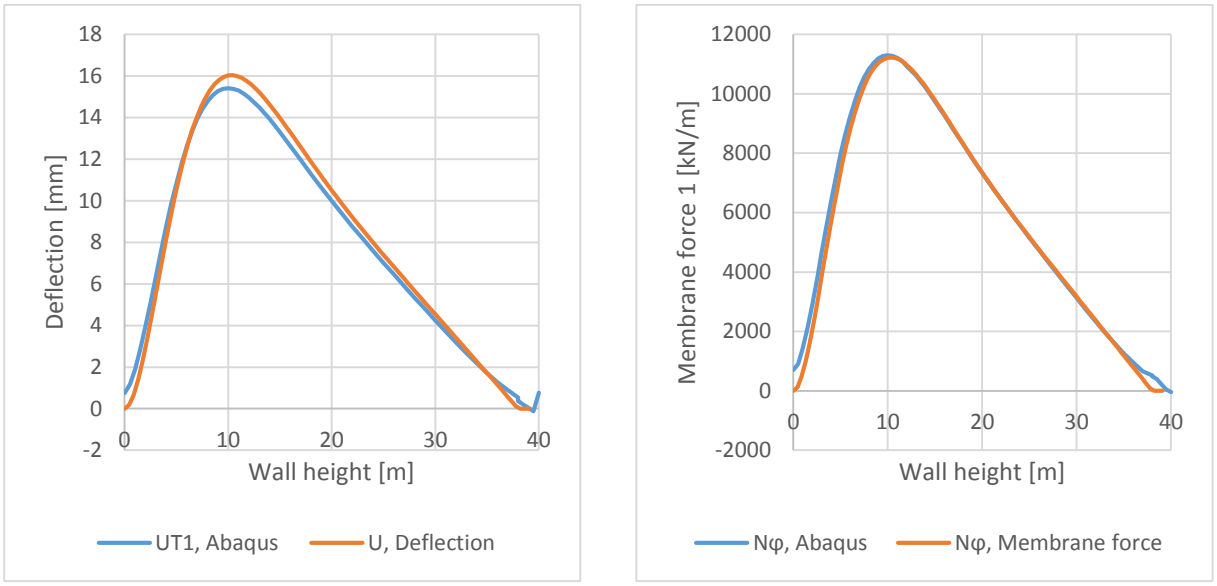

Figure 3-21: Deflection (L) and membrane force (R) by hydrostatic load

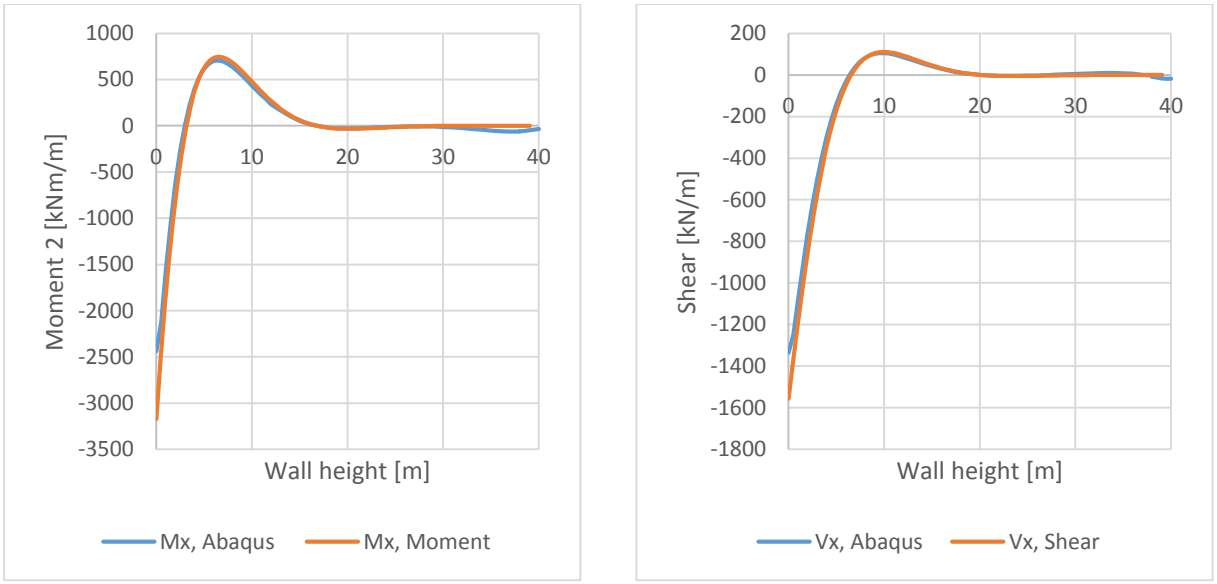

Figure 3-22: Longitudinal moment (L) and shear force (R) by hydrostatic load

Again, the FEM model does not replicate the hand calculation exactly, but the results are very close. A small deformation at the wall-slab connection and some inaccuracy at the ring beam should be noted. The ring beam creates another set of boundary constraints, which is not discussed in this thesis. However, in accordance with (4), Axisymmetric Shells - Sørensen 1999, the solution should be correct.

3.5 Verification of prestressed tendons

For the circumferential prestress, the following properties was decided in accordance with (1)

Table 3-1: Prestress

Circumferential Prestress	Vertical Prestress
$N_{ph} = 7.0\ \frac{MN}{m}$	$N_{pv} = 4.2\ \frac{MN}{m}$
$A_p = 4200\ mm^2$	$A_p = 4200\ mm^2$
$P_0 = -1000\ MPa$	$P_0 = -1000\ MPa$
$s_v = 600\ mm$	$s_v = 1000\ mm$

The resulting stress in the tendons and the inflicted concrete stress is shown in Figure 3-23. The concrete stress is measured from the middle of the wall section.

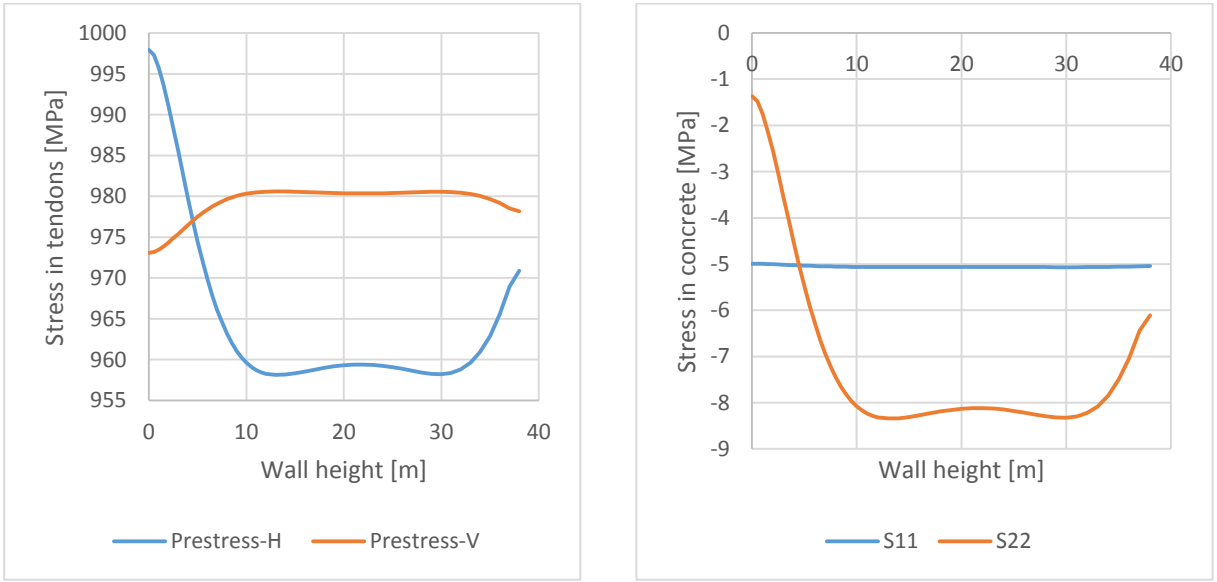

Figure 3-23: Stress in tendons (L) and stress in concrete (R)

A quick hand calculation shows that the prestressing acts as desired, where h represents the thickness of the wall.

$$n_{ph} = \frac{N_{ph}}{h} = -8.75\ MPa \qquad \textit{Eq. 3-1}$$

$$n_{pv} = \frac{N_{pv}}{h} = -5.25\ MPa \qquad \textit{Eq. 3-2}$$

By common literature idealizes prestress for the circumferential direction as a uniform pressure load. This means that the circumferential prestress could be replaced by an outer pressure load, defined as p_{ph}, where r_w is radius from centre to outside of the wall

$$p_{ph} = \frac{N_{ph}}{r_w} = -0.172\ MPa \qquad \textit{Eq. 3-3}$$

The main difference between applying the prestress as prestressed tendons or as an outer pressure load is when it is applied. Abaqus handles the prestressed tendons as an initial condition, which means that the shell section forces include the prestress forces. The pressure load will instead be a load force, which is not included in the shell section force.

This difference may been seen when shell sectional forces are analysed. Shell Force N1 is shifted by N_{ph} in Figure 3-24, but there is no change in the compressive stress in the middle of the wall, S22. No differences could be found for either Vx, Mx, S11 or S22.

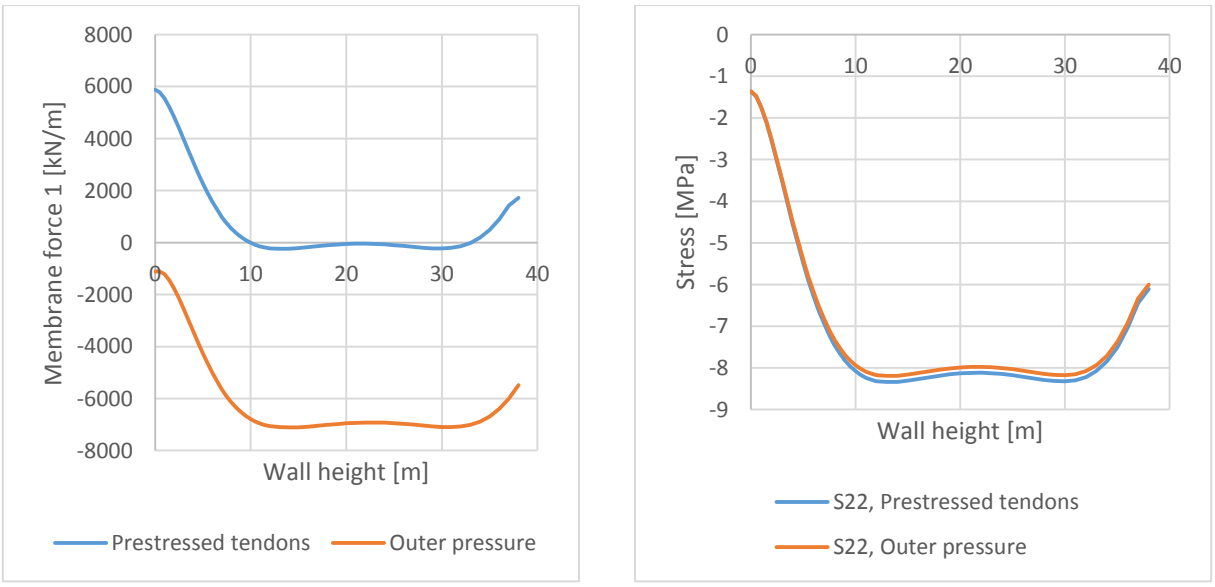

Figure 3-24: Shell section force N1 and concrete stresses

3.6 Verification of thermal load

The heat transfer was the foundation of the thermal loading in Abaqus, imported as a predefined field into a strength analysis. Reasonable tests were done in order to verify that the thermal load was assigned correctly, and that the FEM program provided the correct outputs.

A verification of the stresses at the concrete's surface and the rebar stresses at the clamped connection were done in order to verify the thermal stresses in Abaqus. The control was done at this location since no clamping constraints would interfere with the stresses, just the thermal expansion. Because of the clamped condition, the wall was not able to deform and the Poisson's ratio was therefore excluded from the calculation. Eq. 2-62 was used in order to calculate the expected stresses. See Appendix D for calculations.

Table 3-2: Concrete and rebar stresses from thermal load

Material and position	**Temperature load**	**Expected**	**Results from Abaqus**
Inner concrete surface	Load case 10	57.8 MPa	62.5 MPa
Outer concrete surface	Load case 10	-12.3 MPa	-17.7 MPa
Inner circumferential rebar	Load case 10	300.0 MPa	301.4 MPa
Outer circumferential rebar	Load case 10	-40.0 MPa	-34.5 MPa
Inner concrete surface	Load case 11	57.8 MPa	59.0 MPa
Outer concrete surface	Load case 11	-12.3 MPa	-14.7 MPa
Inner circumferential rebar	Load case 11	300.0 MPa	301.2 MPa
Outer circumferential rebar	Load case 11	-40.0 MPa	-35.8 MPa

An evaluation of the clamped moment and the flare moment was also done by use of Eq. 2-68 and Eq. 2-73. The wall was modelled as fixed at the wall/slab connection. No reinforcement was put in the wall to reduce stress concentrations, and simplify the concrete's stiffness.

Table 3-3: Clamped- and flare moment due to thermal load

Material and position	Temperature load	Expected	Results from Abaqus
Clamped moment at connection	Load case 10	3850 kNm/m	3647 kNm/m
Clamped moment at thermal unloading	Load case 10	-5692 kNm/m	-4684 kNm/m
Flare moment at edge of thermal load	Load case 11	3850 kNm/m	3759 kNm/m
Flare moment at edge of thermal load	Load case 11	-5692 kNm/m	-5576 kNm/m

The expected results, and the results from Abaqus does not match entirely, but are fairly close. The hand calculation does not consider the clamped constrains, and some difference was therefore expected for the flare moment. Load case 11 fits better than load case 10, which implies that the hand calculation would be better suited when the boundary effects are damped out.

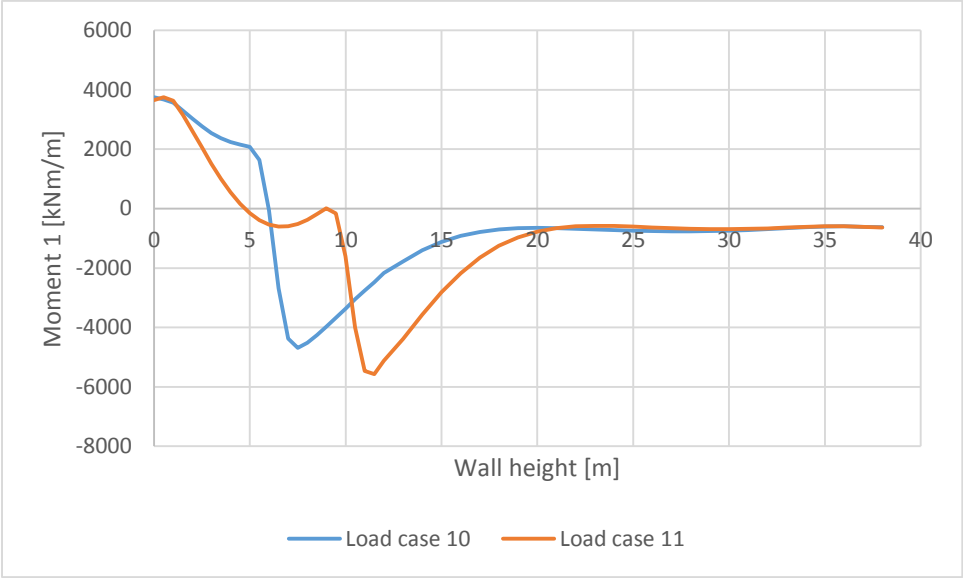

Figure 3-25: Thermal moments

A verification of the slab was also done, in order to certificate the correct faces for the thermal load. The wall was still fixed by a boundary condition, in order to prevent stresses from the clamped wall moment.

To determine the stresses at the concrete's surfaces, max principal stresses was used. For the reinforcement, which was modelled as wire elements, S11 was checked.

Table 3-4: Concrete and rebar stresses from thermal load

Material and position	**Temperature load**	**Expected**	**Results from Abaqus**
Inner concrete surface	Load case 10	57.8 MPa	63,8 MPa
Outer concrete surface	Load case 10	-7 MPa	-43,2MPa
Inner radial rebar	Load case 10	293.0 MPa	280.0 MPa
Outer radial rebar	Load case 10	3 MPa	0.7 MPa

Inner concrete surface	Load case 11	57.8 MPa	66,4 MPa
Outer concrete surface	Load case 11	-7 MPa	-38.8 MPa
Inner radial rebar	Load case 11	293.0 MPa	289.8 MPa
Outer radial rebar	Load case 11	3 MPa	10.8 MPa

The slab was prevented from vertical deformations. Some constraint stresses should therefor be expected. The hand calculation is rather close, but misses at the bottom surface. Still, the results verifies that the thermal loading has been modelled correctly in terms of temperature degree of freedom, so the model is promising for further analysis.

3.7 Elastic analysis

A complete model with all its properties was analysed in order to verify the load combinations, and consider whether the effects on the containment tank were realistic. Elastic materials properties was used for the concrete and the reinforcement, by supressing its non-linearity's.

The circumferential prestress was assigned as an outer pressure load, in order to have a similar basis for comparison between Abaqus and ShellDesign. The vertical prestress remained as an initial load, since a shell line load not was permitted as an edge load for each shell section.

The analysis had three steps, each simulated the expected loads in the assumed order

1. Prestress
2. Pressure
3. Thermal

Two different load combinations regarding different spill height was ran and analysed. The load cases refers to Table 1-2 and the load combinations are described in Table 3-5.

Table 3-5: Load combinations

Load combination 101	Load case 1	Load case 2	Load case8	Load case 9	Load case 10
Load combination 102	Load case 1	Load case 3	Load case 8	Load case 9	Load case 11

Overall deformation is shown for the end of each step in Figure 3-26. UT1 Pressure includes both the deformation for prestress and pressure loads, while UT1 Thermal consist of the deformation for prestress, pressure and thermal loads.

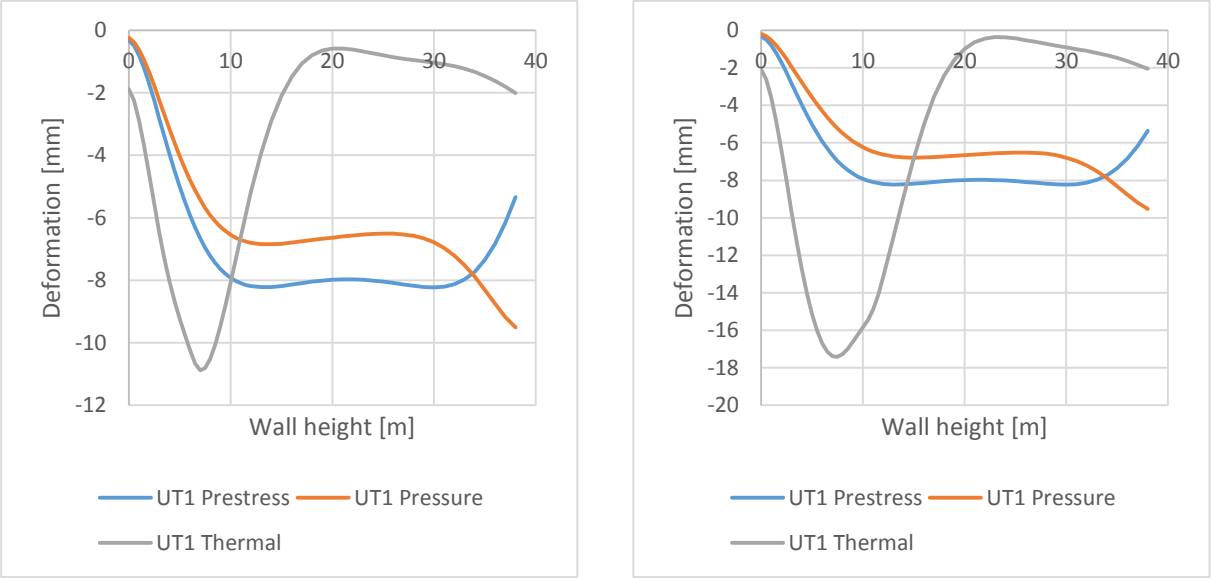

Figure 3-26: Radial deformation, load combination 101 and 102

The UT1 Prestress shows the radial deformation encouraged by the circumferential and vertical prestress. The deformation stabilizes around -8 mm when it is not constrained by the boundary conditions from the slab or the ring beam.

UT1 Pressure shows the deformation at the final increment for step two, including both the prestressing and the pressure deformation. The internal pressure works as intended, deflection the wall in the positive direction. The deformation increases close to the ring beam instead of decrease to zero. This is because the internal pressure load at the roof stretches the roof vertically and deform the ring beam radially.

UT1 Thermal deforms toward centre of the cylinder because of the shrinkage from the liquid spill. LC2 result in a larger radial deformation than LC1.

Figure 3-27 shows the final stresses for LC1 and LC2 through the wall by stresses in the thickness integration points. The integration points was defined in Figure 3-6, and the number increases from inside towards outside of the wall.

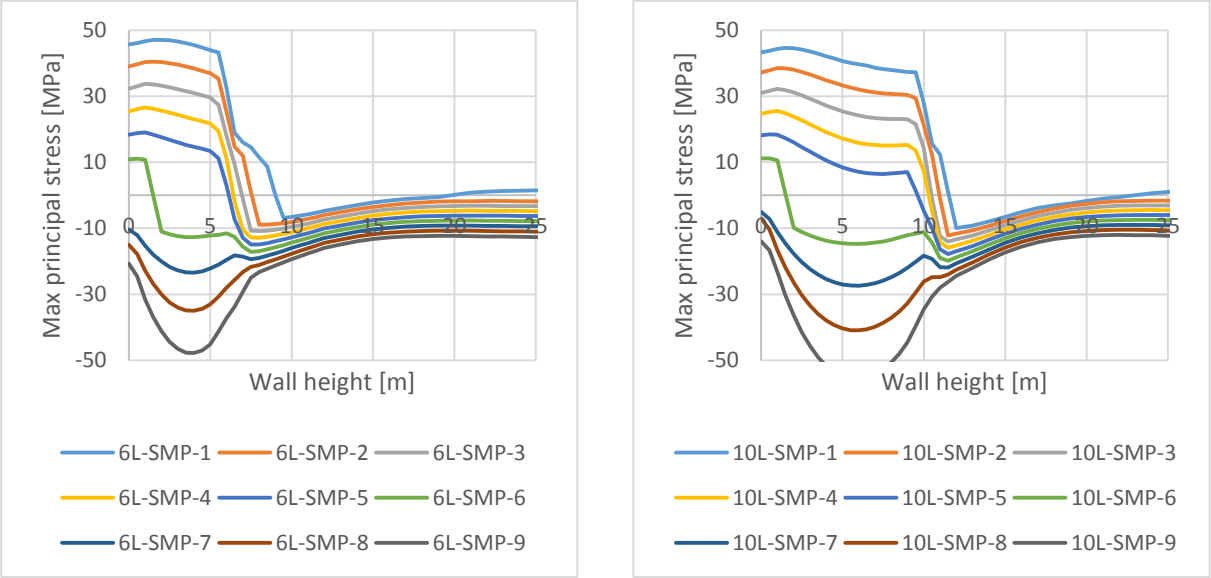

Figure 3-27: Max linear principal stress for wall, LC1 (L) and LC2 (R)

As can be seen of the elastic figures, a lot of tension stresses is obtained at the inner part of the wall. Compression can only be seen in thickness integration point 7 or higher, which is 600 mm from the inside of the wall. Tension stresses at about 50 MPa is impossible for concrete, and large cracks would have occurred if non-linear materials were used in the analysis.

It is also important to mention that the stresses in the thermal load area decline linearly trough the wall until thickness integration point 6. The drop is hard to explain, but apparently, is has nothing to do with the prestressing since the drop is identical for both models.

It should be noticed how the temperature variation in Figure 3-16 and Figure 3-17 dictate the tension and compression for the principal stresses. From the temperature variation figures, only two thickness integration points were heated and compressed, while three (and a half) thickness integration points are in compression for the max principal stresses. This indicates that the prestressing force has worked as intended. An increase of 8.75 MPa for the max principal stresses would reduce the thickness integration points in compression by one. This is in accordance with temperature variation.

Compression stresses at the inside of the wall would indicate inelastic compression strains in the concrete since 50 MPa is larger than the concrete's max elastic compression stress.

An overall presentation of the deformations, sectional forces and rebar stresses for the wall are compared with the non-linear results for both load cases in Appendix E and Appendix F.

The same scene was found for the slab. The tensile and compressive stresses are similar to the wall, with the same tension peak for the stresses. The compression force is lower for the slab, because the outside temperature was set to 20 °C (due to a heating system in the slab), instead of 35 °C for the wall.

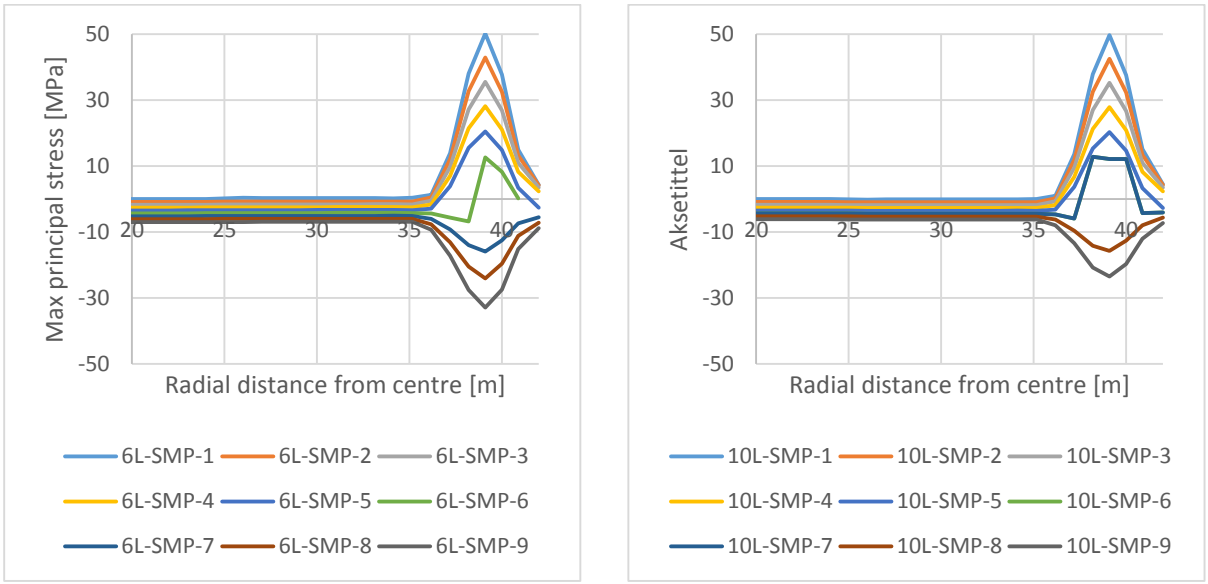

Figure 3-28: Max principal stress for slab, LC1(L) and LC2 (R)

3.8 Verification of non-linear analysis

The non-linear results show an expected change for the section forces and rebar stresses. The shell section forces have lower outcomes, and there is no longer any high tensile membrane forces or shear forces in the wall section. The section moments are also drastically reduced, which are expected since the concrete's tensile amendment has decreased.

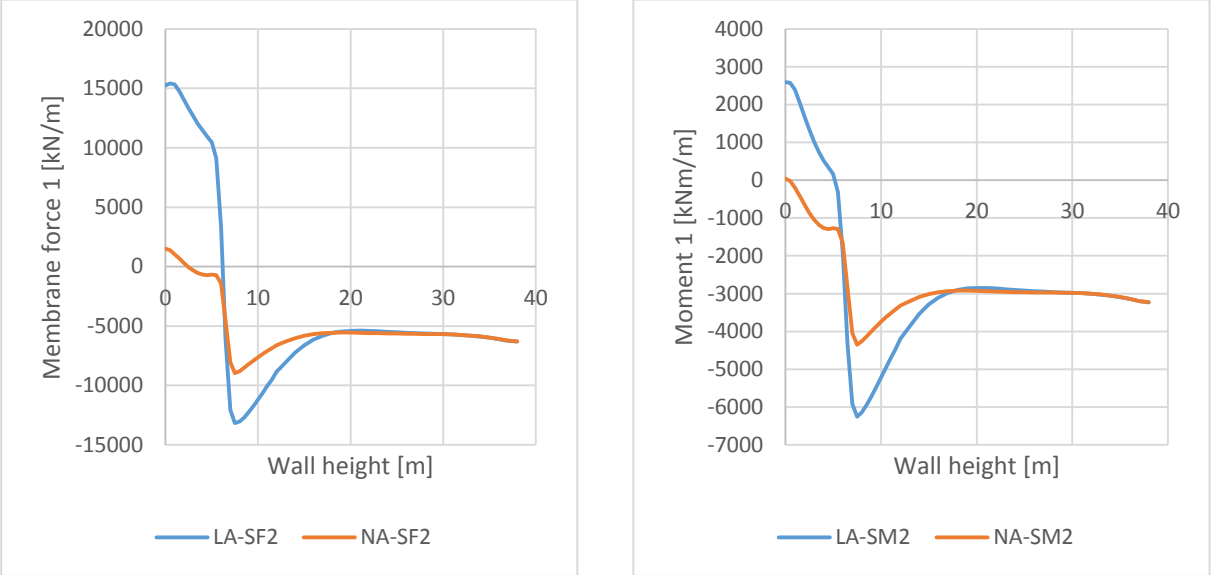

Figure 3-29: Linear/ non-linear comparison of membrane force 1 and moment 1, LC1

The rebar stresses were therefore expected to be higher than the linear ones, for both the stresses at the inside and outside of the wall section to compensate for the concrete's lower tensile stresses. The differences were rather small, considering the great difference in shell section forces. This is because the circumferential reinforcement is almost only dependent of the thermal expansion. In addition to the thermal expansion, the vertical reinforcement needs to prevent radial deformation, which explains why the tensile stresses for the vertical reinforcement has increased.

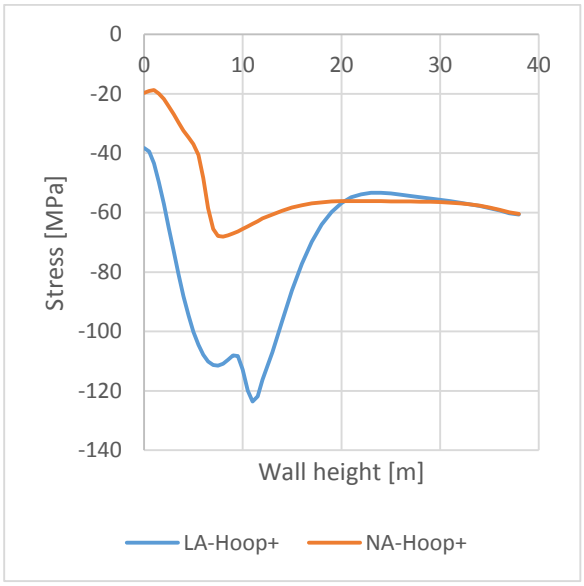

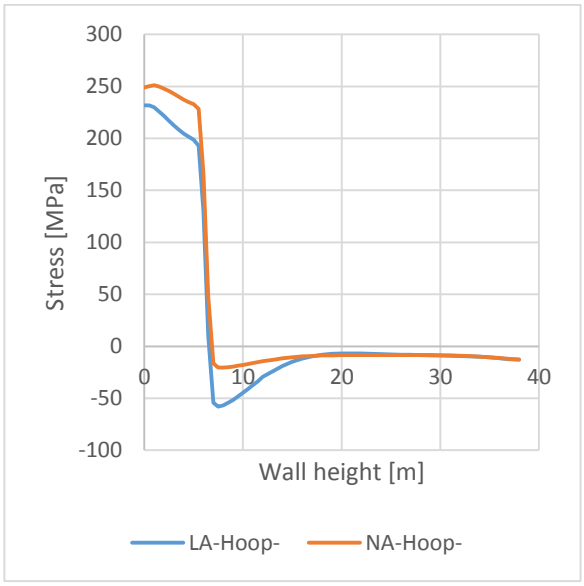

Figure 3-30: Linear/non-linear reinforcement stresses in circumferential direction, LC1

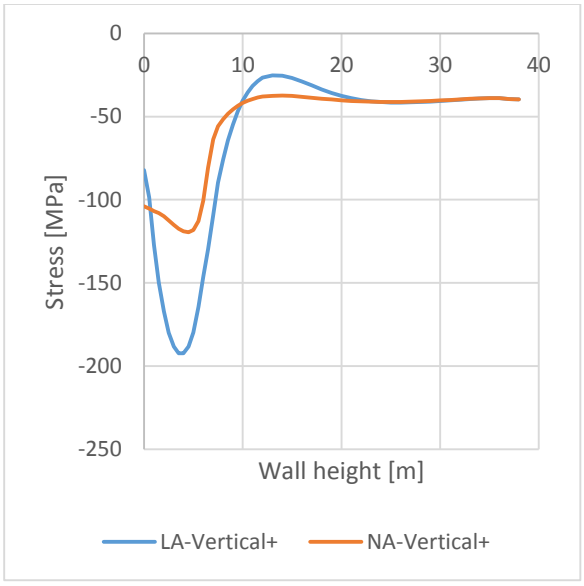

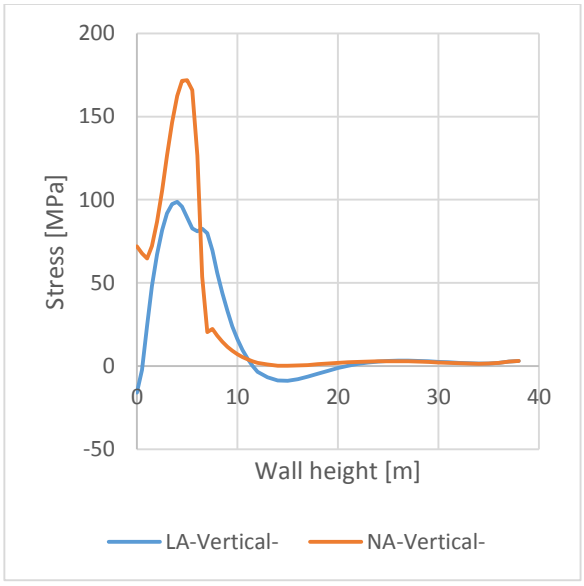

Figure 3-31: Linear/non-linear reinforcement stresses in circumferential direction, LC1

Both models have a positive radial deformation at the slab/wall connection. This is due to the pressure forces, pushing the wall outwards. The radial deformation has however decreased by more than the radial slab/wall deformation in the non-linear analysis. After the concrete has cracked, it has no longer ant needs to shrink radially as a structure. The reinforcement however is assumed to have the same temperature in the linear and non-linear analyses, and will therefore try to deform equally in both analysis.

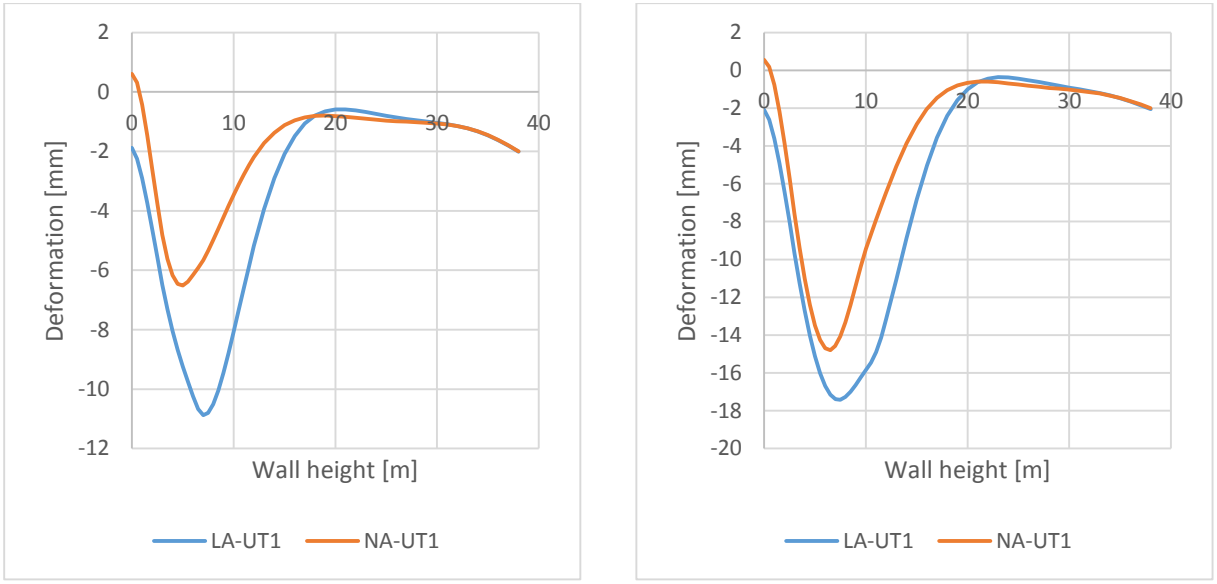

Figure 3-32: Linear/non-linear deformation plots

3.9 Non-linear results from Abaqus

The max principal stress was evaluated for both the concrete wall and the slab. Max principal stress determines the stress resultant in a thickness integration point. The direction of the stress may be in all directions, and are not limited by a coordinate system.

Furthermore, PEEQ and PEEQT were used to determine tensile plastic strain, in order to determine cracks depth and cracks width. PEEQ is denoted “Compressive equivalent plastic strain”, and PEEQT is denoted as “Tensile equivalent plastic strain” in Abaqus. Both plastic strains are determine on behalf of the max principal stresses.

The non-linear results for the wall show that the wall section will not fail for either load combination due to the minimum compression zone. Both load combinations have more than 200 mm in the compressive zone, which is more than the 100 mm required by the regulations. High compressional forces should however be noted at outside of the wall at the wall/slab connection.

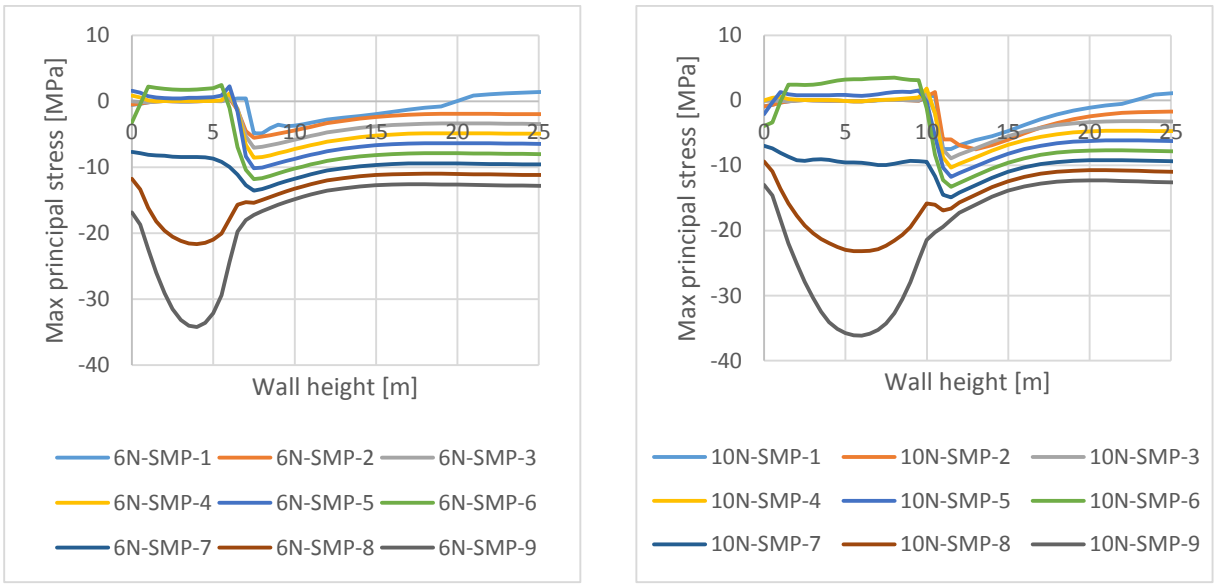

Figure 3-33: Max non-linear principal stresses for wall, LC1 (L) and LC2 (R)

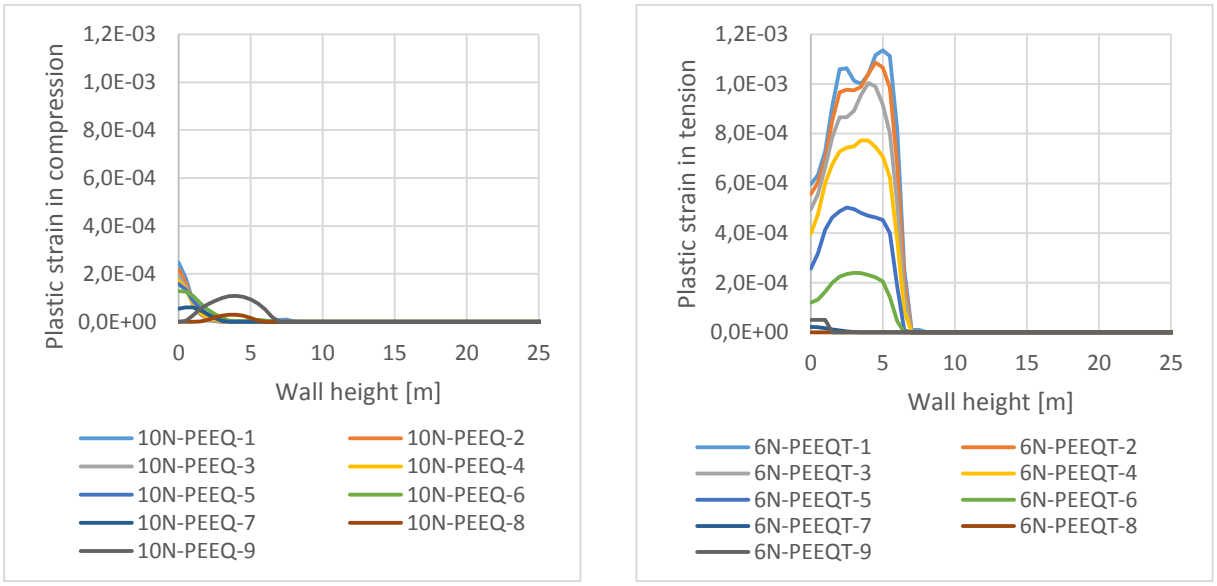

Figure 3-34: Plastic strain in uniaxial compression (L) and tension (R) for LC1

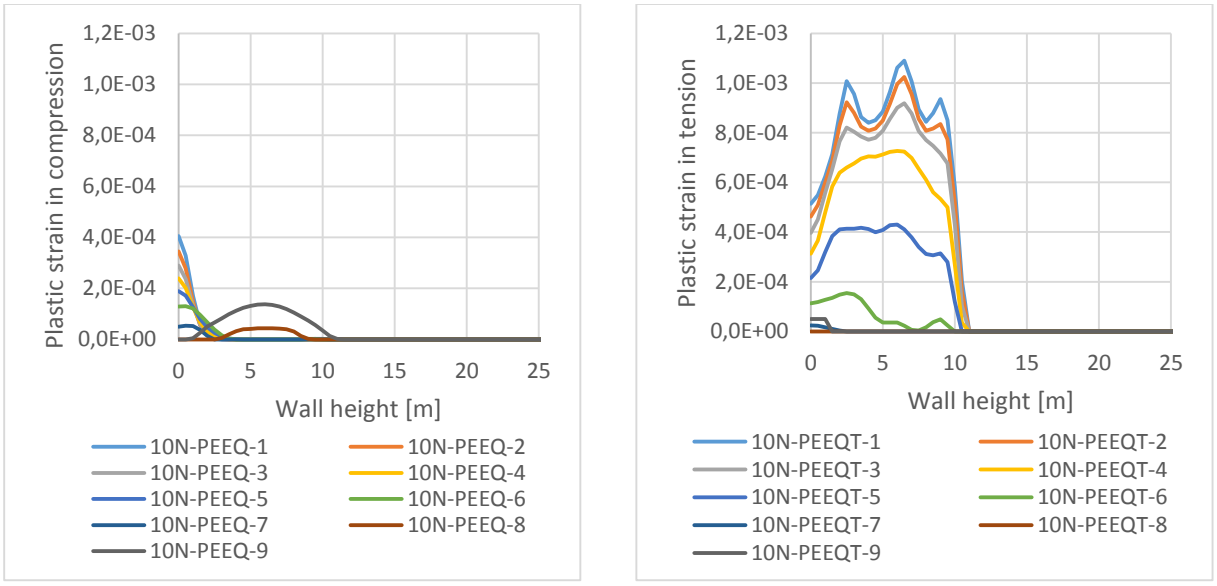

Figure 3-35: Plastic strain in uniaxial compression (L) and tension (R) for LC2

High plastic tensile strains at the inside of the wall will not fulfil the recommended limitation for crack widths, which was set to 0.5 mm. There is also a risk of through cracks, because of the plastic tensile strains at the outside of the wall. The tensile strains at the outside appear since the slab inhibits the rotation of the wall. Thickness integration point 8 has no tensile strains, which indicate that no through cracks will occur.

The non-linear results for the slab show a satisfactory compressive zone at 150 mm for the entire slab. The plastic tensile strains are on the other hand too large; the recommended crack width is exceeded by 0.5 mm (100 %). Plastic compression strains were examined for the slab, but no plastic strains were found through the section.

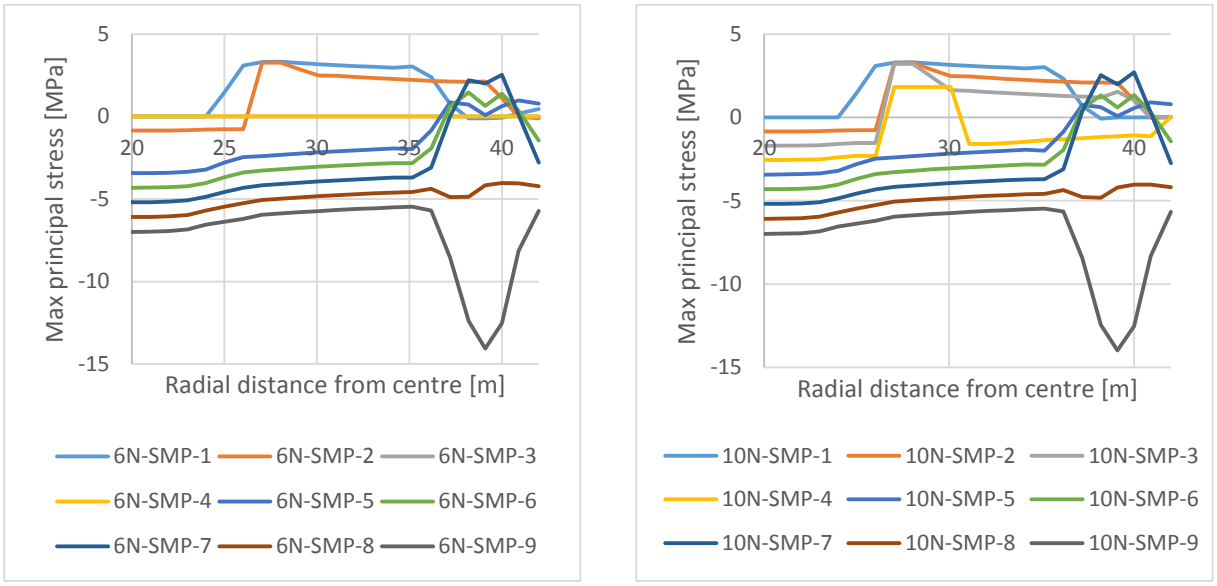

Figure 3-36: Max non-linear principal stresses for slab, LC1 (L) and LC2 (R)

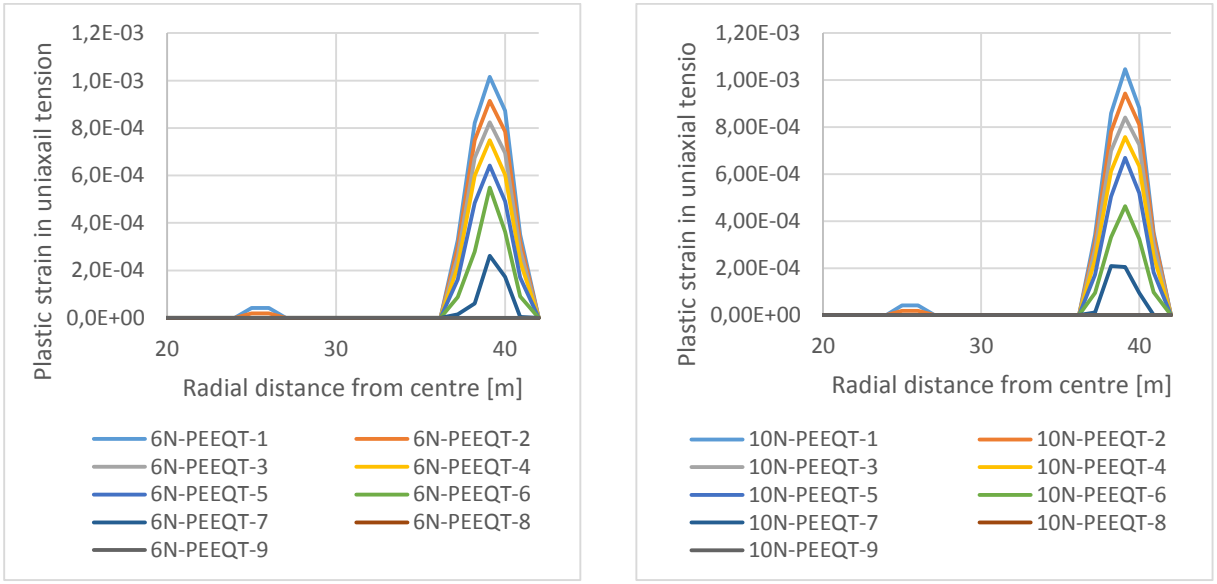

Figure 3-37: Plastic strain in uniaxial tension for slab, LC1 (L) and LC2 (R)

3.10 Conclusion

The outer containment tank exposed for the current load combinations will not fulfil the recommended maximum crack width. The suggested design criteria is not met. The results obtained in this study exceeds the recommended value about 100 %. The largest crack width was found in the wall section in the middle of the thermal load.

The minimum compressive zone criteria to ensure impermeability is fulfilled and the outer containment tank will withstand a major leak event, and serve as catch basin in case of failure of the inner tank.

The results are summarized briefly in Table 3-6.

Table 3-6: Abaqus requirements and results

Section	Suggested/required value	Load combination 1	Load combination 2
Compressive zone, wall	100 mm	200 mm	200 mm
Crack width, wall	0.5 mm	1.0 mm	1.1 mm
Compressive zone, slab	100 mm	150 mm	150 mm
Crack width, slab	0.5 mm	1.0 mm	1.0 mm

4 Sesam and ShellDesign

4.1 General description

Sesam is DNV GL's software for a complete strength assessment system for engineering of ships, offshore structures and risers based on the finite element methodology. Sesam includes a great variety of different programs, for instance Patran and Sestra. Patran is a modelling tool that creates an output file based on geometry, boundary conditions, mesh and load cases. The output file from Patran is a t1.fem file, which later on can be analysed in Sestra. Sestra is a general-purpose finite element program for linear analysis (13). The result file Sestra creates, the r1.sin file, may be analysed or used as the basic for a post processor program.

ShellDesign is a design tool and a post processor for reinforced concrete shell structures. It is used to perform code checks of reinforced concrete structures according to either NS3473 or EuroCode 2. The main tasks for ShellDesign are to combine load cases, perform code checks, run updated stiffness analyses with the "Consistent Stiffness Method" and provide data for documentation and verification (14).

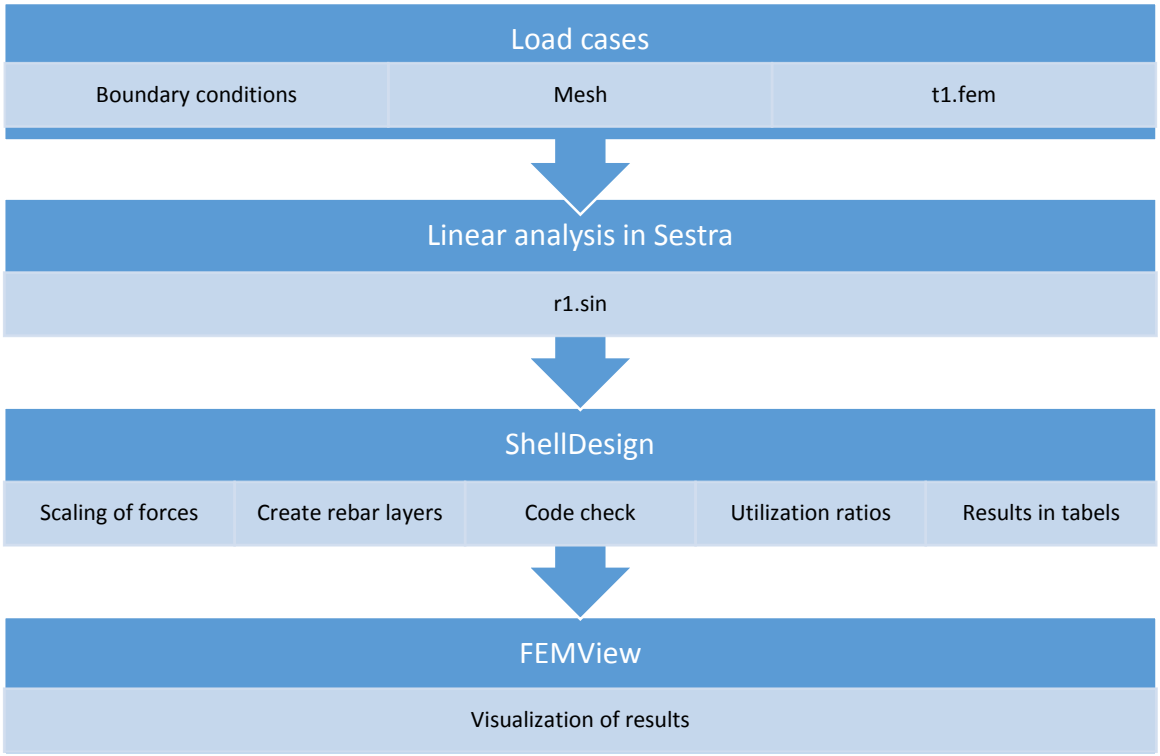

Figure 4-1: Sesam-ShellDesign eco system

4.2 ShellDesign

ShellDesign performs design checks using the iteration method, which calculates a non-linear section response for sections in a current structure. A section is defined in the user manual as "a line through the shell/membrane/plate structure". Sections can either be designed in ShellDesign or be made of existing Gauss-points from elements in a finite element program. The section have two faces, and the reinforcement is normally placed in accordance with the faces, in at least two directions. A section have eight section forces, which is normal by common shell theory. The shell section forces in Figure 4-2 is in accordance with the forces achieved in the latter analysis.

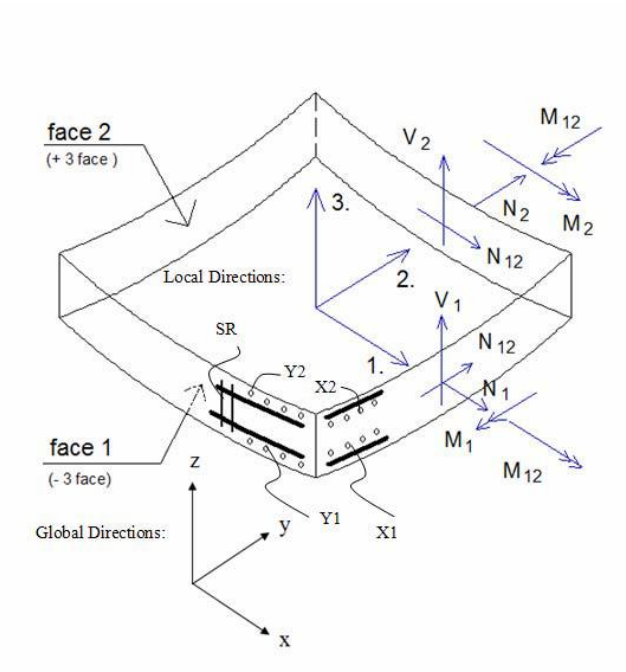

Figure 4-2: Section forces, faces and rebar definitions in ShellDesign (14).

The common way of using ShellDesign is to import linear analysis data from Sestra and perform non-linear section design with the iteration method based on linear elastic stress resultants. ShellDesign has the ability to scale load cases, combine load combinations, change coordinate systems and perform code checks based on results from the linear FEM analysis. The basis for the iteration method is to split a thin shell section into several layers and find the strain distribution from the stress resultants from a FEM analysis. However, there is an inconsistency between what is assumed in the structural analysis and the section design. By use of the iteration method, and ShellDesign's "Consistent Stiffness method", this can be solved.

The consistent stiffness method is a non-linear structural analysis performed with ShellDesign. The method ensures that the stiffness parameters used in the linear finite element model are consistent with the stiffness obtained in the cracked section analysis (14). The method was presented and described at the *fib* Symposium in PRAGUE 2011 (17).

Furthermore, this method is well described at page 21 in the Shell Design User Manual v1.7. "The method builds on an iterative linear-elastic procedure, in which the element stiffness matrix is progressively refined for the non-linear material response until a specified stiffness convergence criterion is satisfied. The stiffness parameters calculated in the sectional design is fed back to the finite element analysis, which is run several times until stiffness converges."

The finite element analysis will for this thesis be Sestra. This iteration procedure stated above is sketched in the same user manual, and gives a good understanding of the procedure. See Figure 4-3.

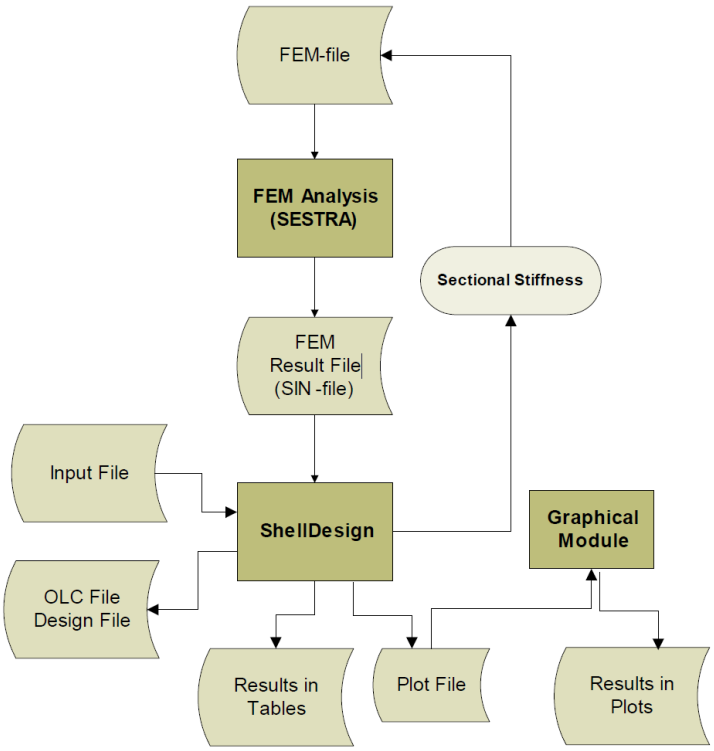

Figure 4-3: Design flow based on the consistent stiffness method (14).

Two graphical modules are available. Dr. tech. Olav Olsen has developed a 2D plot viewer in ShellDesign Manager. 3D presentations can be seen in FEMView, created by TNO Diana.

4.3 Loads

Identical geometry and material properties were used in the Patran model. However, the dimensions was defined in meter instead of millimetre and kilo Newton instead of Newton to fulfil ShellDesign's default units.

The load cases were split and defined one by one, so they later could be combined in ShellDesign. The prestressing tendons could not be defined in Patran, so the circumferential prestressing force was instead applied as an outer pressure load, calculated by Eq. 3-3. The vertical prestressing load was assigned as opposite line loads at the centre of the wall and the ring beam.

The area prestress pressure horizontal load $p_{ph}$was defined in Eq. 3-3. The prestress line load for the wall was calculated by use of the prestress area A_p, the prestress stress P_0, the circumference length O_w, and the distance between the tendons s_w.

$$p_{ph} = \frac{N_{ph}}{r_0} = -172\ kPa \qquad \textit{Eq. 3-3}$$

$$r_w = 40.4m, r_{rb} = 40.6m, A_p = 4200mm^2, s_w = 1.0\ m \qquad \textit{Eq. 4-1}$$

$$P_0 = -1 * 10^6 kPa$$

$$O_w = 2\,\pi\,r_w = 254\ m \qquad \textit{Eq. 4-2}$$

$$P_{lw} = A_p P_0 \frac{O_w}{s_w} = -1.07 * 10^6\ kN \qquad \textit{Eq. 4-3}$$

$$P_{lw} = \frac{P_w}{O_w} = -4200\,\frac{kN}{m} \qquad \textit{Eq. 4-4}$$

$$O_{rb} = 2\,\pi\,r_{rb} = 255\ m \qquad \textit{Eq. 4-5}$$

$$P_{rb} = A_p P_0 \frac{O_{rb}}{s_w} = -1.07 * 10^6\ kN \qquad \textit{Eq. 4-6}$$

$$P_{lrb} = \frac{P_{rb}}{O_{rb}} = -4221\,\frac{kN}{m} \qquad \textit{Eq. 4-7}$$

A minor change has also been done for load case 10 and load case 11. Due to the sharp temperature drop at the inside of the wall and the slab around the liquid spill, a large, unrealistic membrane force was the result from the linear analysis. This peak with the high utilization ratio entailed difficulties for the non-linear analysis, which was not able to start. The temperature loads were therefore modified to give a more smooth transition between the liquid spill and the inside air temperature. The thermal loads were therefore adjusted to drop linearly over 0.5 meter.

Table 4-1: Load cases modelled in Patran

Load case	Section	Location	Surface	Magnitude
1	Wall-Pressure	0.0 – 40.0	Internal Surface	29 kPa
2	Wall-Liquid-6	0.0 – 6.0	Internal Surface	5*(6-Z) kN/m^2
3	Wall-Liquid-10	0.0 – 10.0	Internal Surface	5*(10-Z) kN/m^2
4	Wall Prestress_H	0.0 – 38.0	Pressure load	-172 kPa
5	Wall Prestress_V	0.0 – 38.0	Line load, top/ bottom centre	4200 kN/m
6	Ring Beam Prestress_H	38.0 – 40.0	Pressure load	-174 kPa
7	Ring Beam Prestress_H	38.0 – 40.0	Line load, top/ bottom centre	42 kN/m
8	Roof-Gravity	Entire Section	Internal Surface	-10 kPa
9	Roof-Pressure	Entire Section	Internal Surface	29 kPa

10	Slab	0.0 – 37.4	Inside	0 °C
	Slab	37.4 – 38.2	Inside	0 °C → 165 °C
	Slab	38.2 – 40.0	Inside	-165 °C
	Slab	40.0 – 40.7	Inside	-165 °C → 0 °C
	Slab	40.7 – 42.0	Inside	0 °C
	Slab	0.0 – 42.0	Outside	35 °C
	Wall	0.0 – 6.0	Inside	-165 °C
	Wall	6.0 – 6.5	Inside	-165 °C → 0 °C
	Wall	6.5 – 40.0	Inside	0 °C
	Wall	0.0 – 40.0	Outside	35 °C
	Roof	Entire Section	Inside	0 °C
	Roof	Entire Section	Outside	35 °C
11	Slab	0.0 – 37.4	Inside	0 °C
	Slab	37.4 – 38.2	Inside	0 °C → 165 °C
	Slab	38.2 – 40.0	Inside	-165 °C
	Slab	40.0 – 40.7	Inside	-165 °C → 0 °C
	Slab	40.7 – 42.0	Inside	0 °C
	Slab	0.0 – 42.0	Outside	35 °C
	Wall	0.0 – 10.0	Inside	-165 °C
	Wall	10.0 – 10.5	Inside	-165 °C – 0 °C
	Wall	10.5 – 40.0	Inside	0 °C
	Wall	0.0 – 40.0	Outside	35 °C
	Roof	Entire Section	Inside	0 °C
	Roof	Entire Section	Outside	35 °C

4.4 ShellDesign linear analysis results

ShellDesign version 4.3.2 is the available software on the marked. V4.3.2 overrides the concrete tensile strength during the code check, and calculates the non-linear sectional response without the concrete tensile strength. The sectional response assumes a linear strain distribution over the thickness. This is a rather efficient and well-examined method. In this thesis, high tensile stresses was expected at the inside of the wall.

A development version of ShellDesign, version 4.3.2A7 is used in this thesis, which has been developed to also account for the concrete tensile strength in iteration procedure in the non-linear sectional response. This development version has been developed to include different coefficient parameters of thermal expansion for concrete and reinforcement to be able to calculate the correct response for concrete structures exposed to high temperature variations. Different temperature profiles can also be specified to give the distribution of the temperature through the section depth.

In addition, this version of ShellDesign differ from V4.3.2 by using the strains from the linear elastic analysis directly into the code check when the Consistent Stiffness method is carried out, instead of calculate shell section forces to be used in the iteration procedure to calculate the strain profile. This approach has from an experience point of view, provided better results for ultimate capacity calculations.

The elastic analyses for load combination 101 and 102 have good correlation with the Abaqus sectional forces, except for N1, M1 and M2. N2 differ from Abaqus' SF1 (shell force 1 – the coordinate system is defined differently) by 4200 kN/m, which is the initial compression from the prestressing tendons.

M1 is the moment about the wall's circumferential direction, and have a different form including an almost opposite starting value. All load cases in load combination 101 has been examine, and the only different load effect for M1 is load case 10. ShellDesign and Abaqus respond differently at the temperature load.

M2 is the moment about the radial direction. The differences for the clamped moment and the peak moment has been examined by looking at each load case separately. No major, nor minor load case was able to explain the difference, not even the initial condition for the vertical prestressing. The difference between Abaqus and ShellDesign may be related to an overall load combination effect.

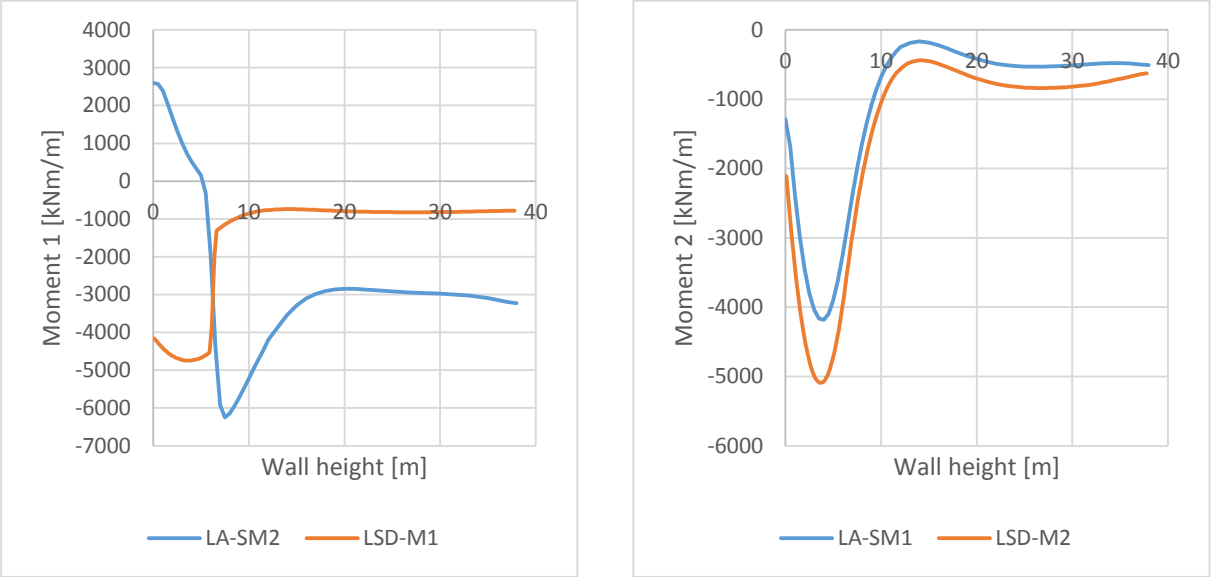

Figure 4-4: Moment 1 and moment 2 due to LC1

On the other hand, the rebar stresses differ a lot, with high utilization ratios with some scatter in the curvature. Especially at the inside of the wall, where the cryogenic load is present. No non-linear reinforcement properties was defined, even though LSD-Y12 stops at yielding stress.

LA-Hoop+ represents the rebar in the circumferential direction at the outer face, analysed linearly in Abaqus. LSD-X11 represents the rebar layer aligned from face 1 (the outer face), analysed linearly in ShellDesign. NA-vertical- means the vertical rebar layer at the inner face, analysed non-linearly in Abaqus. NSD-Y22 will then be the vertical rebar layer at the inner face, analysed non-linearly in ShellDesign.

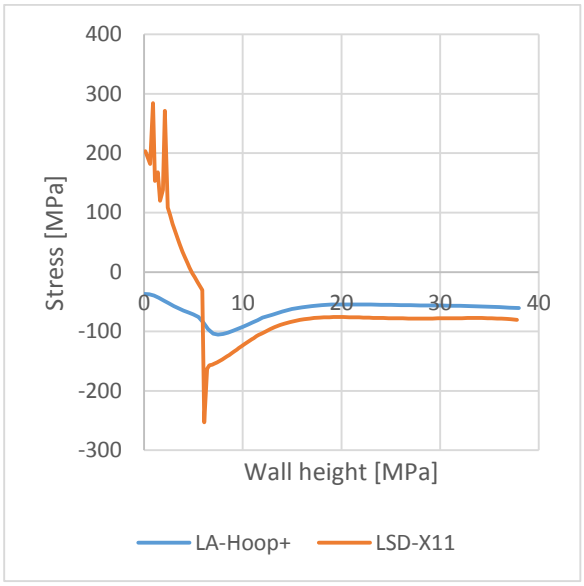

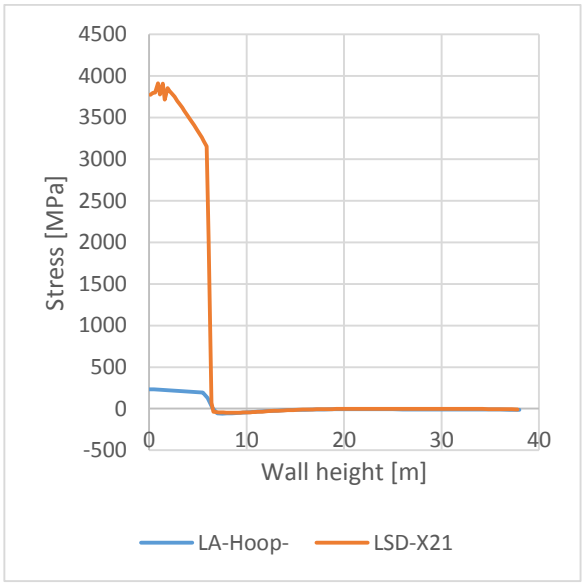

Figure 4-5: Linear analysis for rebar stresses in circumferential direction, LC1

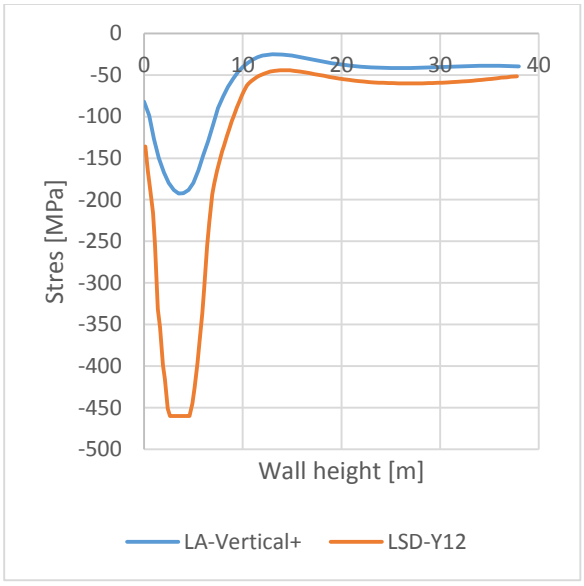

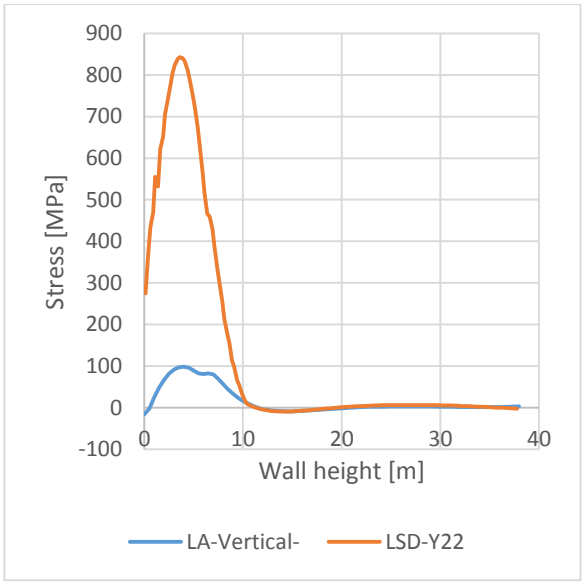

Figure 4-6: Linear analysis for rebar stresses in circumferential direction, LC1

A similar reinforcement analysis was done for the slab in order to investigate how the linear stresses are in a cut of the base slab. The same results were found in the slab as in the wall – high rebar stresses at the inside of the plate.

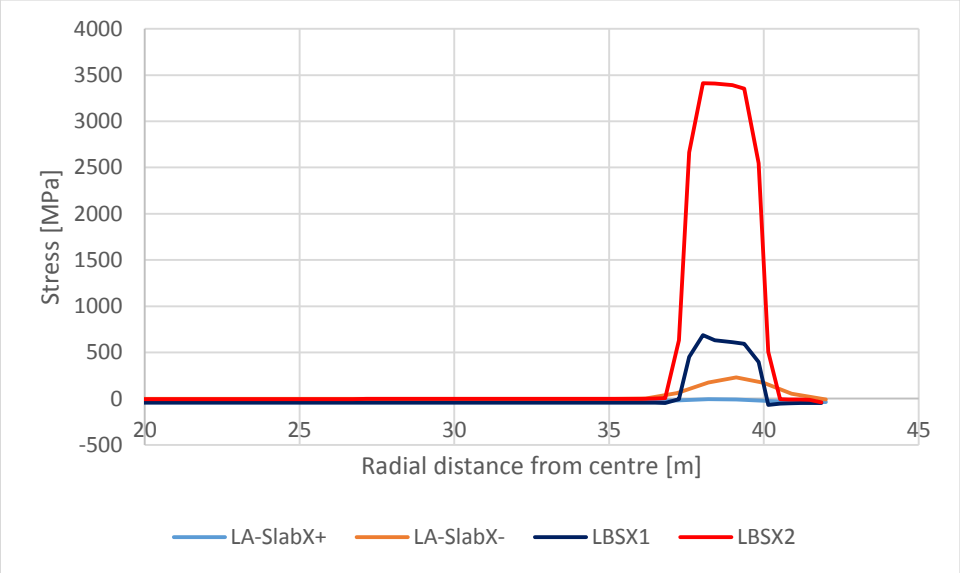

Figure 4-7: Comparison of linear rebar stresses for slab, LC1

4.5 ShellDesign non-linear analysis results

The non-linear analyses results provided much more expected section forces and accurate rebar stresses, compared to the Abaqus results. Redistribution of section forces occurred for all forces, resulting in less membrane forces and lower moments. This was expected, since the cracked concrete carry very small tensile forces, which result in less membrane forces and lower sectional moments. One exception is present, which is the thermal moment M1. ShellDesign is not able to determine a logical moment about the wall's circumferential direction.

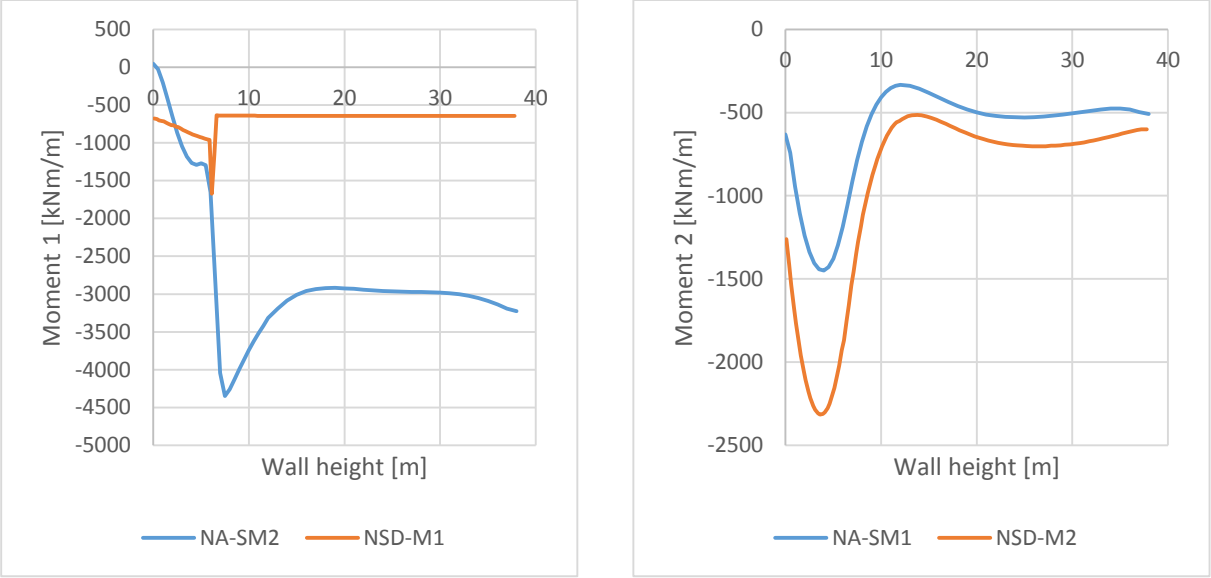

Figure 4-8: Non-linear section moments for LC1,, ftn=3 MPa

The rebar stresses were all comparable with the stresses achieved from Abaqus. In the compressive zone at the outside of the wall, the rebar stresses in the thermal area coincided, leaving some more compression in ShellDesign for the rest of the wall. In the tensile area, tensile stresses were higher in the thermal exposure area, but still similar curves, including a rather big scatter at the edge of the temperature load.

Higher rebar stresses at inside of the wall correspond well with the higher moment 2 (LSD-M2) from the section forces. Moment 2 must be in equilibrium from rebar tensile stresses from the inner side, and concrete and rebar compressive stresses from the outer side.

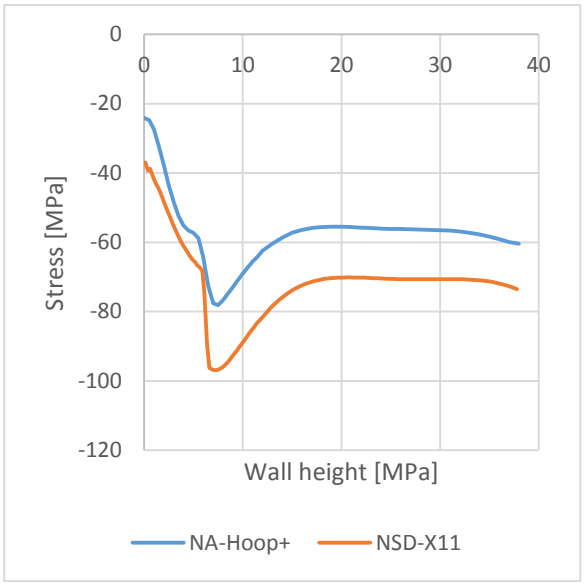

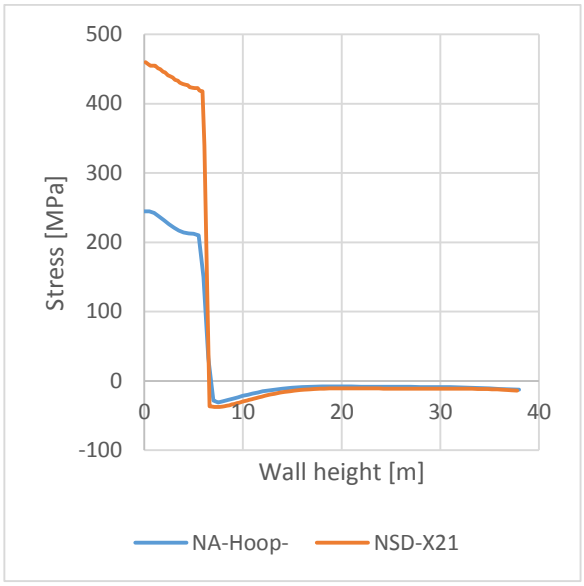

Figure 4-9: Non-linear rebar stresses in circumferential direction for LC1, ftn=3 MPa

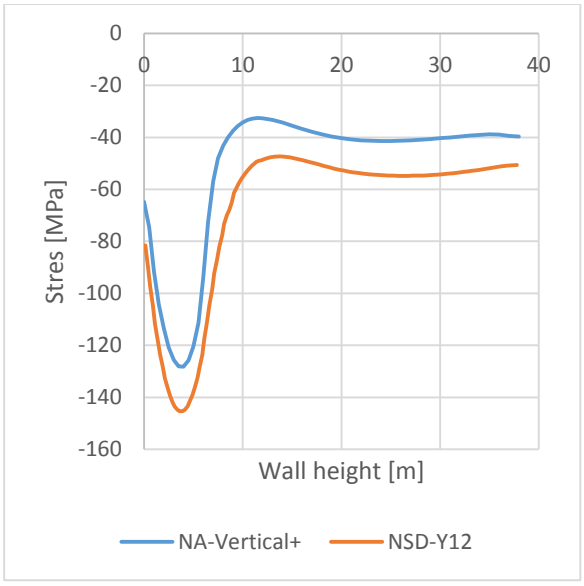

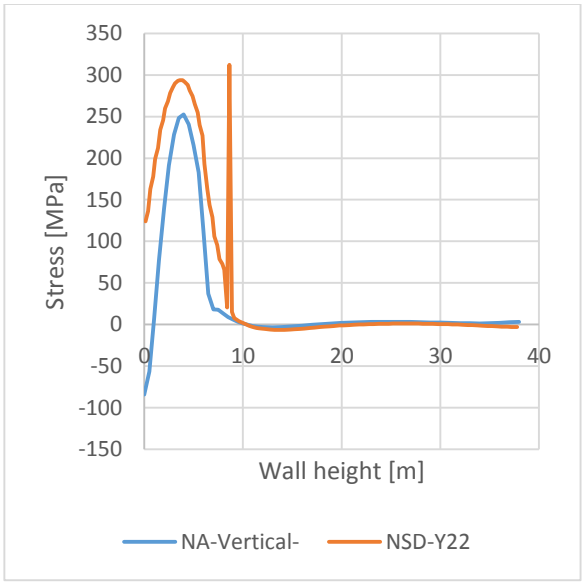

Figure 4-10: Non-linear rebar stresses in vertical direction for LC1, ftn=3 MPa

The non-linear rebar stresses for the slab also proved itself comparable with Abaqus results. Higher rebar stresses was achieved in the thermal exposure area, with a scatter for LC1 at the inner face.

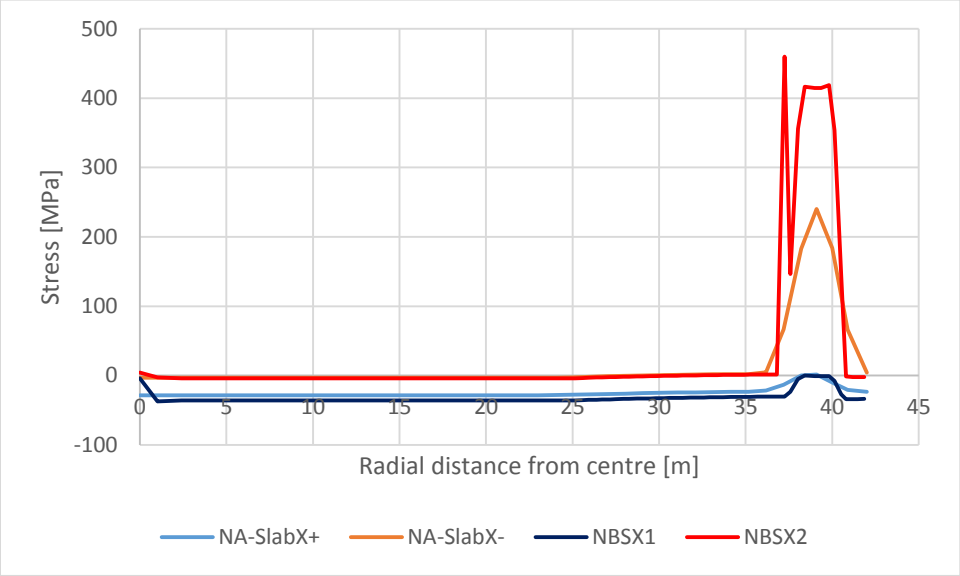

Figure 4-11: Comparison of non-linear rebar stresses for LC1

4.6 Discussion of results in ShellDesign

ShellDesign calculates the rebar stresses from section forces. For linear membrane force 1, N1 is 16463 kN/m, which require 0.035789 m^2/m reinforcement in the tensile area at yielding. From the input file, the reinforcement in the X21 direction is set to 0.003272 m^2/m, which is about a reinforcement ratio at 0.09 of what ShellDesign needs for equilibrium in the section. In this case, the rebar stresses should be 5011 MPa. The difference between 4022 MPa and 5011 MPa must therefore be captured by the prestressing tendons from the middle of the section, with a minor contribution from the concrete's tensile capacity. The prestressing tendons will be in the tensile part of the section. The high linear rebar stresses in ShellDesign can therefore be explained by the calculation method

Abaqus does not calculate the rebar stresses from the section forces, but directly from the thermal loading. The linear expected value at 300 MPa from load case 10, has decreased to about 230 MPa for load combination 101. The drop of stresses is believed to be caused by the other load cases.

Every test in ShellDesign was also done with another tensile property as well. Ftn, which regulates the max concrete tensile stress, was set to 0 in order to consider the effects without any concrete tensile stress capacity.

The shell section forces are primarily the same, with only very small differences. The peak values for the non-linear membrane force 1 with ftn = 3 MPa are overall higher, and some differences were found for the non-linear section forces.

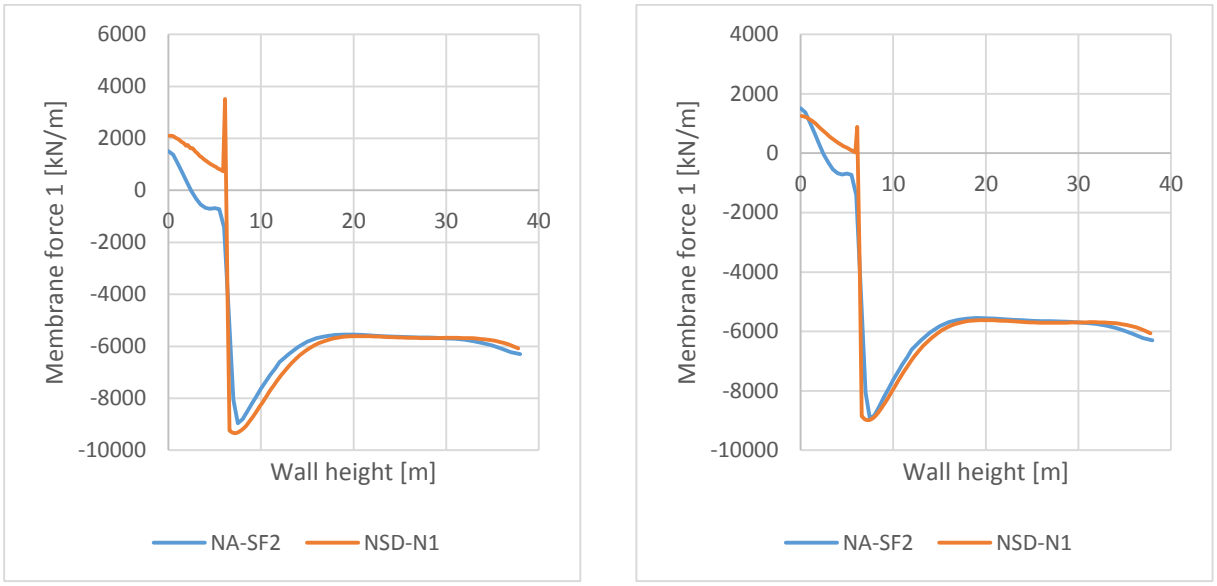

Figure 4-12: Peak values for membrane force 1, ftn = 3MPa and ftn = 0 MPa

For the reinforcement stresses, higher stresses were found in the models with 3 MPa as max tensile capacity. In these figures, scatter was also found.

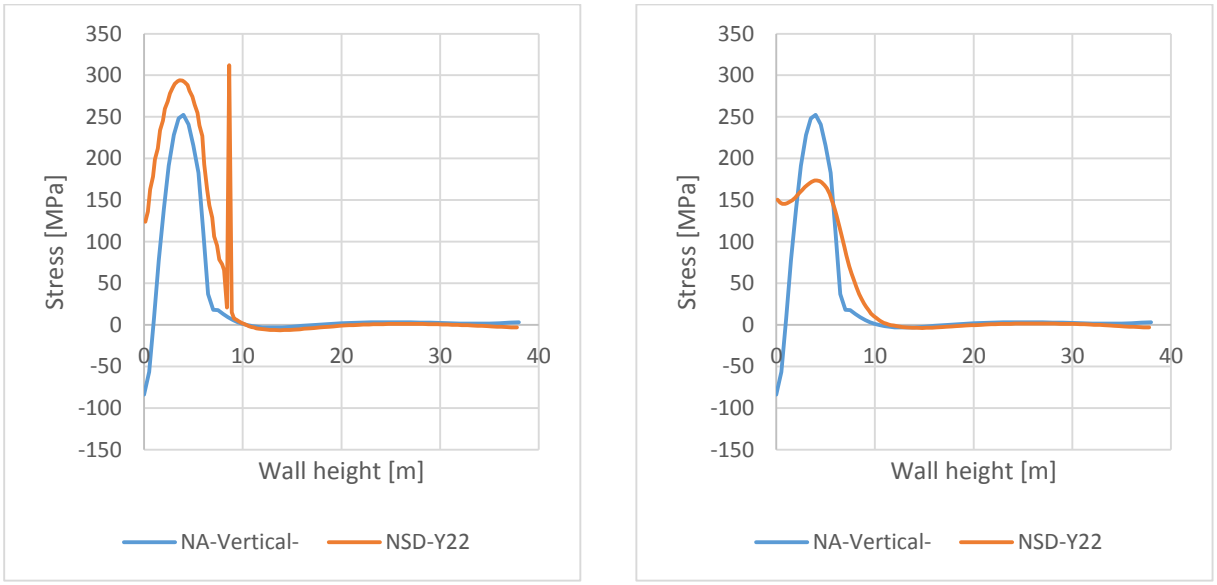

Figure 4-13: Non-linear reinforcement stress, FTN = 3 MPa and FTN = 0 MPa

The iteration process in ShellDesign may explain the scatter. Perfect bonding between the steel and reinforcement was assumed, and the steel stresses were calculated from the concrete element strain. When the concrete crack, a sudden change in the stiffness occurs which may cause a significant scattered results in the analytical model. A finer mesh may smooth out the scatter, and should be examine further analysis.

Overall, the Consistent Stiffness Method seems to work rather good by updating the stiffness, before re-run the analysis with new stiffness parameters. Section moment 1 is off, but the reinforcement stresses should be considered as solid, at least the analyses done with ftn = 0 MPa.

See Appendix G – Appendix P for the background data for all section forces and rebar stresses. The input analysis file is attached in Appendix Q.

It is impossible to determine whether the results from ShellDesign would fulfil the common requirements stated in chapter 1. No code check was done, no concrete stresses were evaluated but the reinforcement stresses look promising.

5 Comparison of Methodology

5.1 Analysis setup and software organization

Abaqus is an "all-in-one" performer, having all utilities built-in for non-linear concrete analysis. The whole operation is transparent, adjustment can be controlled prior analysis, and most features can be assigned by point and click. DNV GL's Sesam suit is on the other hand a huge package of different programs, fitting together by exporting files in an eco-system. ShellDesign is a post processor program, re-analysing the linear results from Sestra. This analysis path hardened transparency and adjustments, and is dependent of users with great knowledge in all programs.

5.2 Creation of models and running the analysis

Performing a correct analysis in Abaqus demand expertise in the program and general insight in finite element methodology. The great number of different inputs and options require an available and well-explained user manual, which Abaqus provide. Abaqus got tutorials, examples, programming manuals and an extensive theory manual. The prestressing ability was also appreciated, which entail bonding properties for the tendons. One feature was however missed in Abaqus: the possibility to assign a different thermal expansion coefficient for the reinforcement.

I personally did not create the Patran model, nor run the Sestra analysis. Learning different programs are time consuming, and errors are often done in complex analysis. I was told that Patran and Sestra should be quite straight forward, but I decided to focus on ShellDesign. ShellDesign is limited for concrete structures, and therefore got less input variables in the program. The input variables are well explained in the brief user manual, and some tutorials are provided. Fault messages however, are difficult to understand due to the limited or no-existing reported error.

The process with Patran/Sestra/ShellDesign and FEMView require at least one input/output file each, which expand the uncertainties and enlarges the verification operation. For instance, before the linear temperature variation was modelled in Patran, non-linear analysis was not

possible in ShellDesign. No error was created, the ShellDesign analysis just would not start. In an eco-system as this, troubleshooting is hard and time consuming.

5.3 Analysis post processing

Abaqus is a good visualization tool, with extensive opportunities for plotting. The thickness integration points in the shell sections should be considered as a gold mine, providing convincing results. No visualization through the sections is available, nor code check or the ability of calculation of minimum reinforcement. Exporting curves to Excel is cumbersome, but the opportunities with the thickness integration points outweigh the restrictions. Abaqus also provide results through the analysis, which is helpful troubleshooting errors.

ShellDesign provides section tables and reinforcement stresses well arranged in a text file. A code check can also be performed, including utilization ratios and crack widths. FEMView is a proper utilization tool for view 3D results from ShellDesign.

The total CPU time for the non-linear load combination 102 in Abaqus was 17682 seconds. Two CPUs were used for the analysis, which means that clock time was 9431 seconds (2 hours and 37 minutes). During this analysis, the limitary factor should be the CPU since there was available ram at all times. An integrated flash drive was used was used for storage.

The non-linear ShellDesign analyses were ran at DNV GL Concrete Structure's main analysis computer. This computer, designed for calculations used just less than 30 minutes.

It is rather difficult, if not impossible to determine the faster analysis process, but I believe that both analysis were solved rather fast, considering the great amount of elements and non-linearity involved.

6 Further Work

In general, this study has resolved many questions due to non-linear material properties and design requirements. The most important parameter is however the thermal load, defining the shrinkage of concrete and the reinforcement. A small variation in the initial temperature would change the outcome in the matter of residual compression zone.

A verification of reinforcement properties due to cryogenic conditions would also be interesting, especially since thermal expansion coefficient for reinforcement is known to be 6E-6 K^{-1} instead of 1E-5 K^{-1} for temperatures lower than -10 °C. The lower thermal expansion coefficient for the reinforcement would potentially reduce the strain by almost 40 % in the cracked area.

A major investigation in Abaqus Analysis User's Manual was done in order to make the reinforcement's thermal expansion coefficients dependent for another value than defined in the concrete's properties. No solution was found for this feature, but it is expected to be resolved in a future version.

The development version of ShellDesign has the opportunity to define a separate thermal expansion coefficient for the reinforcement, but some uncertainties must be solved prior usage of this feature.

The thermal connection between Sestra and ShellDesign must be verified and the moment about the circumferential direction should be controlled. For the analyses with concrete tensile capacity, a finer mesh around the temperature-exposed areas should be considered in order to resolve the scatter in the reinforcement.

7 Bibliography

1. Baumann T, Roetzer J. Outer Concrete Containments of LNG-Tanks - Design against Thermal Shock. Munich:; 2013.

2. Poologasingam N, Tatematsu H, Takuwa D, Duque A. Analysis and Design for Spill Condition of Liquefied. ACI STRUCTURAL JOURNAL. 2008 March: p. 189-195.

3. Standard Norway. NS-EN 1992-1-1:2004+NA:2008. Standard. ; 2004.

4. Sørensen SI. Aksesymmetriske skall, del 2. In.; 1999.

5. Cook RD, Young WC. Advanced Mechanics of Materials: Pearson Education; 1999.

6. Dassult Systémes. Simula Finite Element Analysis. [Online].; 2014. Available from: http://www.3ds.com/products-services/simulia/portfolio/abaqus/abaqus-portfolio/.

7. Cook RD, Malkus DS, Plesha ME, Witt JR. Concepts and Applicatios of Finite Element Analysis. John iley & Sons ed.; 2002.

8. Dassult Systémes. 29.6.5 Using a shell section integrated during the analysis to define the section behaviour. [Online].; 2012. Available from: http://abaqus.me.chalmers.se/v6.12/books/usb/default.htm.

9. Dassult Systémes. 16.1.2: Sequentially coupled thermal-stress analysis. [Online].; 2012. Available from: http://abaqus.me.chalmers.se/v6.12/books/usb/default.htm.

10. Dassult Systémes. 6.5.2 Uncoupled heat transfer analysis. [Online]. Available from: http://abaqus.me.chalmers.se/v6.12/books/usb/default.htm?startat=pt03ch06s05at18.html.

11. Dassult Systémes. 6.3.2 Implicit dynamic analysis using direct integration. [Online]. Available from: http://abaqus.me.chalmers.se/v6.12/books/usb/default.htm.

12. Systémes D. 2.2.3 Defining Reinforcement. [Online].; 2012. Available from: http://abaqus.me.chalmers.se/v6.12/books/usb/default.htm.

13. Dassult Systémes. 2.2.5 Orientations. [Online]. Available from: http://abaqus.me.chalmers.se/v6.12/books/usb/default.htm.

14. Systémes D. 33.6.1 Predefined fields. [Online]. Available from: http://abaqus.me.chalmers.se/v6.12/books/usb/default.htm.

15. DNV GL. DNV GL software. [Online]. Available from: http://www.dnv.com/services/software/products/sesam/sesam_genie/sestra.asp.

16. Olsen DtO. ShellDesign User Manual v1.7 Oslo: Dr. techn. Olav Olsen; 2013.

17. Due IKH, Godejord SA, Weider O. A new and practical method for non-linear design of concrete structures - the consistent stiffness method: fib. Symposium; 2011.

18. Dassult Systémes. 33.6.1 Predefined fields. [Online].; 2012. Available from: http://abaqus.me.chalmers.se/v6.12/books/usb/default.htm.

19. Dassult Systémes. 29.6.5 Using a shell section integrated during the analysis to define the section behavior. [Online].; 2012. Available from: http://abaqus.me.chalmers.se/v6.12/books/usb/default.htm.

20. Ugural AC. Stresses in Beams, Plates and Shells. Third Edition ed.: CRC Press.

21. Dassult Systémes. 2.2.5 Orientations. [Online].: SIMULIA; 2012.

8 Appendix

Appendix A: Non-linear concrete properties

Appendix B: Universal pressure

Appendix C: Hydrostatic pressure load 38 m

Appendix D: Thermal load

Appendix E: Comparison linear-non-linear LC101

Appendix F: Comparison linear-non-linear LC102

Appendix G: Comparison linear shell forces for LC101, ftn = 3 MPa

Appendix H: Comparison linear shell forces for LC102, ftn = 3 MPa

Appendix I: Comparison non-linear shell forces for LC101, ftn = 3 MPa

Appendix J: Comparison non-linear shell forces for LC102, ftn = 3 MPa

Appendix K: Comparison linear shell forces for LC101, ftn = 0

Appendix L: Comparison linear shell forces for LC102, ftn = 0

Appendix M: Comparison non-linear shell forces for LC101, ftn = 0

Appendix N: Comparison non-linear shell forces for LC102, ftn = 0

Appendix N: Comparison of reinforcement for slab, ftn = 3 MPa

Appendix O: Comparison of reinforcement for slab, ftn = 0 MPa

Appendix P: ShellDesign input analysis file

8.1 Appendix A: Non-linear concrete properties

Compression (MPa)	Inelastic Strain	Elastic Strain	Total strain		Compression (MPa)	Inelastic Strain	Elastic Strain	Total strain
0.00	0.0E+00	0.0E+00	0.0E+00		44.10	7.0E-04	4.7E-04	2.0E-03
15.63	0.0E+00	4.7E-04	4.7E-04		44.39	7.4E-04	4.7E-04	2.0E-03
17.19	3.7E-05	4.7E-04	5.2E-04		44.62	7.9E-04	4.7E-04	2.1E-03
18.71	4.6E-05	4.7E-04	5.7E-04		44.79	8.4E-04	4.7E-04	2.1E-03
20.20	5.5E-05	4.7E-04	6.3E-04		44.92	8.9E-04	4.7E-04	2.2E-03
21.64	6.5E-05	4.7E-04	6.8E-04		44.99	9.4E-04	4.7E-04	2.2E-03
23.05	7.6E-05	4.7E-04	7.3E-04		45.00	9.9E-04	4.7E-04	2.3E-03
24.42	8.8E-05	4.7E-04	7.8E-04		44.95	1.1E-03	4.7E-04	2.3E-03
25.76	1.0E-04	4.7E-04	8.3E-04		44.85	1.1E-03	4.7E-04	2.4E-03
27.05	1.1E-04	4.7E-04	8.9E-04		44.69	1.2E-03	4.7E-04	2.4E-03
28.30	1.3E-04	4.7E-04	9.4E-04		44.48	1.2E-03	4.7E-04	2.5E-03
29.51	1.5E-04	4.7E-04	9.9E-04		44.20	1.3E-03	4.7E-04	2.6E-03
30.68	1.6E-04	4.7E-04	1.0E-03		43.86	1.4E-03	4.7E-04	2.6E-03
31.81	1.8E-04	4.7E-04	1.1E-03		43.46	1.4E-03	4.7E-04	2.7E-03
32.90	2.0E-04	4.7E-04	1.1E-03		43.00	1.5E-03	4.7E-04	2.7E-03
33.94	2.2E-04	4.7E-04	1.2E-03		42.47	1.6E-03	4.7E-04	2.8E-03
34.94	2.4E-04	4.7E-04	1.3E-03		41.88	1.7E-03	4.7E-04	2.8E-03
35.90	2.7E-04	4.7E-04	1.3E-03		41.23	1.8E-03	4.7E-04	2.9E-03
36.81	2.9E-04	4.7E-04	1.4E-03		40.51	1.9E-03	4.7E-04	2.9E-03
37.68	3.2E-04	4.7E-04	1.4E-03		39.73	1.9E-03	4.7E-04	3.0E-03
38.50	3.4E-04	4.7E-04	1.5E-03		38.87	2.0E-03	4.7E-04	3.0E-03
39.28	3.7E-04	4.7E-04	1.5E-03		37.95	2.1E-03	4.7E-04	3.1E-03
40.01	4.0E-04	4.7E-04	1.6E-03		36.96	2.2E-03	4.7E-04	3.1E-03
40.69	4.3E-04	4.7E-04	1.6E-03		35.89	2.3E-03	4.7E-04	3.2E-03
41.32	4.6E-04	4.7E-04	1.7E-03		34.76	2.5E-03	4.7E-04	3.2E-03
41.91	5.0E-04	4.7E-04	1.7E-03		33.55	2.6E-03	4.7E-04	3.3E-03
42.45	5.3E-04	4.7E-04	1.8E-03		32.27	2.7E-03	4.7E-04	3.3E-03
42.94	5.7E-04	4.7E-04	1.8E-03		30.92	2.8E-03	4.7E-04	3.4E-03

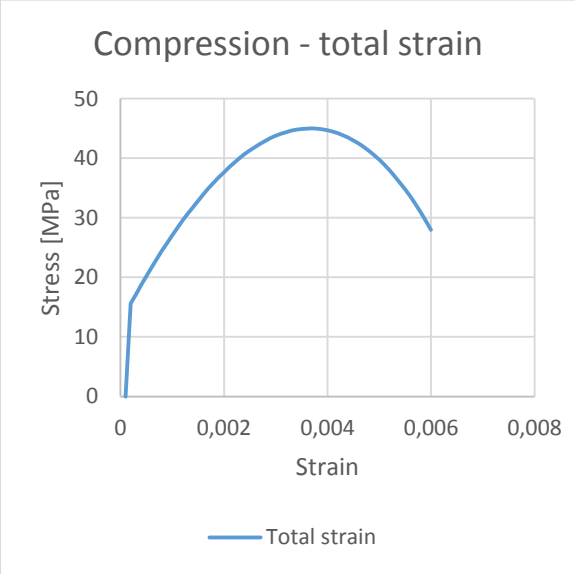

Tension (MPa)	Cracking Strain	Elastic Strain	Total strain
0.00	0.0E+00	0.0E+00	0.0E+00
3.57	0.0E+00	4.7E-04	1.0E-04
3.34	2.7E-05	4.7E-04	1.2E-04
3.12	5.5E-05	4.7E-04	1.4E-04
2.90	8.1E-05	4.7E-04	1.7E-04
2.69	1.1E-04	4.7E-04	1.9E-04
2.49	1.3E-04	4.7E-04	2.1E-04
2.30	1.6E-04	4.7E-04	2.3E-04
2.11	1.9E-04	4.7E-04	2.5E-04
1.94	2.1E-04	4.7E-04	2.7E-04
1.77	2.4E-04	4.7E-04	2.9E-04
1.61	2.6E-04	4.7E-04	3.1E-04
1.45	2.9E-04	4.7E-04	3.3E-04
1.31	3.1E-04	4.7E-04	3.5E-04
1.17	3.4E-04	4.7E-04	3.7E-04
1.04	3.6E-04	4.7E-04	3.9E-04
0.92	3.9E-04	4.7E-04	4.1E-04
0.81	4.1E-04	4.7E-04	4.3E-04
0.70	4.3E-04	4.7E-04	4.5E-04
0.60	4.6E-04	4.7E-04	4.8E-04
0.51	4.8E-04	4.7E-04	5.0E-04
0.43	5.0E-04	4.7E-04	5.2E-04
0.35	5.3E-04	4.7E-04	5.4E-04
0.29	5.5E-04	4.7E-04	5.6E-04
0.23	5.7E-04	4.7E-04	5.8E-04
0.18	5.9E-04	4.7E-04	6.0E-04
0.13	6.2E-04	4.7E-04	6.2E-04
0.10	6.4E-04	4.7E-04	6.4E-04
0.07	6.6E-04	4.7E-04	6.6E-04
0.05	6.8E-04	4.7E-04	6.8E-04
0.04	7.0E-04	4.7E-04	7.0E-04

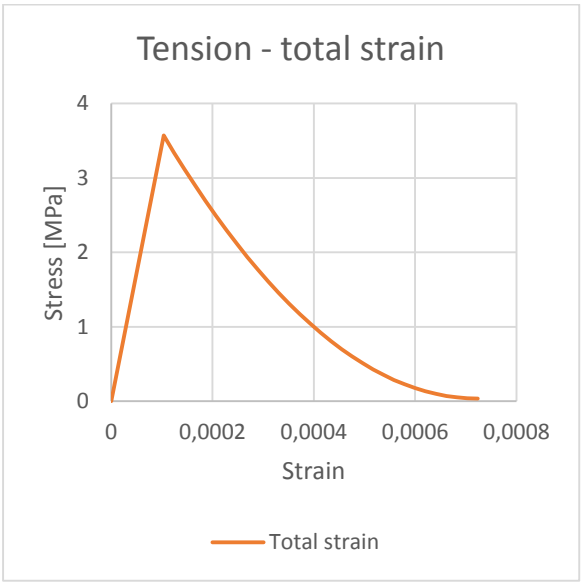

8.2 Appendix B: Universal pressure

$g_1(\xi) := e^{-\xi} \cdot \cos(\xi)$

$g_2(\xi) := e^{-\xi} \cdot \sin(\xi)$

$g_3(\xi) := g_1(\xi) + g_2(\xi)$

$g_4(\xi) := g_1(\xi) - g_2(\xi)$

$L_e := \frac{\sqrt{h \cdot r}}{\sqrt[4]{3 \cdot (1 - \upsilon^2)}} = 4.342\,m$

$h := 0.8m$

$r := 40m$

$E := 35000 \frac{N}{mm^2}$

$D := \frac{E \cdot h^3}{12 \cdot (1 - \upsilon^2)} = 1.556 \times 10^6 \cdot kN \cdot m$

$H := 10m$

$\upsilon := 0.2$

$p := 0.029MPa$

Constants

$M_0 := \frac{p \cdot L_e^2}{2} = 273 \cdot kN \cdot m \cdot \frac{1}{m}$

$V_0 := -p \cdot L_e = -126 \cdot kN \cdot \frac{1}{m}$

$\xi := 0, 0.114 .. 6$

Plotting deflections

$$w_{tot}(\xi) := \frac{p \cdot r^2}{E \cdot h} + \left(g_4(\xi) \cdot M_0 + g_1(\xi) \cdot V_0 \cdot L_e\right) \cdot \frac{L_e^2}{2 \cdot D}$$

$$w_h(\xi) := \left(g_4(\xi) \cdot M_0 + g_1(\xi) \cdot V_0 \cdot L_e\right) \cdot \frac{L_e^2}{2 \cdot D}$$

$$w_p := \frac{p \cdot r^2}{E \cdot h} = 1.7 \cdot mm$$

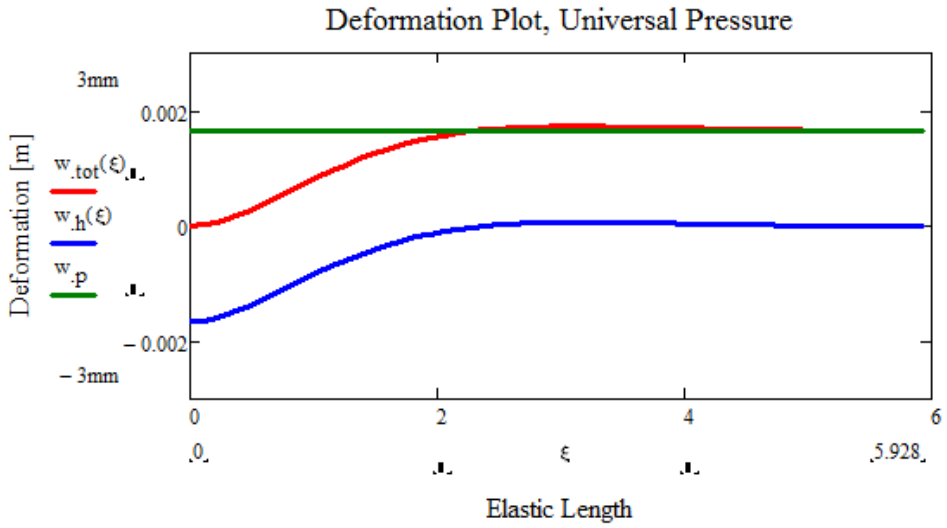

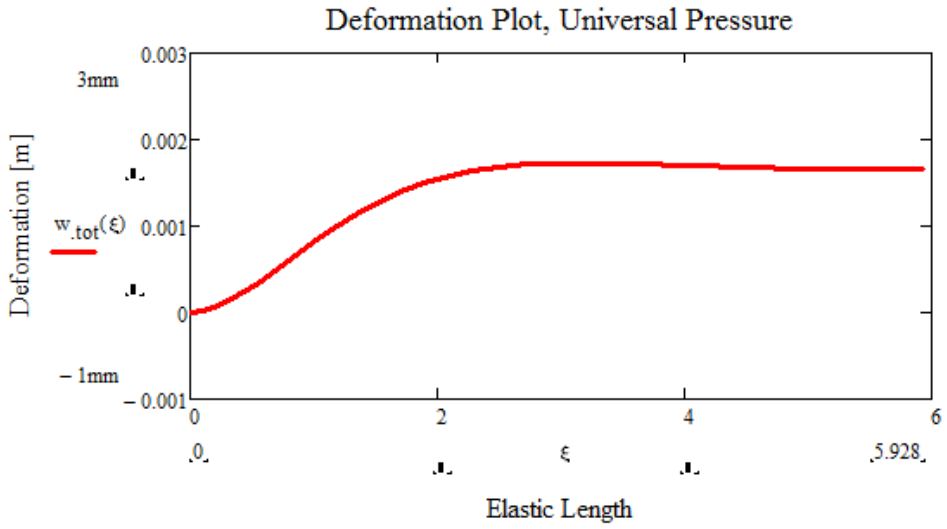

$$N_{\varphi}(\xi) := p \cdot r + \left(g_4(\xi) \cdot M_0 + g_1(\xi) \cdot V_0 \cdot L_e\right) \cdot \frac{2 \cdot r}{L_e^2}$$

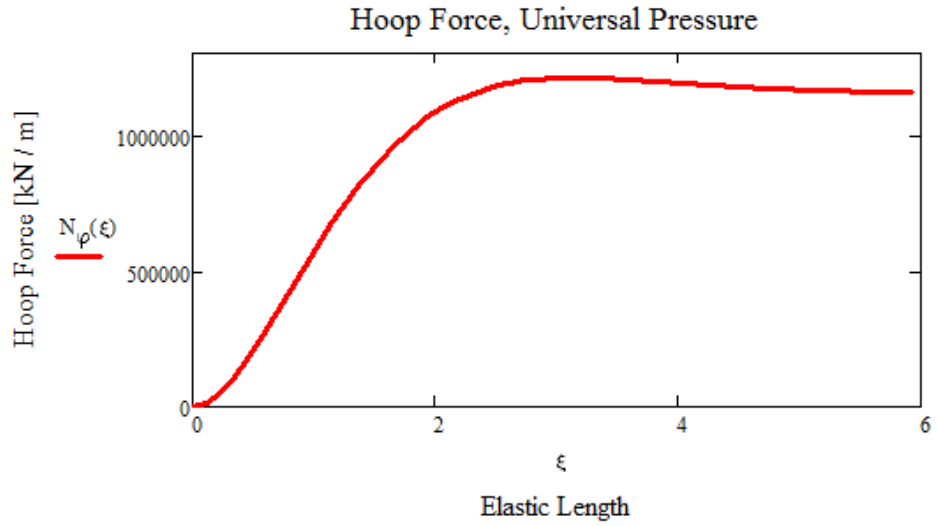

$$w'(\xi) := \frac{L_e}{2 \cdot D} \cdot \left(-2\, g_1(\xi) \cdot M_0 - g_3(\xi) \cdot V_0 \cdot L_e\right)$$

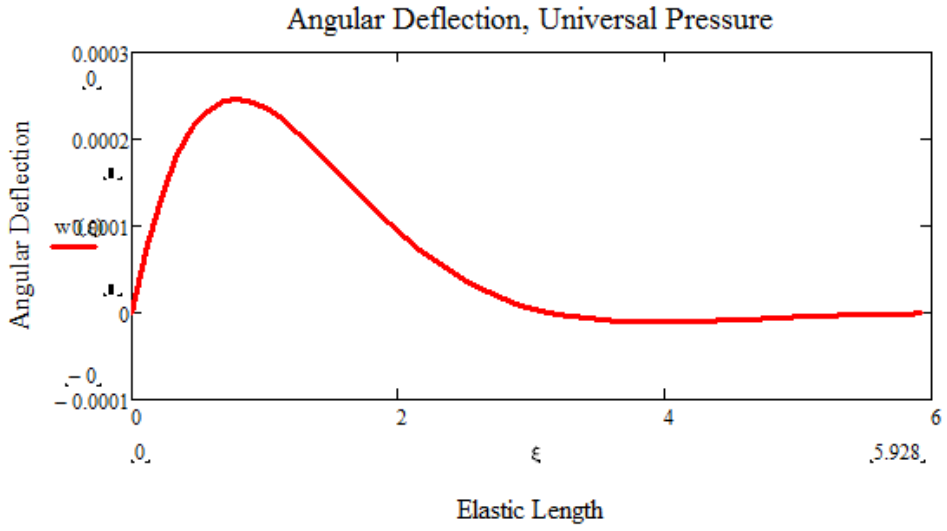

$$M_x(\xi) := g_3(\xi)\cdot M_0 + g_2(\xi)\cdot V_0\cdot L_e$$

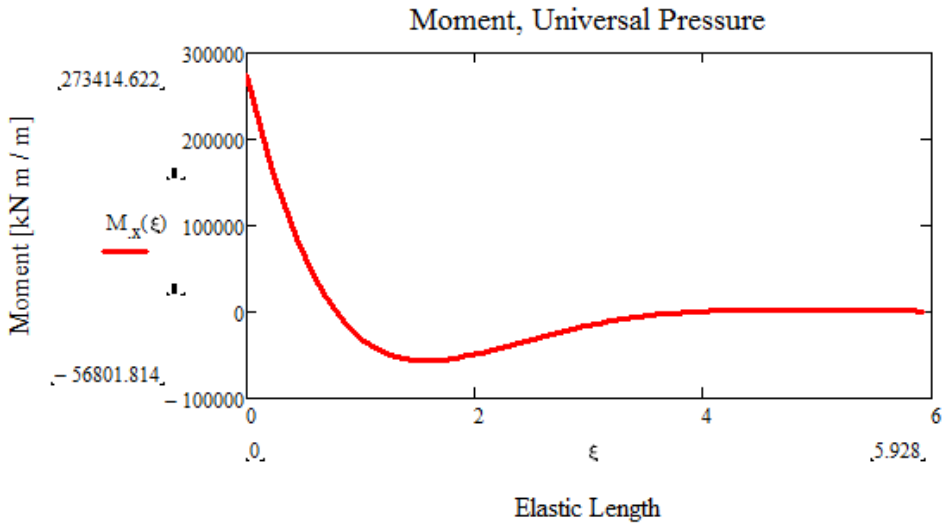

$$V_x(\xi) := \frac{1}{L_e}\cdot\left(-2\cdot g_2(\xi)\cdot M_0 + g_4(\xi)\cdot V_0\cdot L_e\right)$$

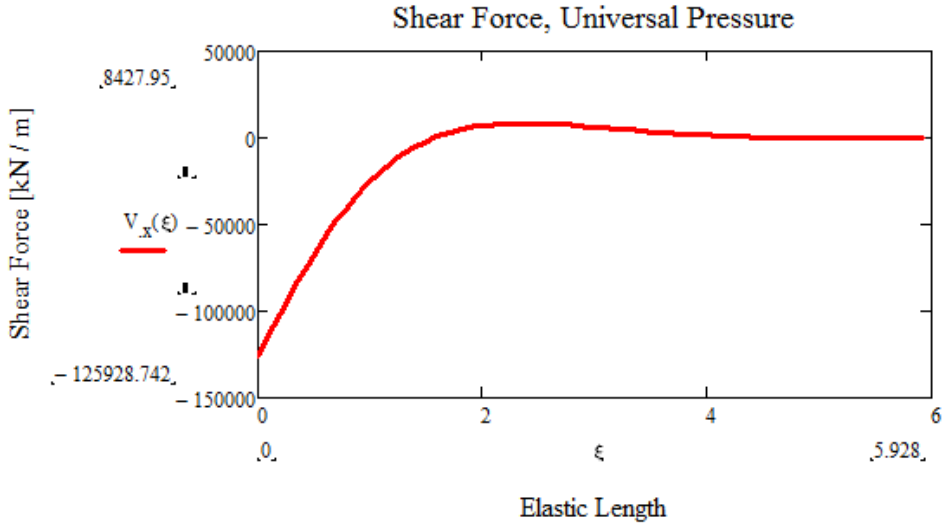

$\xi := 2$

$$w_{tot} := \frac{p \cdot r^2}{E \cdot h} + \left(g_4(\xi) \cdot M_0 + g_1(\xi) \cdot V_0 \cdot L_e\right) \cdot \frac{L_e^2}{2 \cdot D} = 1.5 \cdot mm$$

$$N_{\varphi} := p \cdot r + \left(g_4(\xi) \cdot M_0 + g_1(\xi) \cdot V_0 \cdot L_e\right) \cdot \frac{2 \cdot r}{L_e^2} = 1083 \cdot kN \cdot \frac{1}{m}$$

$$w' := \frac{L_e}{2 \cdot D} \cdot \left(-2\, g_1(\xi) \cdot M_0 - g_3(\xi) \cdot V_0 \cdot L_e\right) = 9.4 \times 10^{-5} \cdot rad$$

$$M_x := g_3(\xi) \cdot M_0 + g_2(\xi) \cdot V_0 \cdot L_e = -49 \cdot kN \cdot m \cdot \frac{1}{m}$$

$$V_x := \frac{1}{L_e} \cdot \left(-2 \cdot g_2(\xi) \cdot M_0 + g_4(\xi) \cdot V_0 \cdot L_e\right) = 7.1 \cdot kN \cdot \frac{1}{m}$$

8.3 Appendix C: Hydrostatic pressure load 38 m

$g_1(\xi) := e^{-\xi}\cdot\cos(\xi)$ $\quad h := 0.8m$ $\quad H := 38m$

$g_2(\xi) := e^{-\xi}\cdot\sin(\xi)$ $\quad r := 40m$ $\quad \upsilon := 0.2$

$g_3(\xi) := g_1(\xi) + g_2(\xi)$ $\quad E := 35000\frac{N}{mm^2}$ $\quad \gamma_s := 10\frac{kN}{m^3}$

$g_4(\xi) := g_1(\xi) - g_2(\xi)$

$L_e := \frac{\sqrt{h\cdot r}}{\sqrt[4]{3\cdot\left(1-\upsilon^2\right)}} = 4.342\,m$ $\quad D := \frac{E\cdot h^3}{12\cdot\left(1-\upsilon^2\right)} = 1.556\times10^6\cdot kN\cdot m$

Constants

$M_0 := \left(\frac{H}{L_e} - 1\right)\cdot\frac{r^2\cdot\gamma_s\cdot 2\cdot D}{E\cdot h\cdot L_e} = 3.173\times10^3\cdot kN\cdot m\cdot\frac{1}{m}$

$V_0 := \left(1 - \frac{2\cdot H}{L_e}\right)\cdot\frac{r^2\cdot\gamma_s\cdot 2\cdot D}{E\cdot h\cdot L_e^{\,2}} = -1.556\times10^3\cdot\frac{N}{mm}$

$\xi := 0, 0.1 .. 9$

$a := \frac{H}{L_e} = 8.751$

Plotting deflections

$$w_h(\xi) := \left(g_4(\xi)\cdot M_0 + g_1(\xi)\cdot V_0\cdot L_e\right)\cdot\frac{L_e^{\,2}}{2\cdot D}$$

$$w_p(\xi) := \max\left[\frac{r^{2}\cdot\gamma_s}{E\cdot h}\left(H - L_e\cdot\xi\right), 0\right]$$

$$w_{tot}(\xi) := w_h(\xi) + w_p(\xi)$$

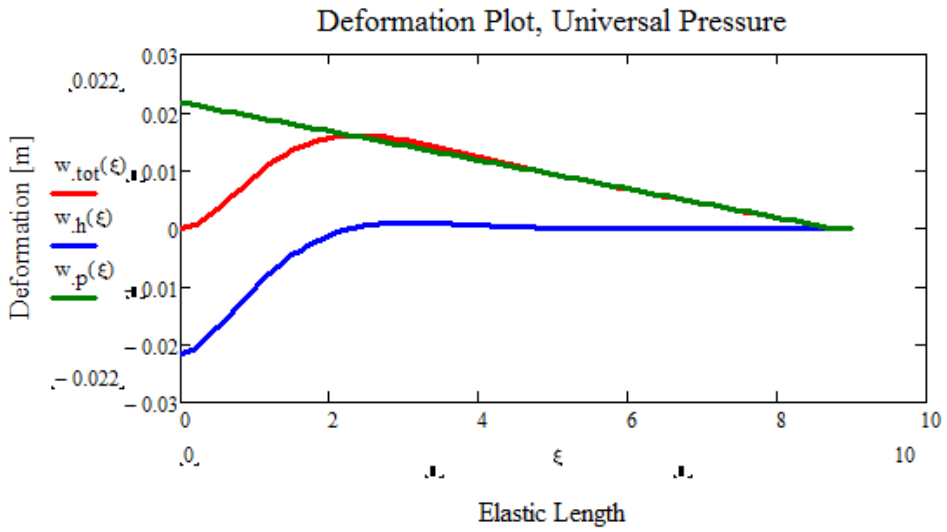

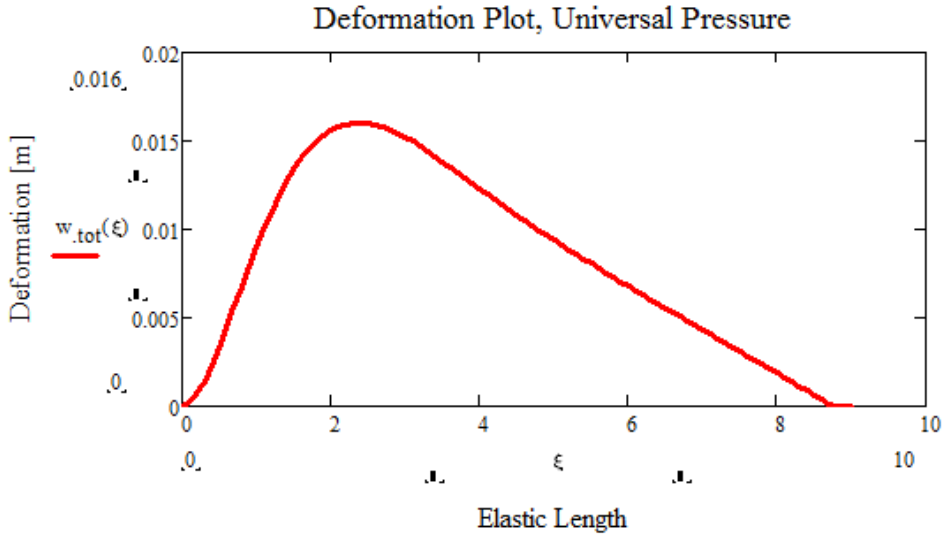

$$N_{\varphi h}(\xi) := \left(g_4(\xi)\cdot M_0 + g_1(\xi)\cdot V_0\cdot L_e\right)\cdot\frac{2\cdot r}{L_e^{\,2}}$$

$$N_{\varphi p}(\xi) := \max\left[r\cdot\gamma_s\cdot\left(H - L_e\cdot\xi\right), 0\right]$$

$$N_{\varphi}(\xi) := N_{\varphi h}(\xi) + N_{\varphi p}(\xi)$$

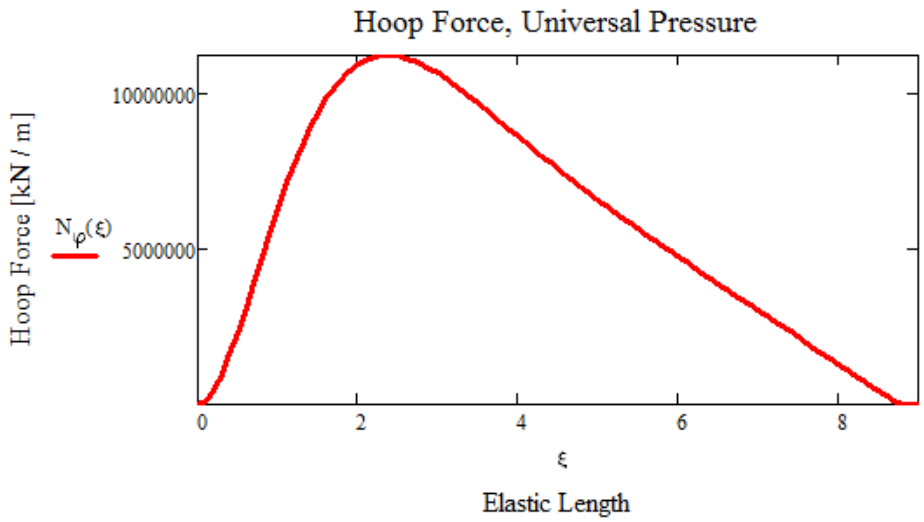

$$w'_{tot}(\xi) := \frac{L_e}{2 \cdot D} \cdot \left(-2\, g_1(\xi) \cdot M_0 - g_3(\xi) \cdot V_0 \cdot L_e\right) - \frac{r^2 \cdot \gamma_s}{E \cdot h}$$

$$w'_h(\xi) := \frac{L_e}{2 \cdot D} \cdot \left(-2\, g_1(\xi) \cdot M_0 - g_3(\xi) \cdot V_0 \cdot L_e\right)$$

$$w'_p := -\frac{r^2 \cdot \gamma_s}{E \cdot h}$$

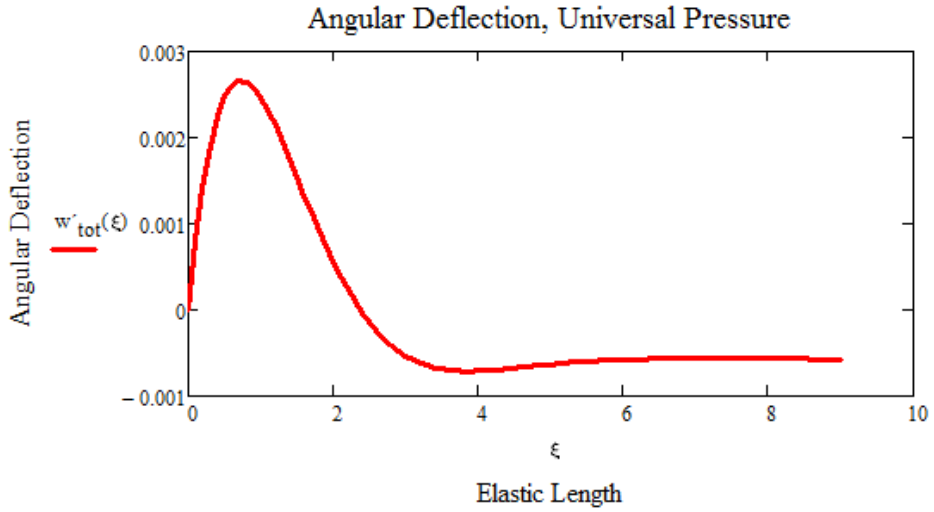

$$M_x(\xi) := g_3(\xi) \cdot M_0 + g_2(\xi) \cdot V_0 \cdot L_e$$

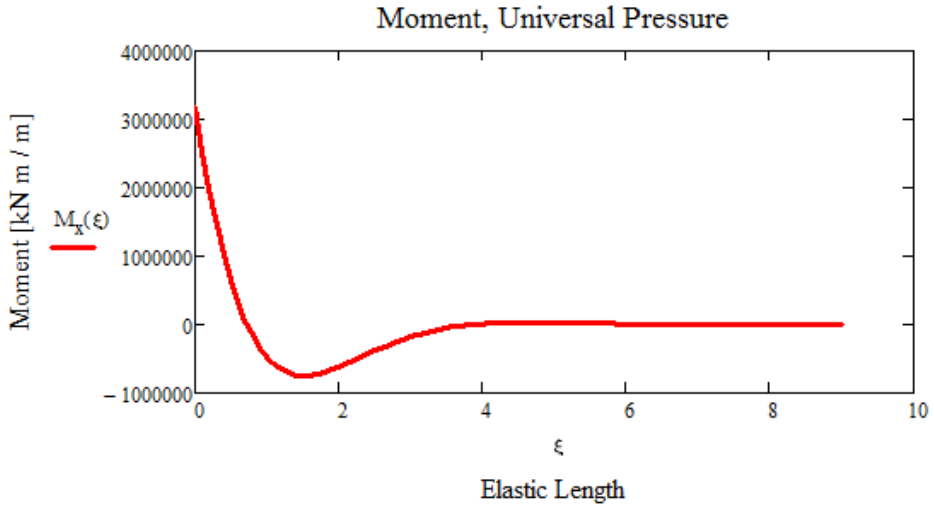

$$V_x(\xi) := \frac{1}{L_e}\cdot\left(-2\cdot g_2(\xi)\cdot M_0 + g_4(\xi)\cdot V_0\cdot L_e\right)$$

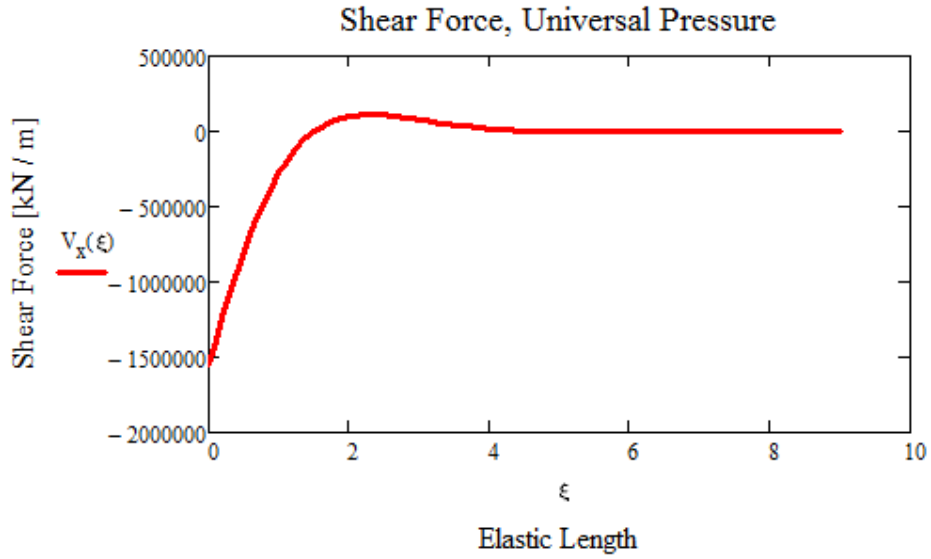

8.4 Appendix D: Thermal load

$E := 35000MPa \qquad \alpha := 1 \cdot 10^{-5} \cdot \frac{1}{K}$

$E_s := 200000MPa \qquad d := 25mm \qquad A_s := \pi \cdot \left(\frac{d}{2}\right)^2$

Thermal stresses and moments in wall section

$T_i := -165K \qquad T_o := 35K$

$h := 800mm \qquad \upsilon := 0.2 \qquad R := 40.4m$

$\sigma_i := -E \cdot \alpha \cdot T_i = 57.8 \cdot MPa$

$\sigma_o := -E \cdot \alpha \cdot T_o = -12.3 \cdot MPa$

Clamped thermal moment

$M_0 := \sigma_i \cdot \frac{h^2}{12(1-\upsilon)} = 3.85 \times 10^3 \cdot kN \cdot m \cdot \frac{1}{m}$

Flare stresses and thermal moment

$\lambda := \left[\frac{3 \cdot \left(1-\upsilon^2\right)}{R^2 \cdot h^2}\right]^{\frac{1}{4}}$

$\sigma_\theta := \frac{E \cdot \alpha \cdot T_i}{1-\upsilon} - \frac{2 \cdot M_0 \cdot \lambda^2 \cdot R}{h} + \upsilon \cdot \frac{6 \cdot M_0}{h^2}$

$\sigma_\theta = -85.4 \cdot MPa$

$M_\theta := \sigma_\theta \cdot \frac{h^2}{12(1-\upsilon)} = -5.692 \times 10^3 \cdot kN \cdot m \cdot \frac{1}{m}$

Thermal stresses and moments in wall section

$a := \frac{|T_i|}{|T_i| + |T_o|} = 0.825$

$b := \frac{|T_o|}{|T_i| + |T_o|} = 0.175$

Temperature in rebar at inside of tank

$$T_{si} := T_i - \frac{60mm}{a \cdot h} \cdot T_i = -150\,K$$

Temperature in rebar at outside of tank

$$T_{so} := T_o - \frac{60mm}{b \cdot h} \cdot T_o = 20\,K$$

Thermal stresses in rebars

$$\sigma_{si} := E_s \cdot \alpha \cdot T_{si} = -300 \cdot MPa$$

$$\sigma_{so} := E_s \cdot \alpha \cdot T_{so} = 40 \cdot MPa$$

$$M_s := \frac{\sigma_{si} \cdot 600mm \cdot A_s}{m} = -88.357 \frac{1}{m} \cdot kN \cdot m$$

$$T_i := -165K \qquad T_o := 20K \qquad h := 1000mm$$

$$\sigma_i := -E \cdot \alpha \cdot T_i = 57.8 \cdot MPa$$

$$\sigma_o := -E \cdot \alpha \cdot T_o = -7 \cdot MPa$$

$$a := \frac{|T_i|}{|T_i| + |T_o|} = 0.892$$

$$b := \frac{|T_o|}{|T_i| + |T_o|} = 0.108$$

Temperature in rebar at inside of tank

$$T_{si} := T_i - \frac{100mm}{a \cdot h} \cdot T_i = -146.5\,K$$

Temperature in rebar at outside of tank

$$T_{so} := T_o - \frac{100mm}{b \cdot h} \cdot T_o = 1.5\,K$$

$$\sigma_{si} := E_s \cdot \alpha \cdot T_{si} = -293 \cdot MPa$$

$$\sigma_{so} := E_s \cdot \alpha \cdot T_{so} = 3 \cdot MPa$$

8.5 Appendix E: Comparison linear-non-linear LC101

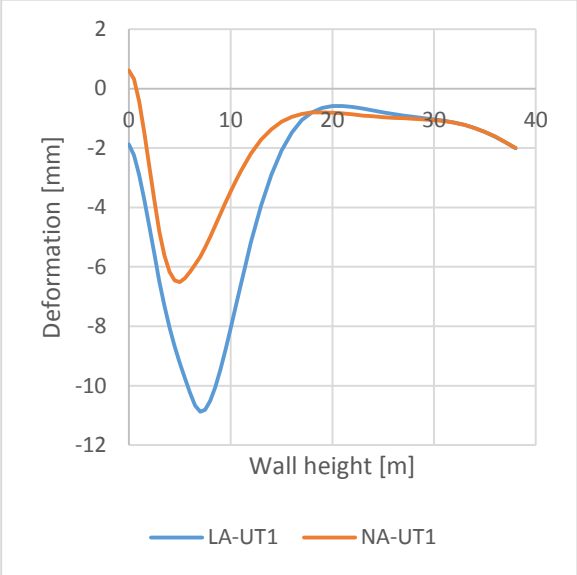

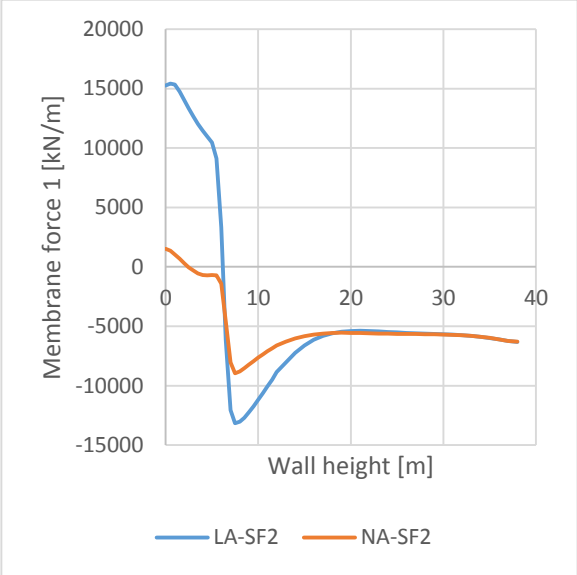

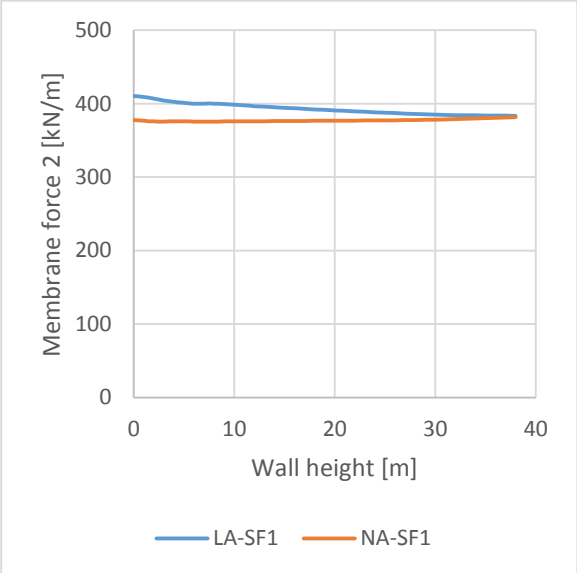

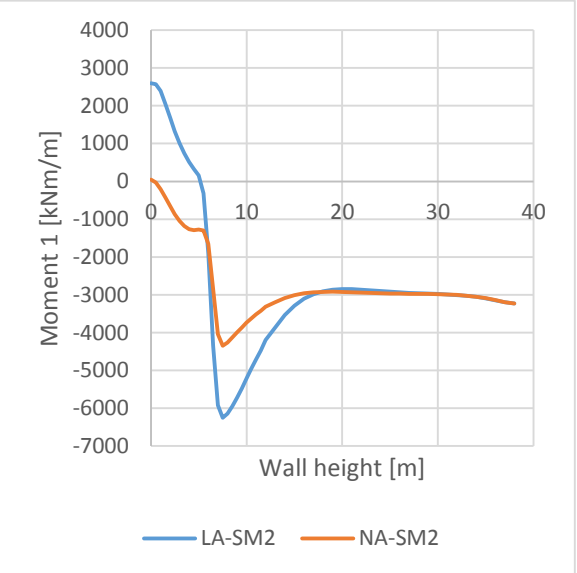

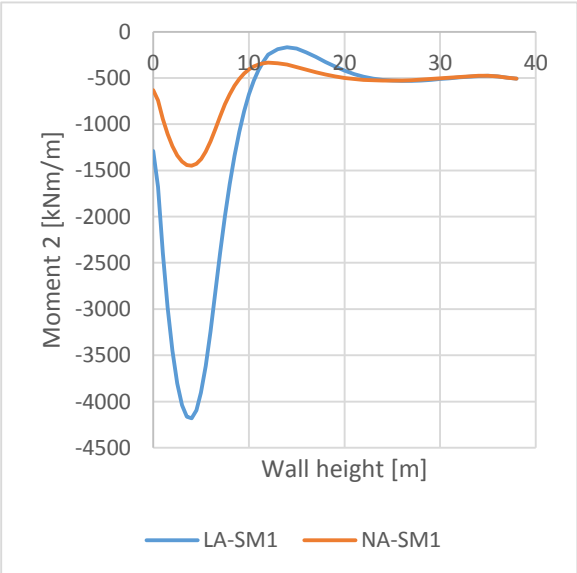

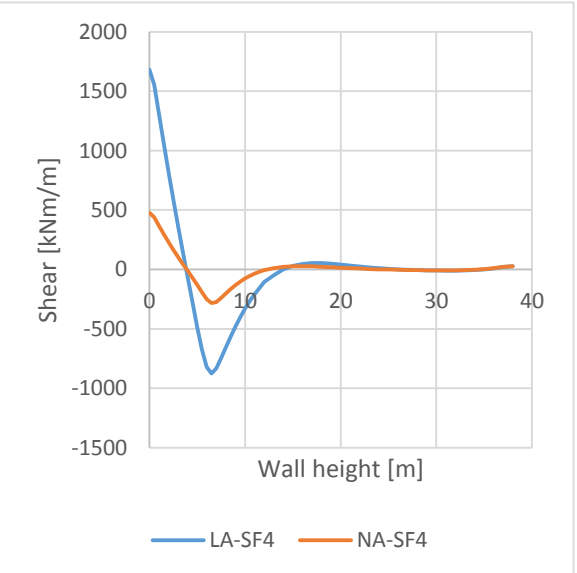

Rebar stresses for wall

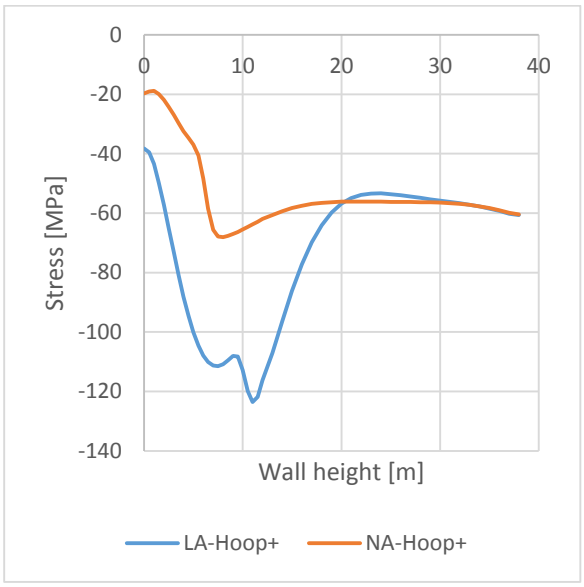

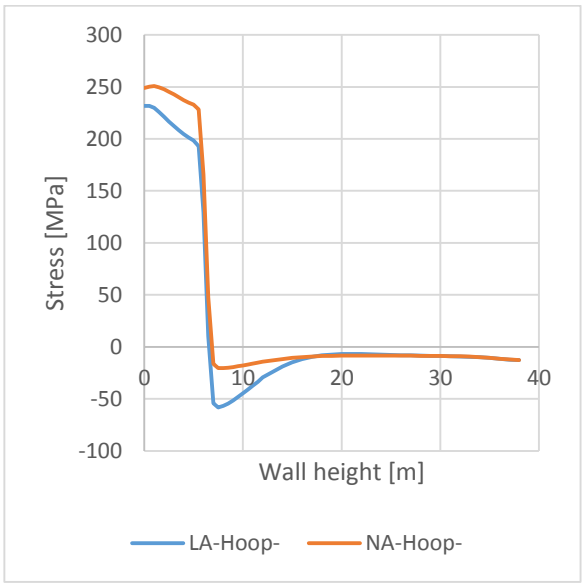

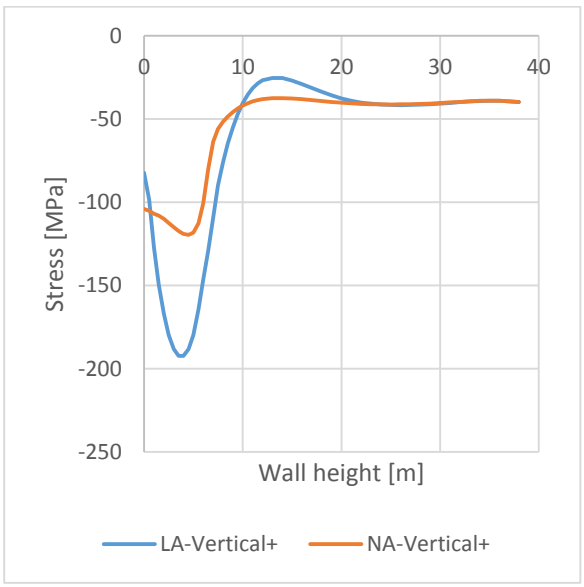

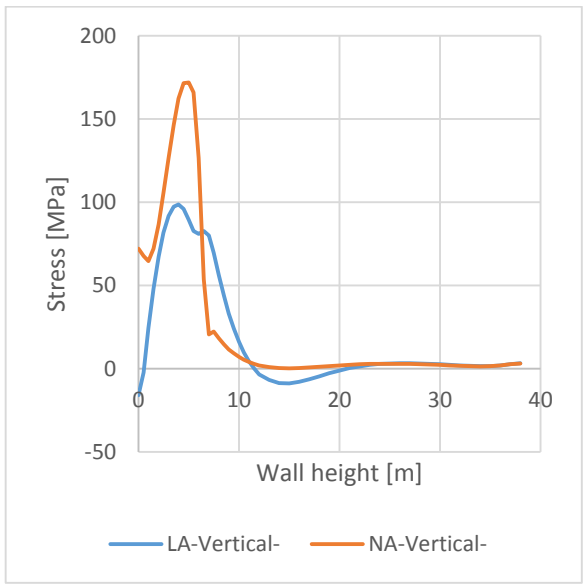

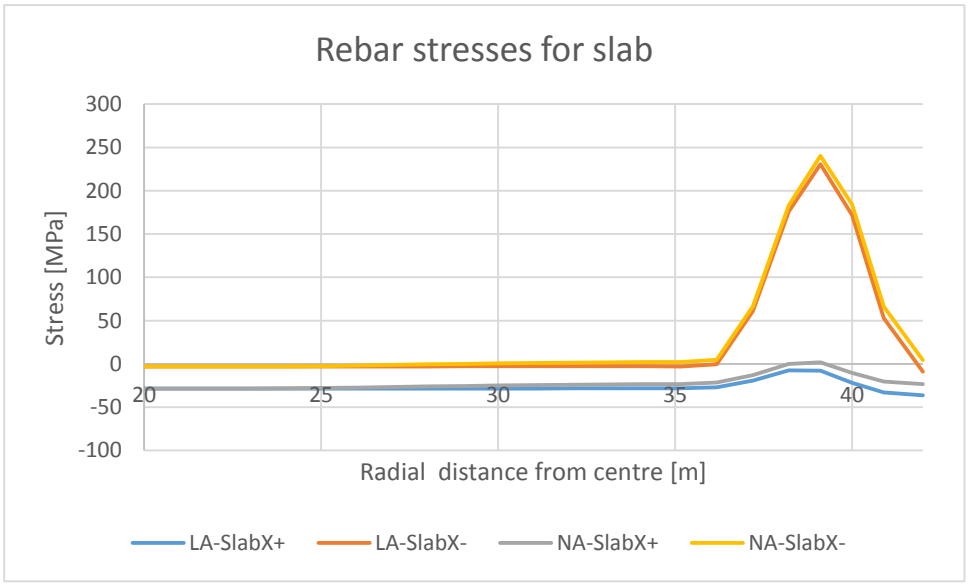

8.6 Appendix F: Comparison linear-non-linear LC102

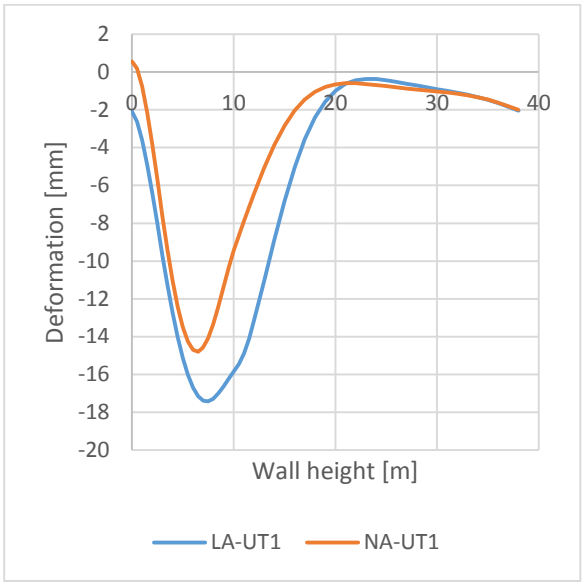

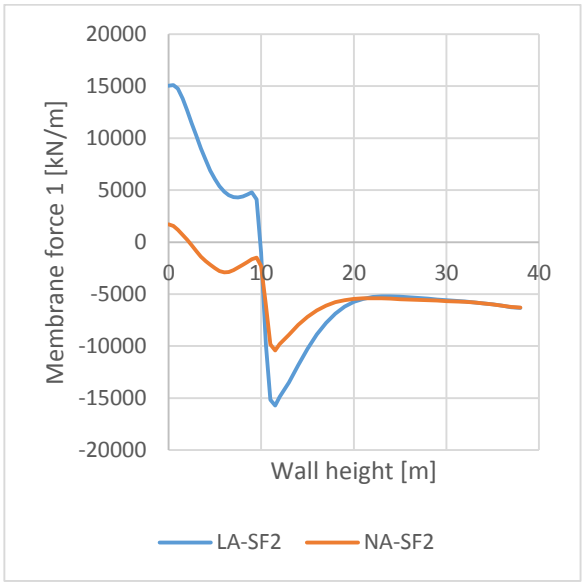

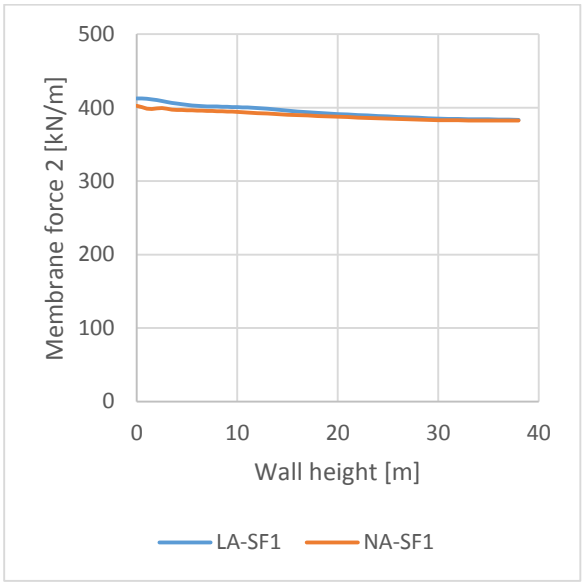

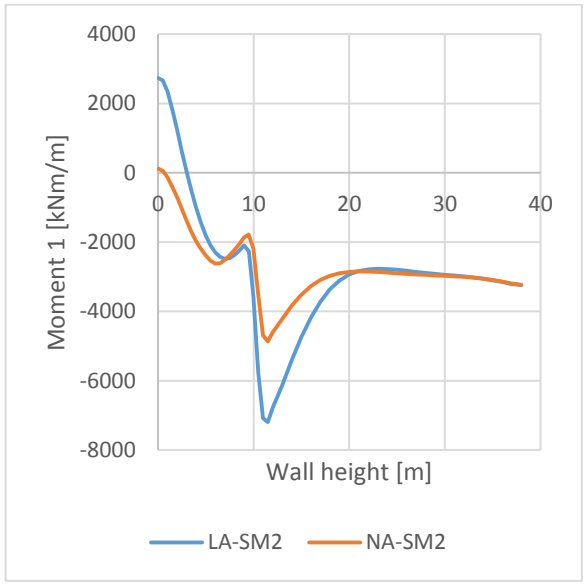

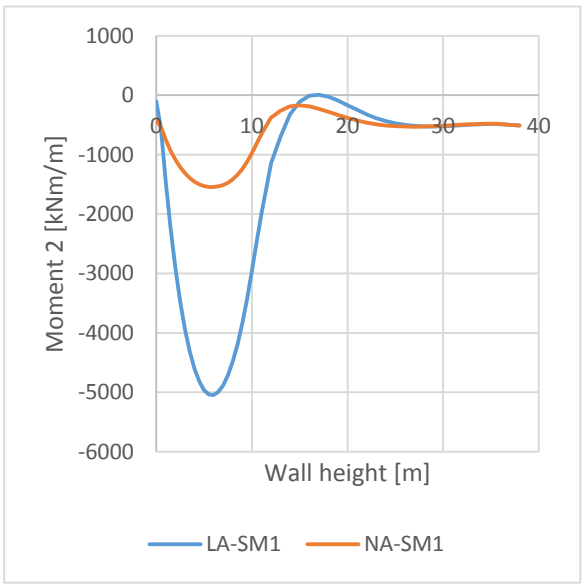

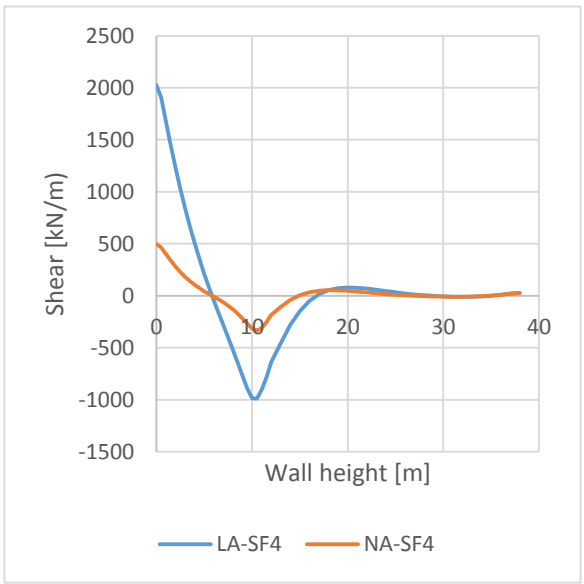

Rebar stresses for wall

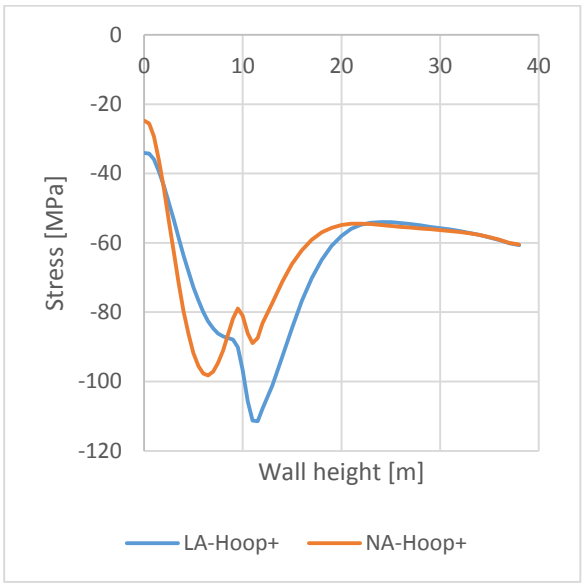

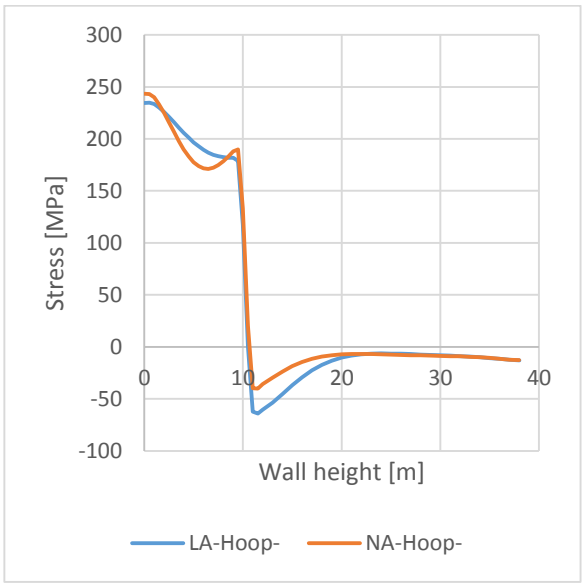

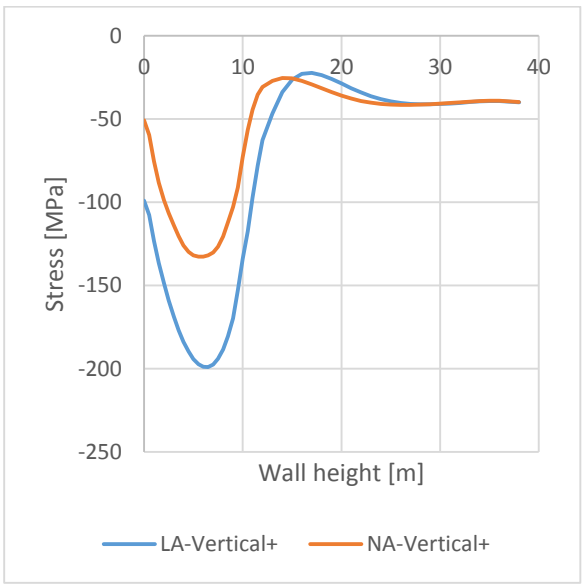

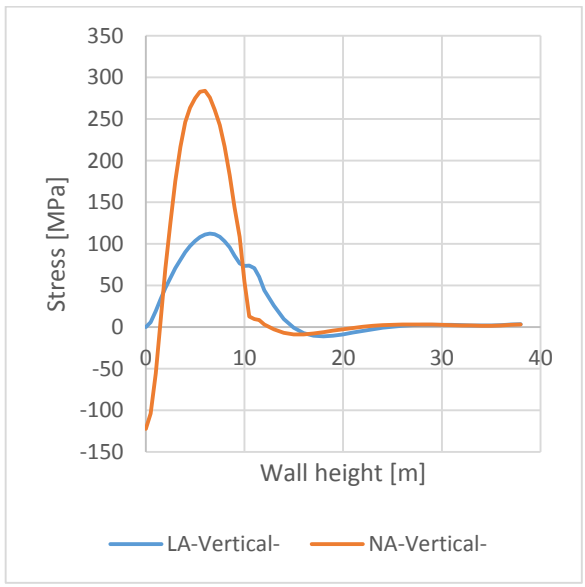

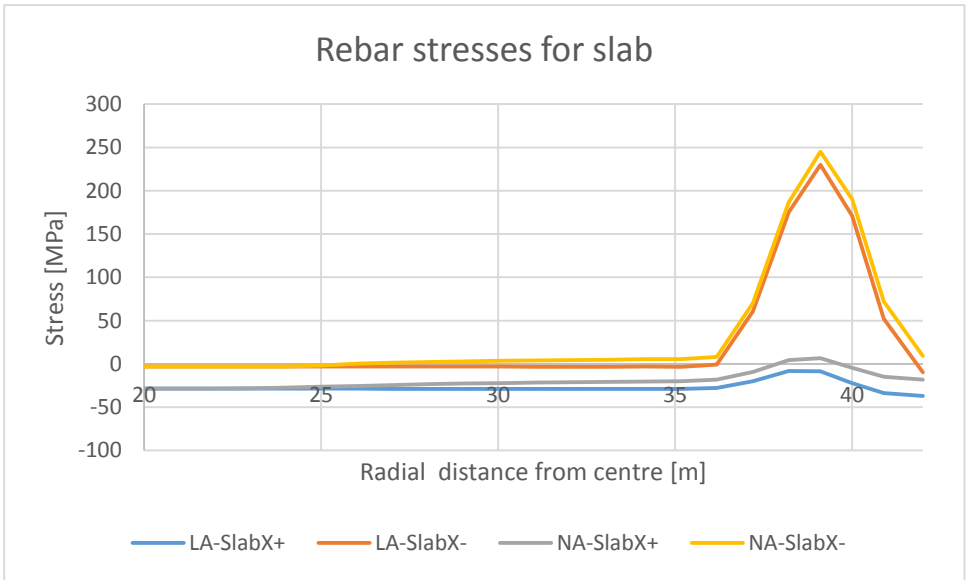

8.7 Appendix G: Comparison linear shell forces for LC101, ftn = 3 MPa

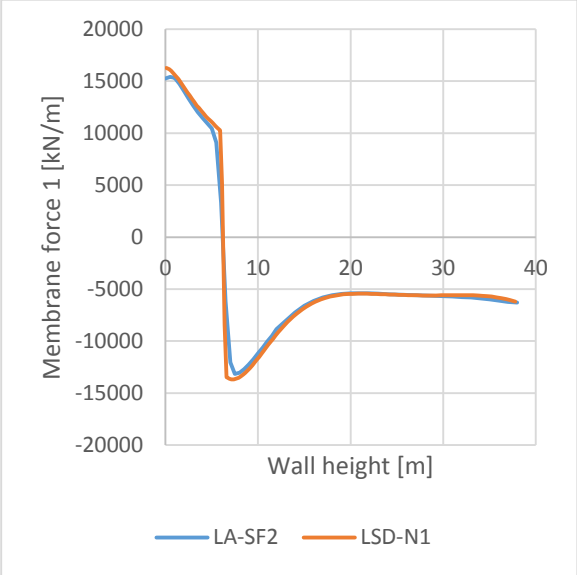

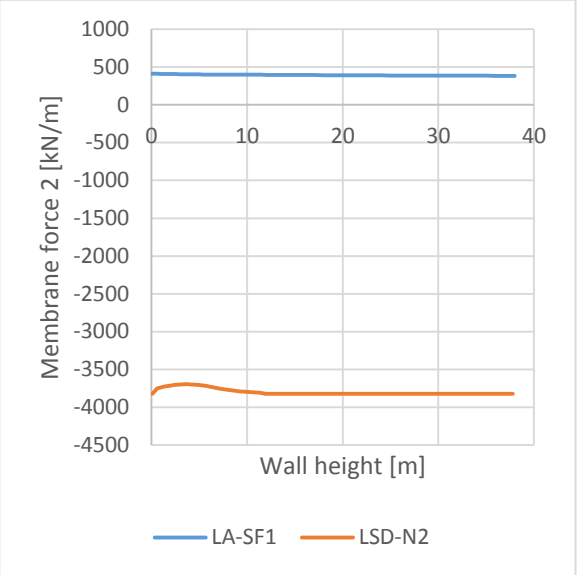

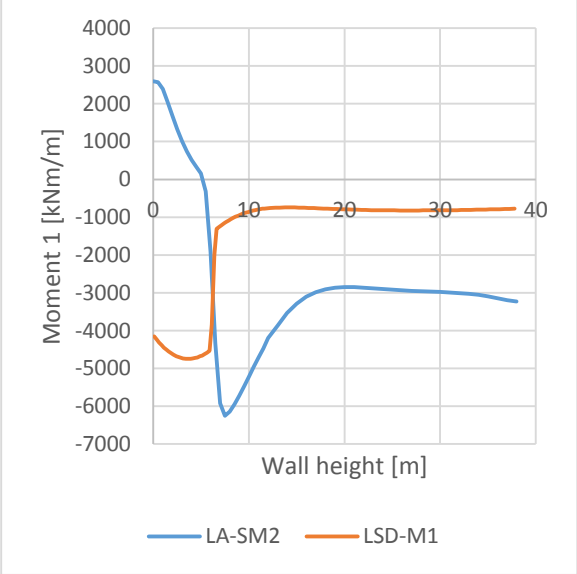

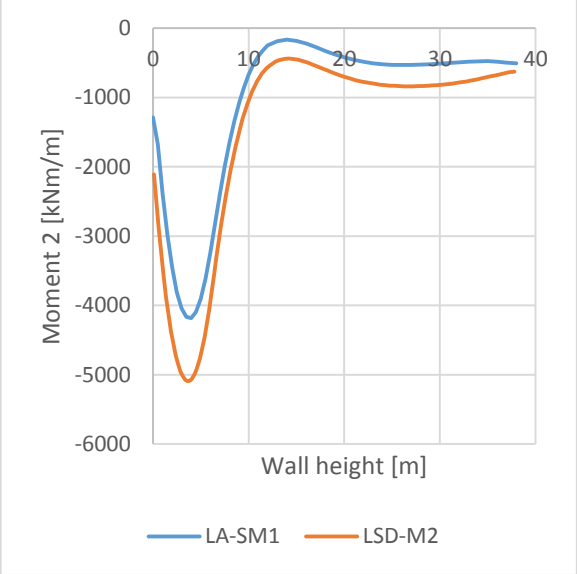

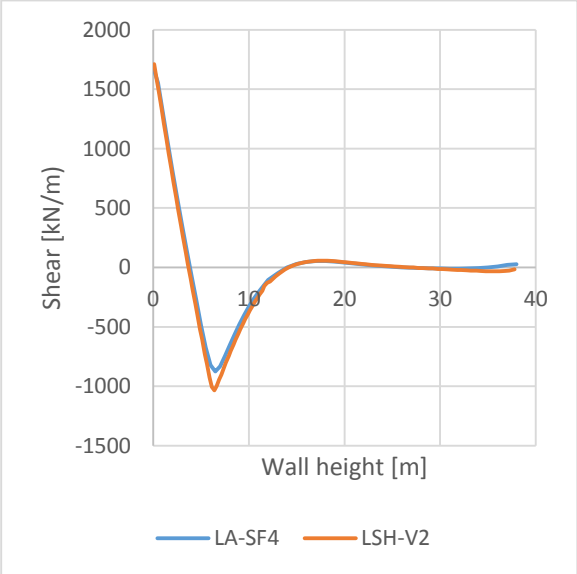

Comparison linear rebar stresses for LC101, ftn = 3 MPa

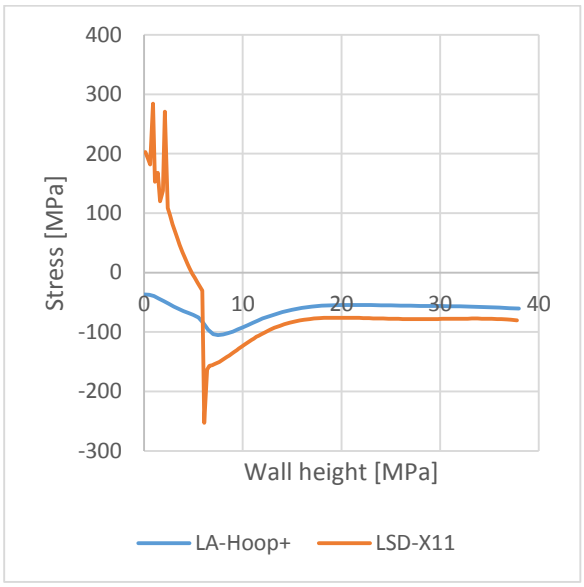

X11 Hoop outside

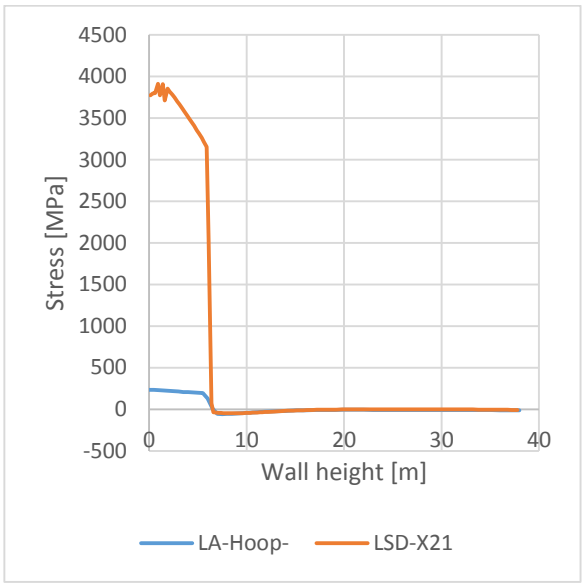

X21 Hoop inside

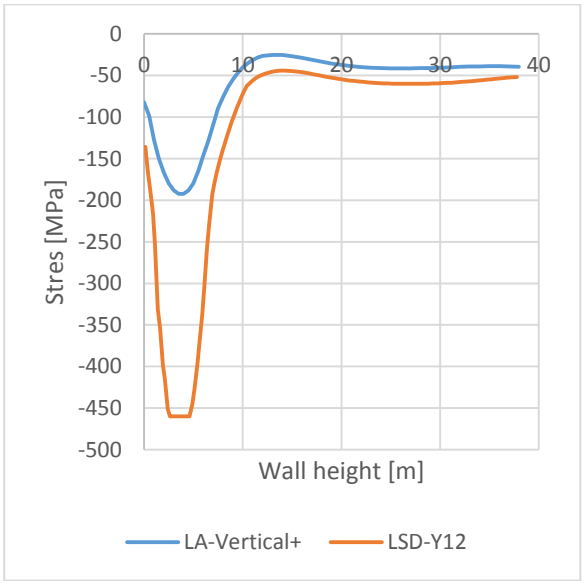

Y21 Vertical outside

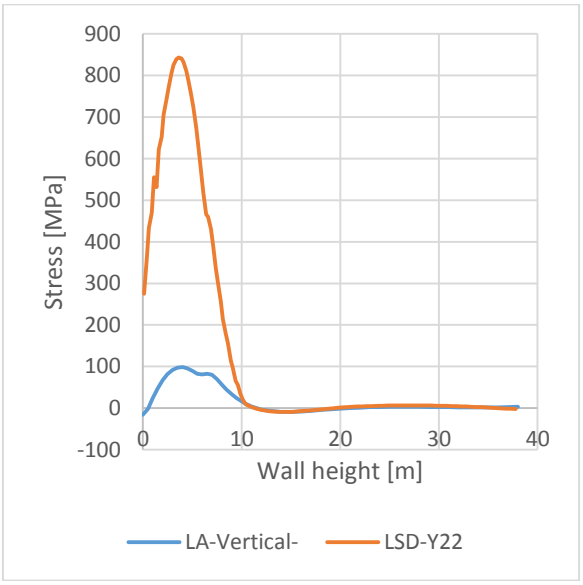

Y22 Vertical inside

8.8 Appendix H: Comparison linear shell forces for LC102, ftn = 3 MPa

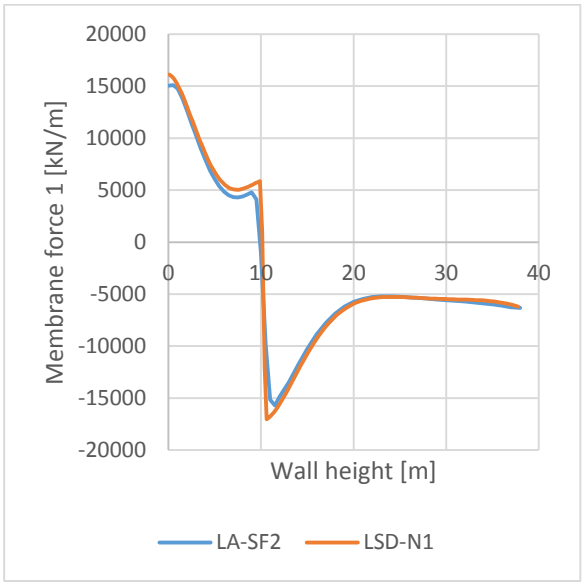

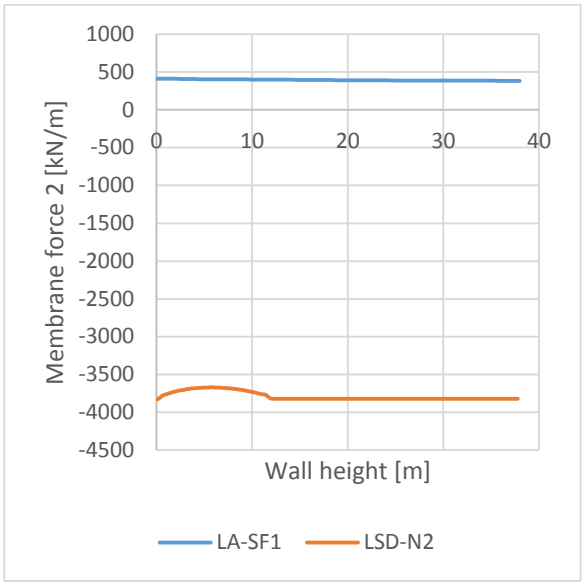

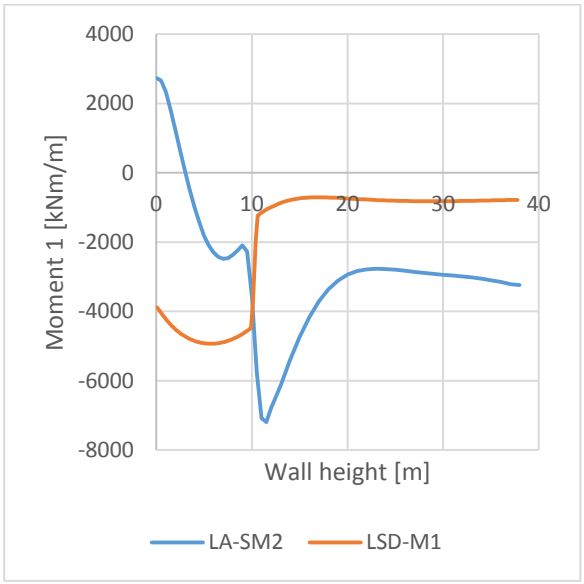

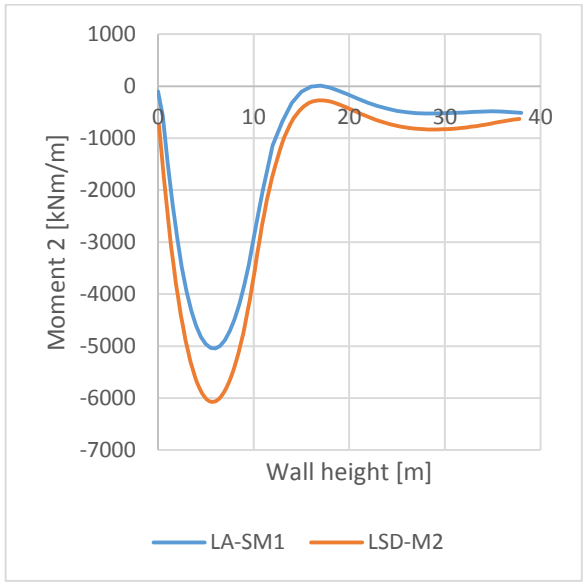

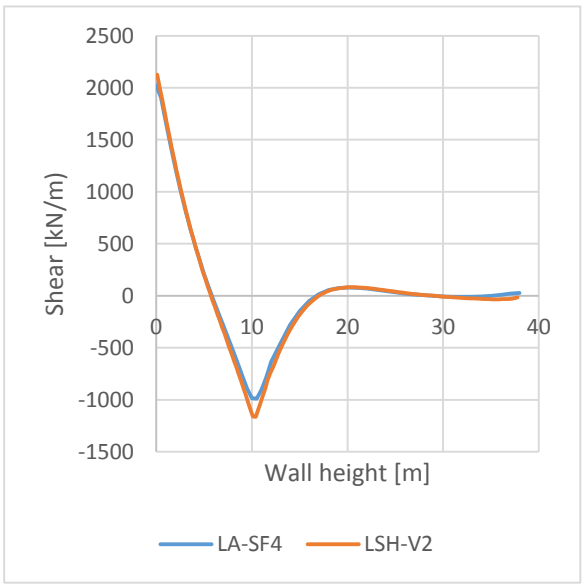

Comparison linear rebar stresses for LC102, ftn = 3 MPa

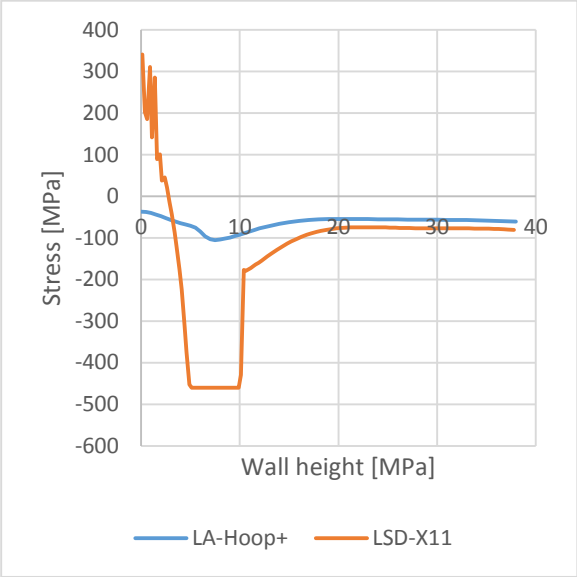

X11 Hoop outside

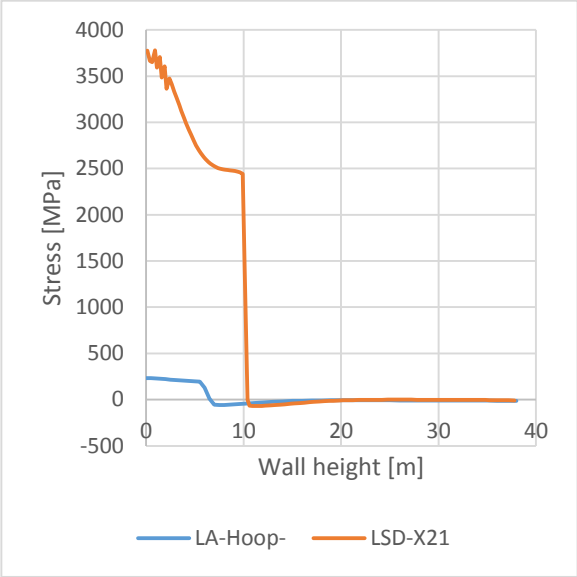

X21 Hoop inside

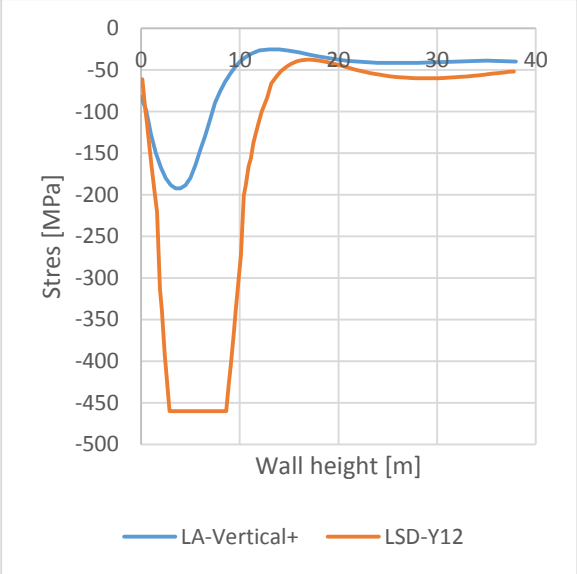

Y21 Vertical outside

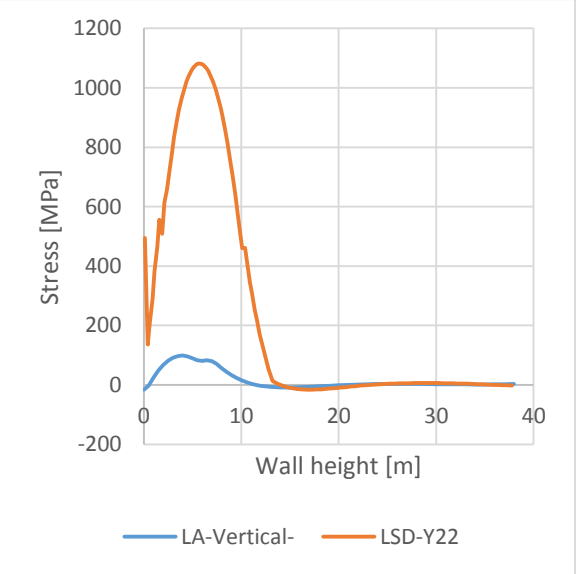

Y22 Vertical inside

8.9 Appendix I: Comparison non-linear shell forces for LC101, ftn = 3 MPa

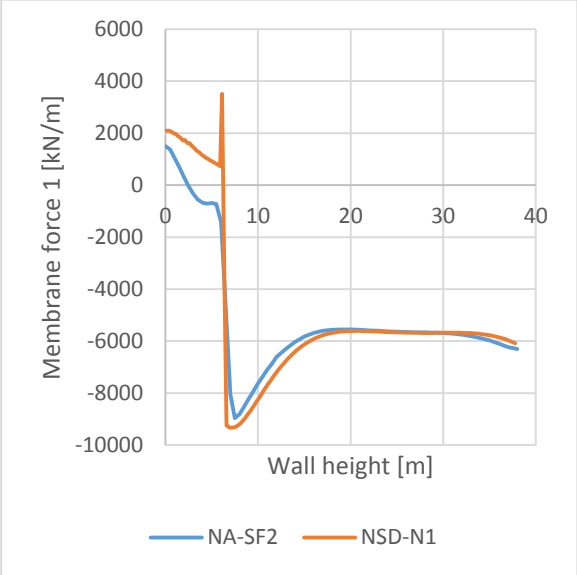

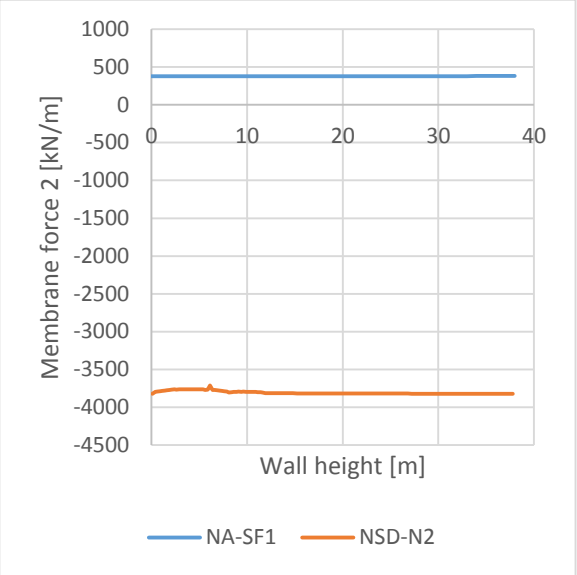

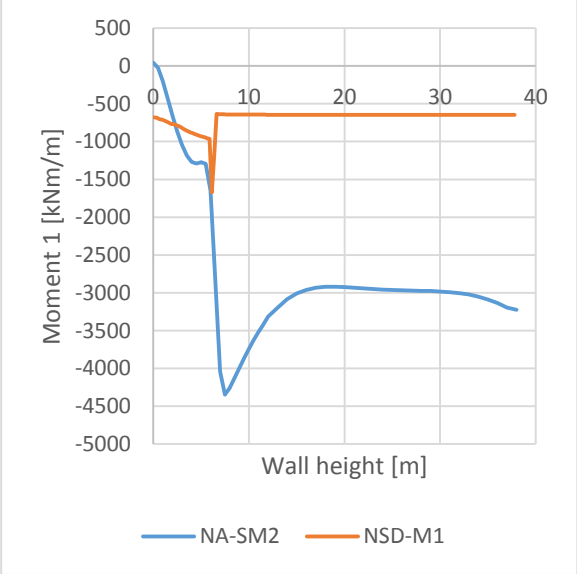

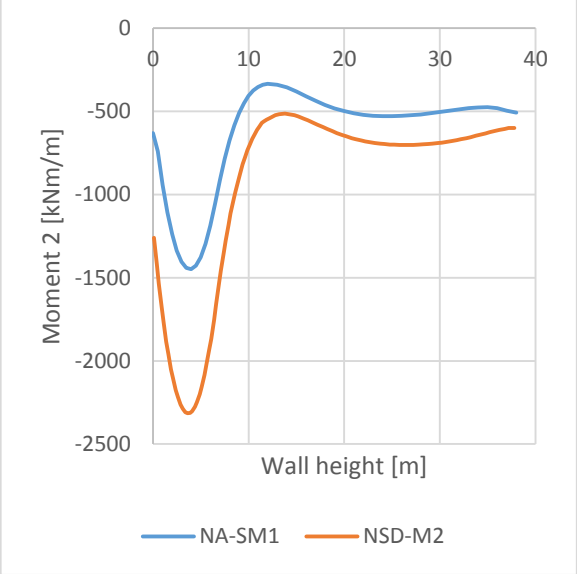

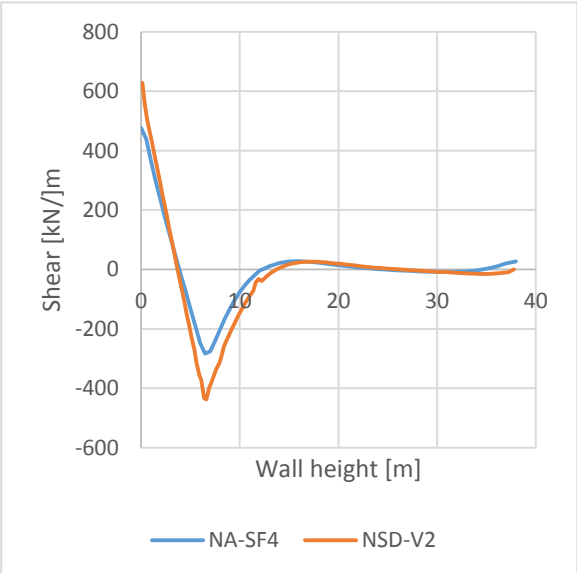

Comparison non-linear rebar stresses for LC101, ftn = 3 MPa

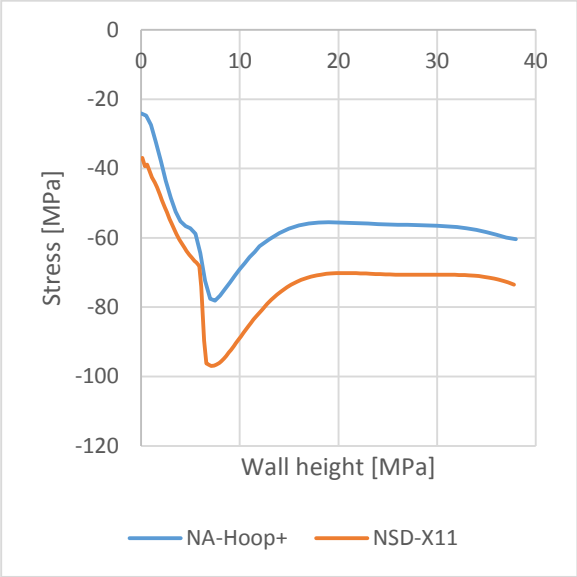

X11 Hoop outside

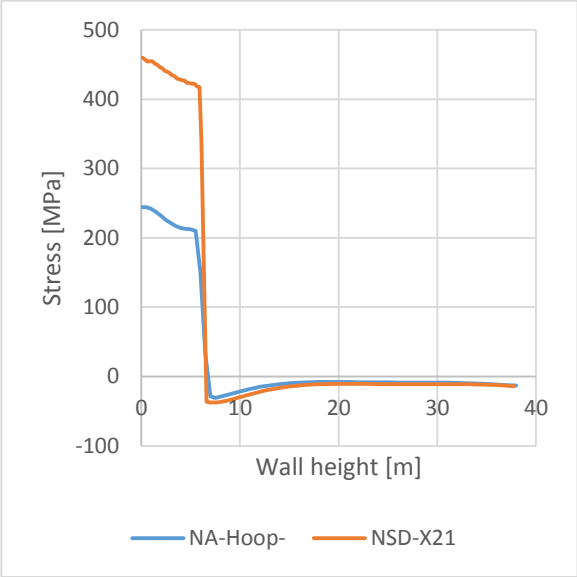

X21 Hoop inside

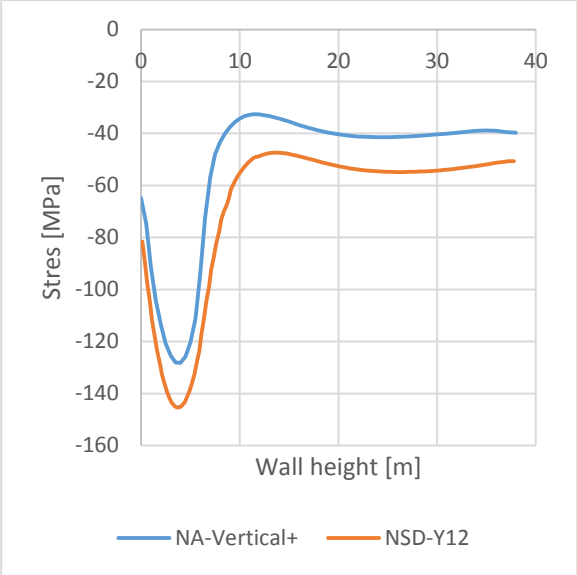

Y21 Vertical outside

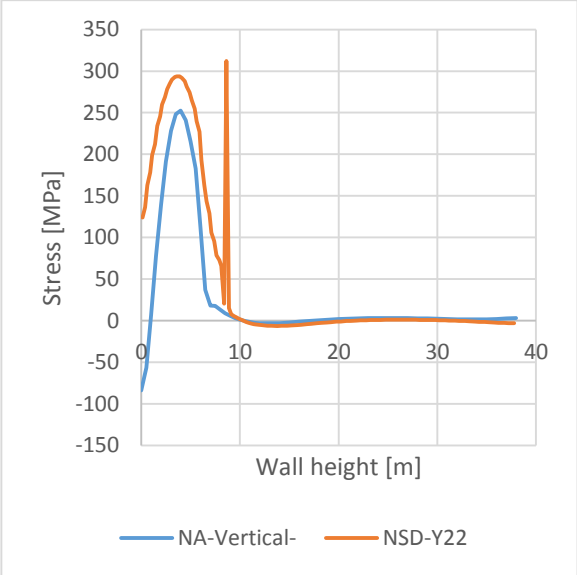

Y22 Vertical inside

8.10 Appendix J: Comparison non-linear shell forces for LC102, ftn = 3 MPa

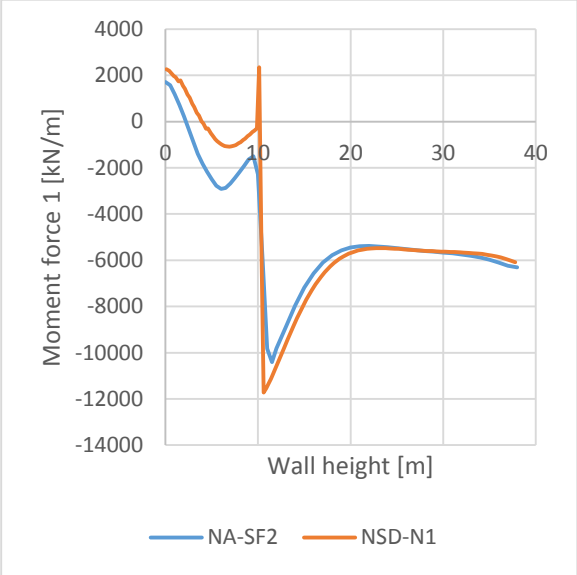

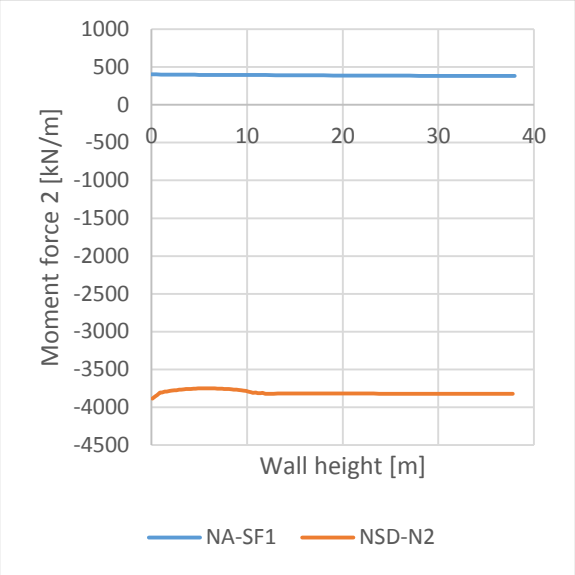

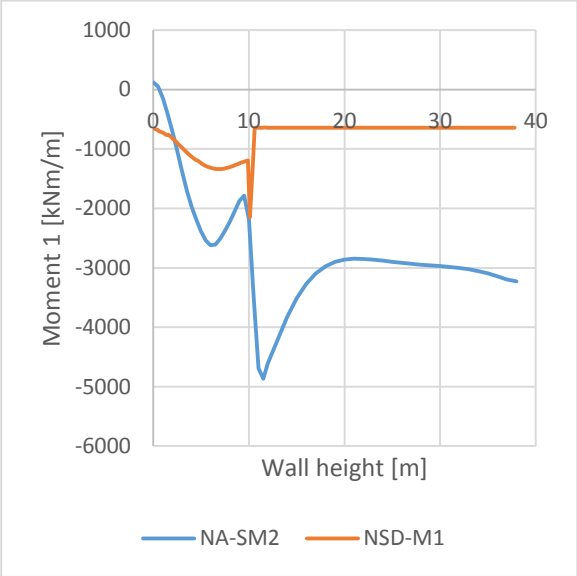

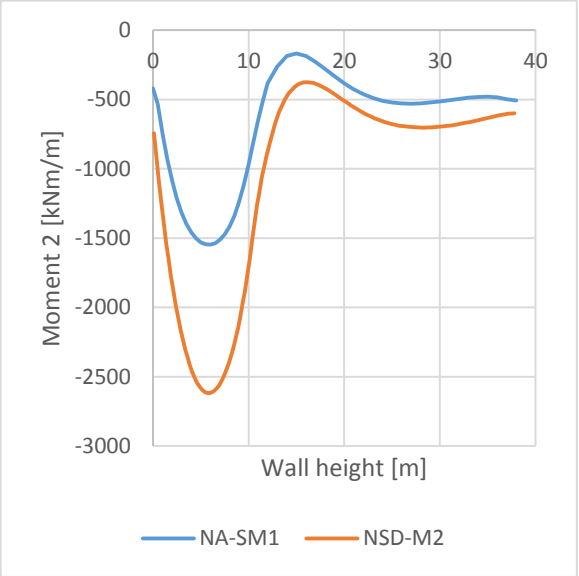

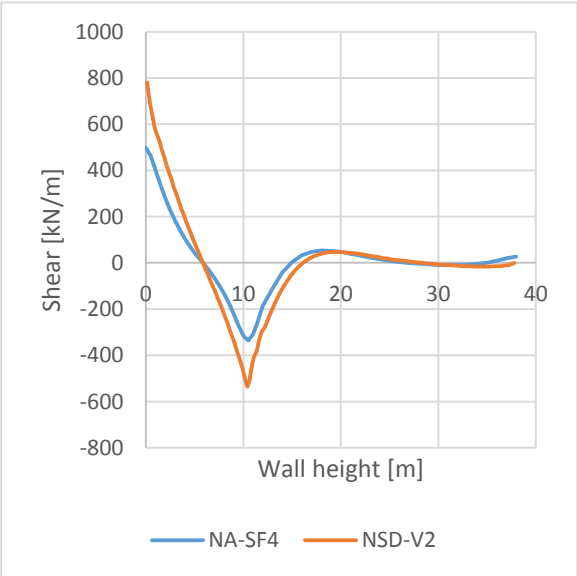

Comparison non-linear rebar stresses for LC102, ftn = 3 MPa

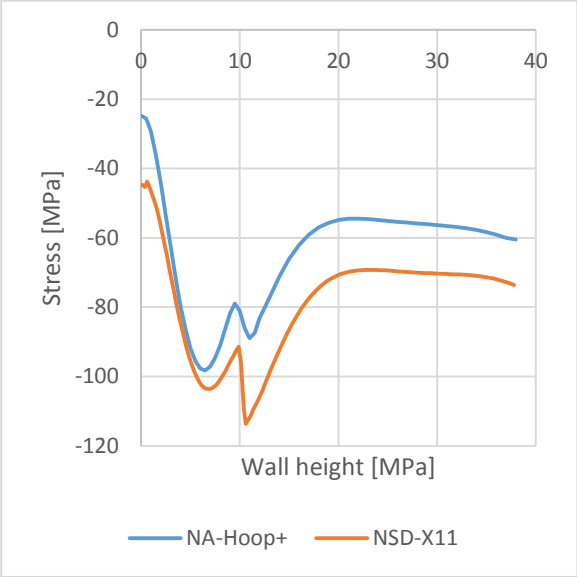

X11 Hoop outside

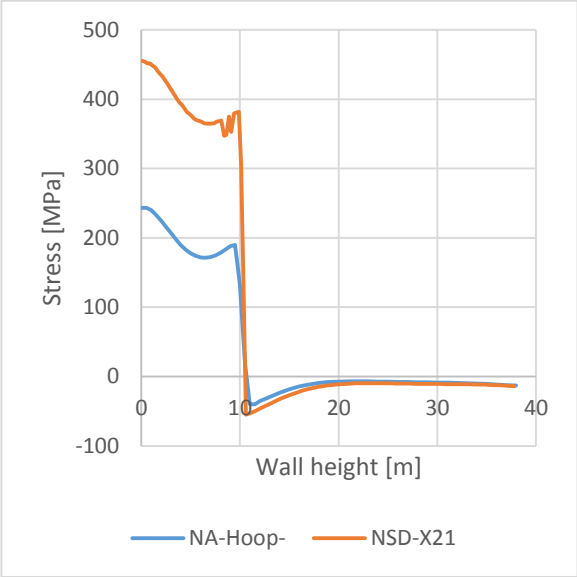

X21 Hoop inside

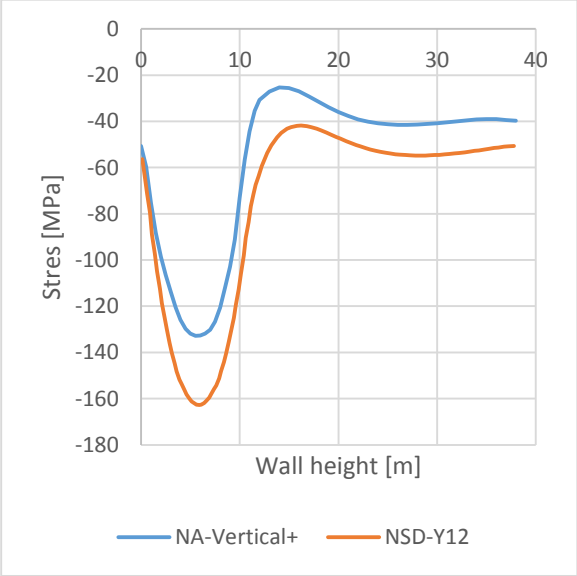

Y21 Vertical outside

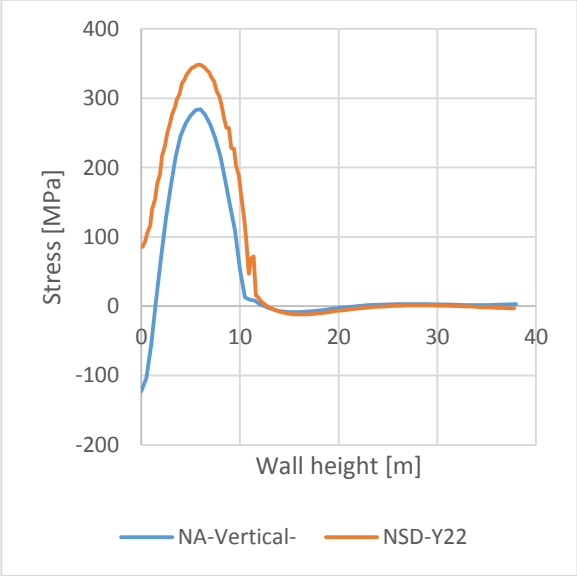

Y22 Vertical inside

8.11 Appendix K: Comparison linear shell forces for LC101, ftn = 0 MPa

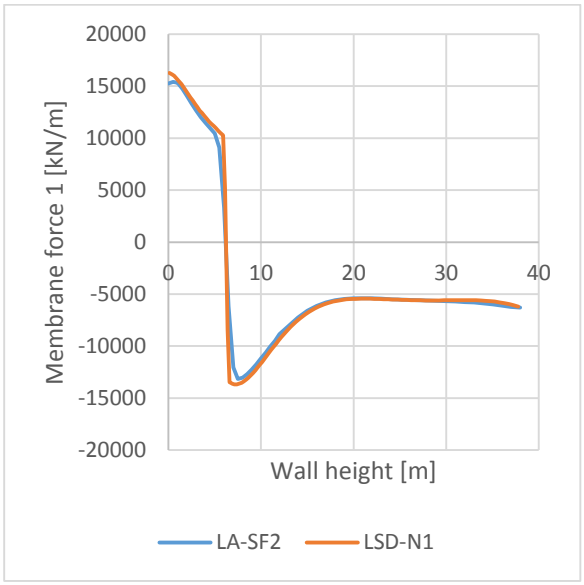

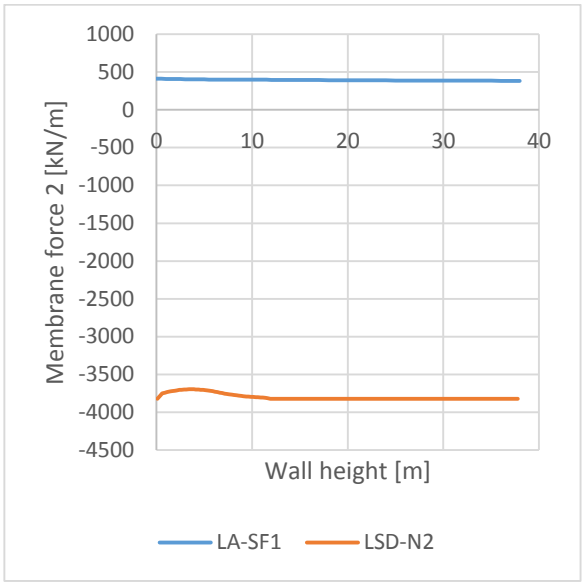

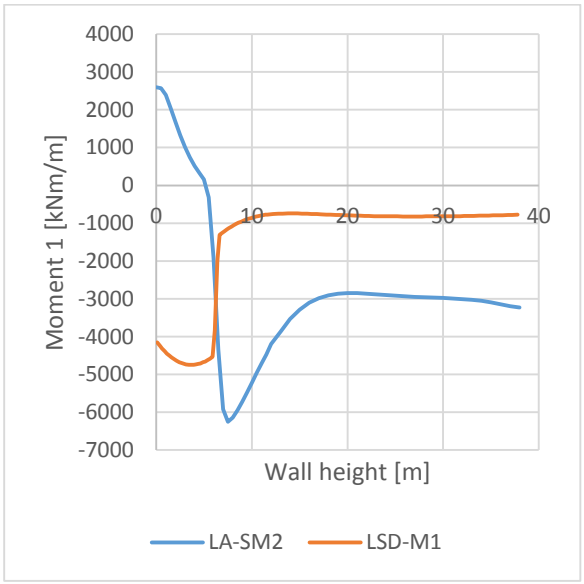

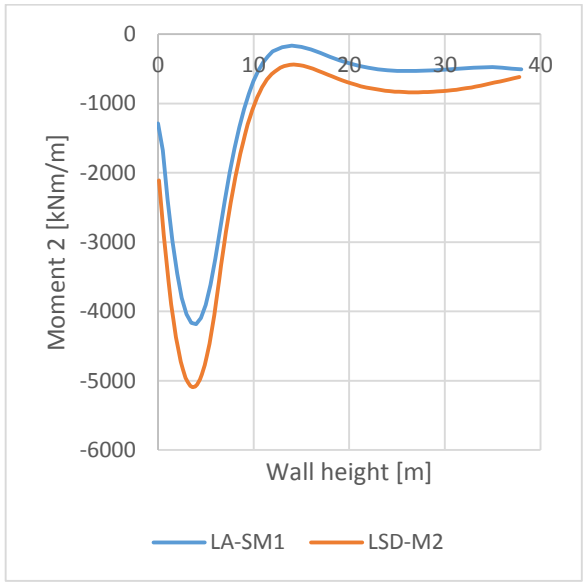

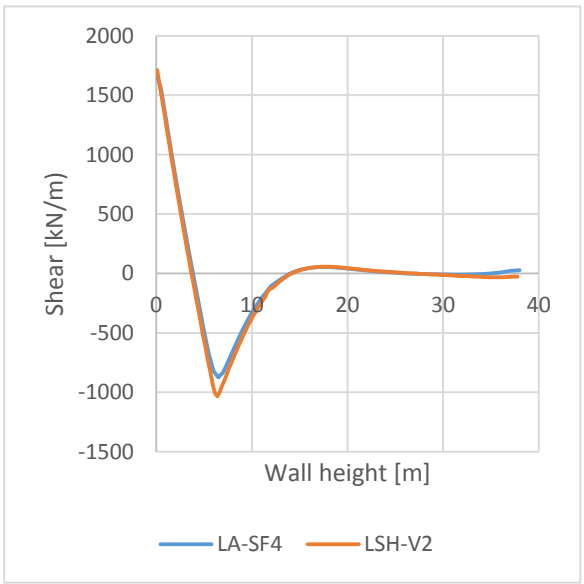

Comparison linear rebar stresses for LC101, ftn = 0 MPa

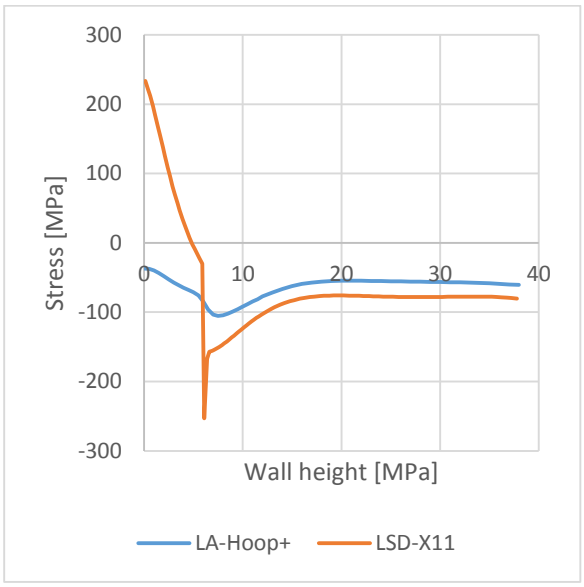

X11 Hoop outside

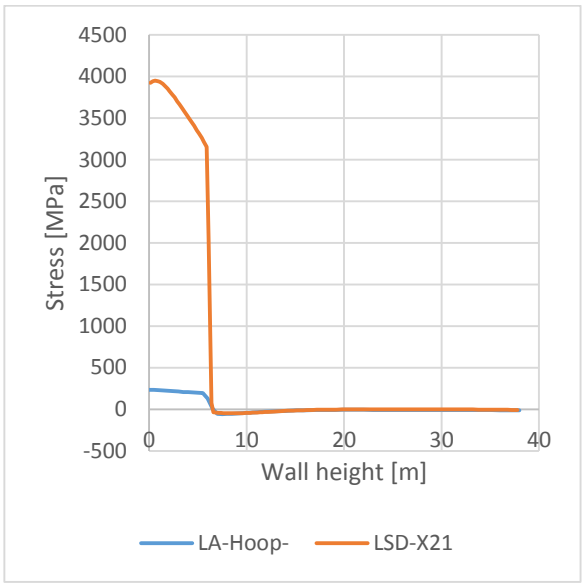

X21 Hoop inside

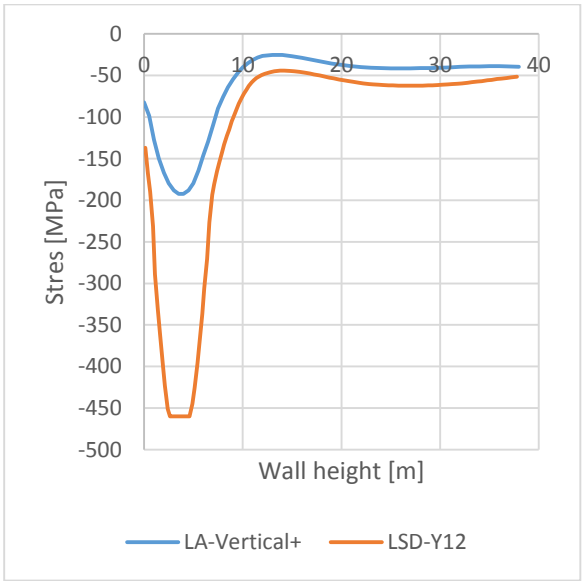

Y21 Vertical outside

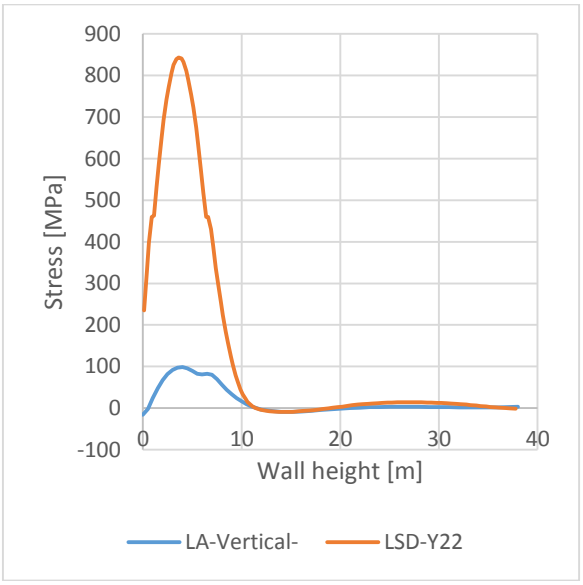

Y22 Vertical inside

8.12 Appendix L: Comparison linear shell forces for LC102, ftn = 0 MPa

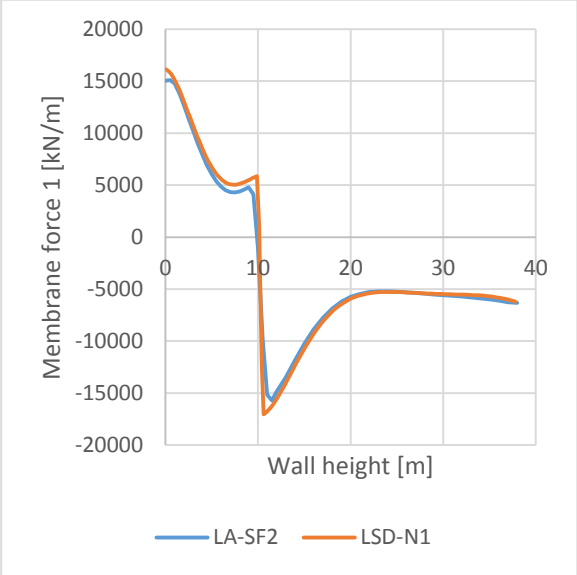

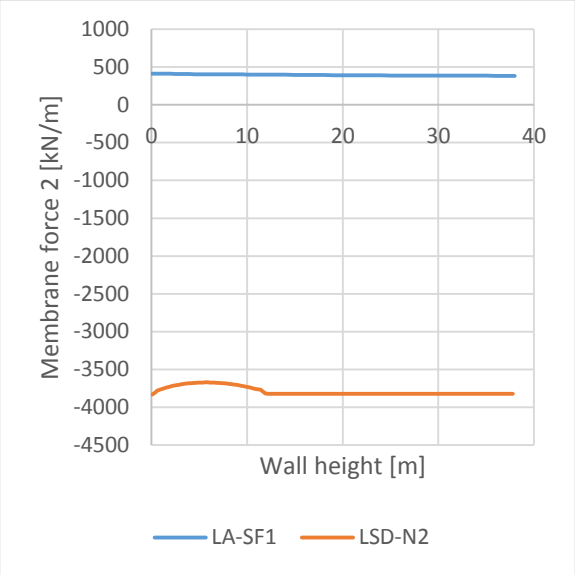

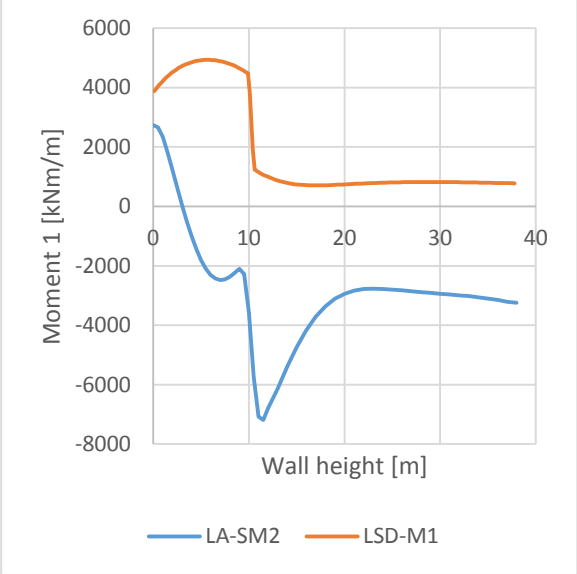

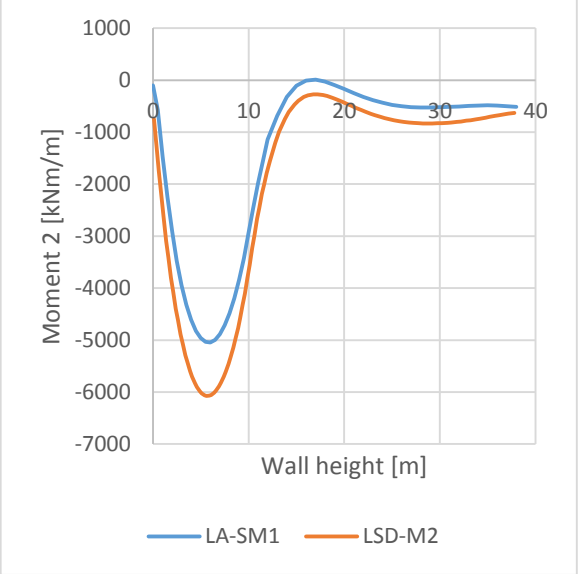

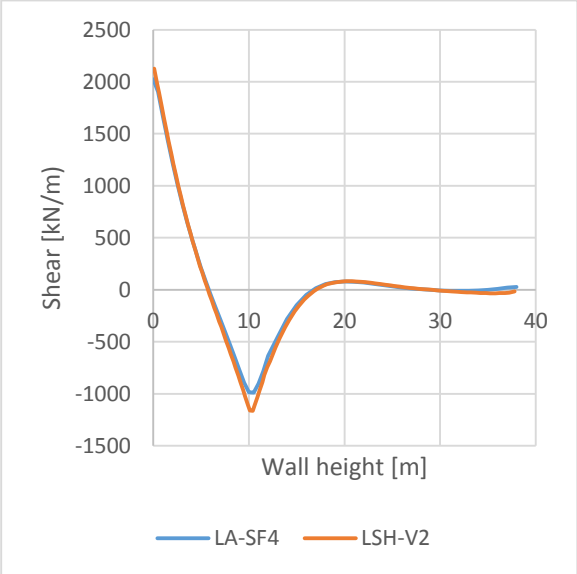

Comparison linear rebar stresses for LC102, ftn = 0 MPa

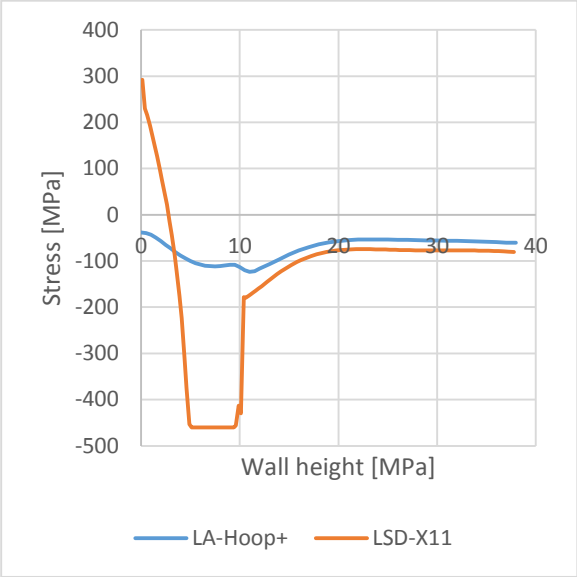

X11 Hoop outside

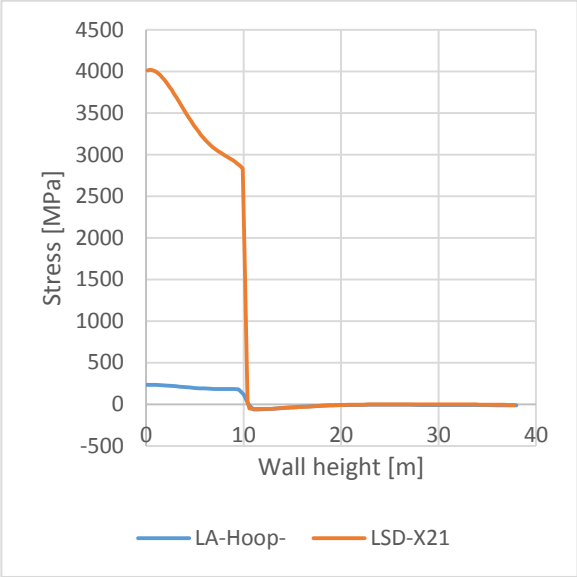

X21 Hoop inside

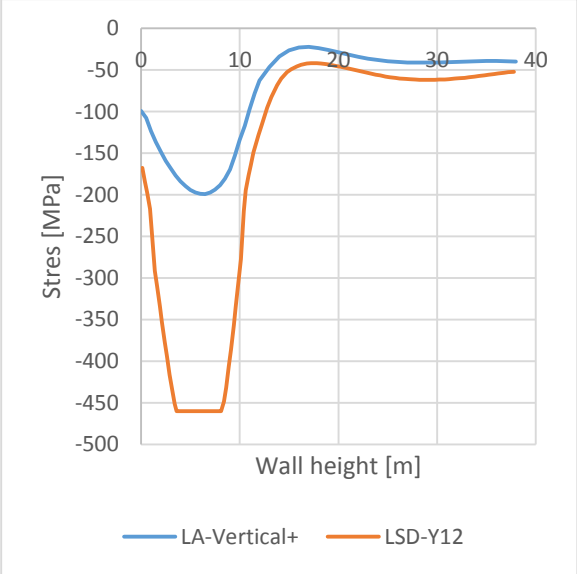

Y21 Vertical outside

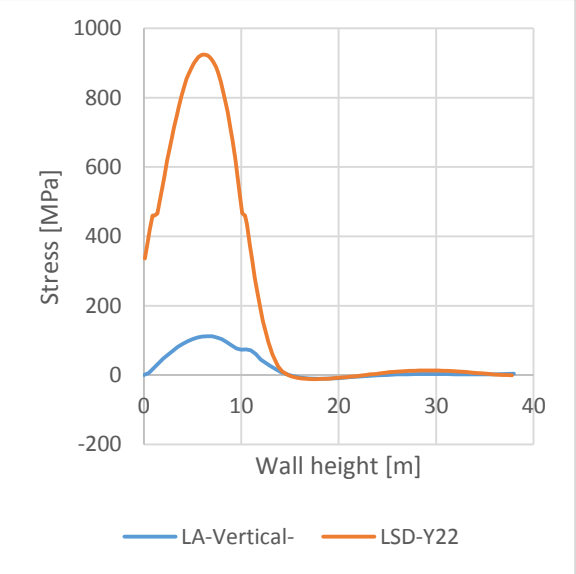

Y22 Vertical inside

8.13 Appendix M: Comparison non-linear shell forces for LC101, ftn = 0 MPa

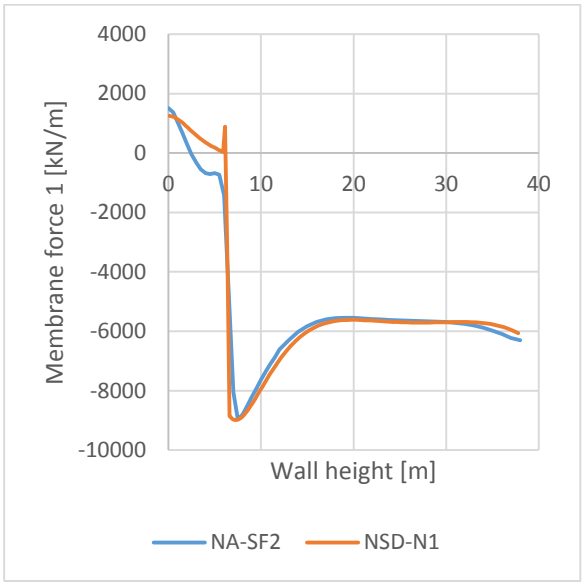

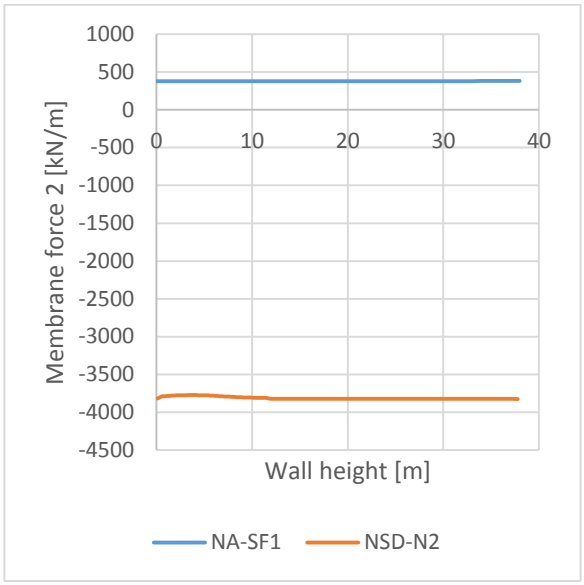

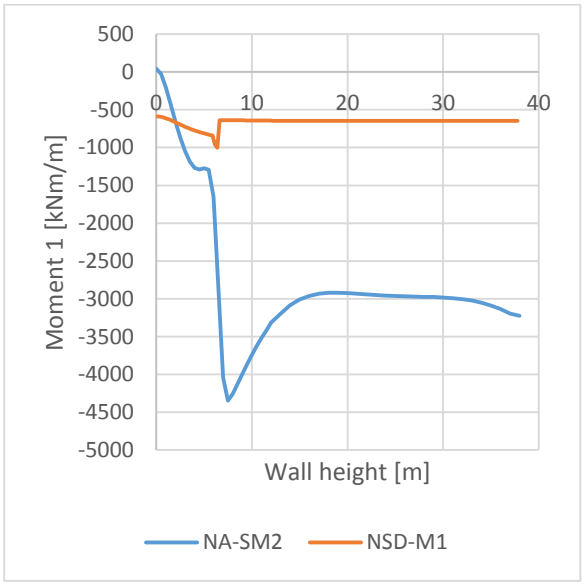

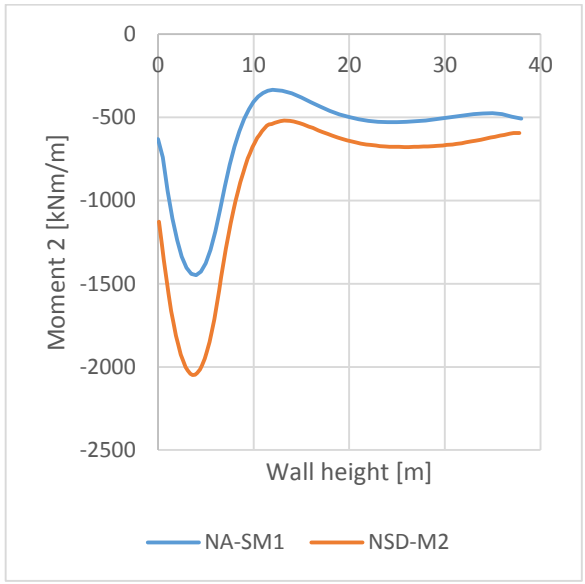

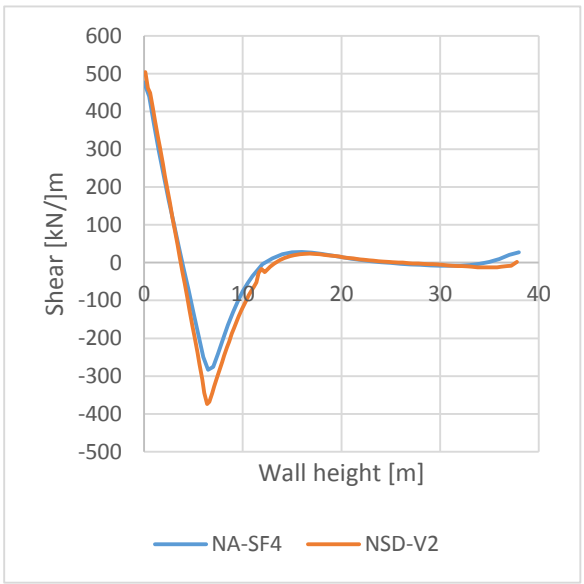

Comparison non-linear rebar stresses for LC101, ftn = 0 MPa

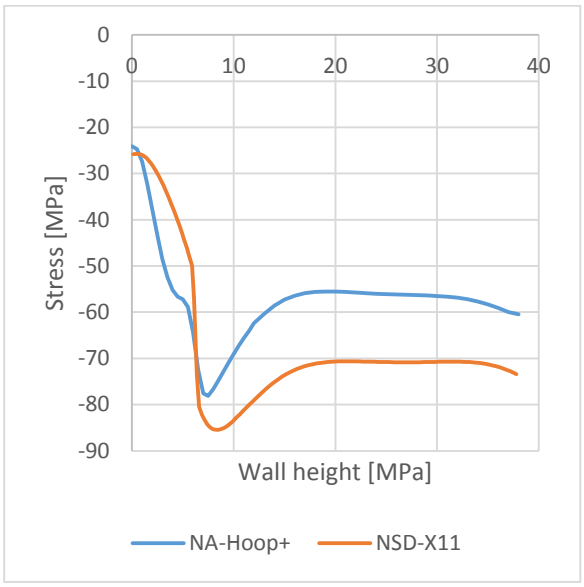

X11 Hoop outside

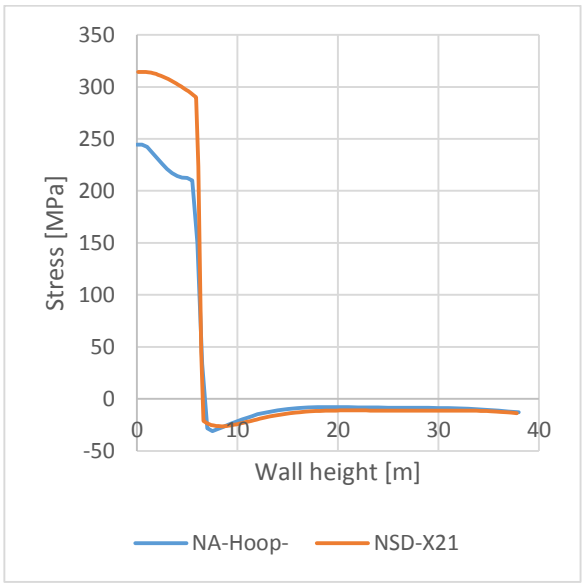

X21 Hoop inside

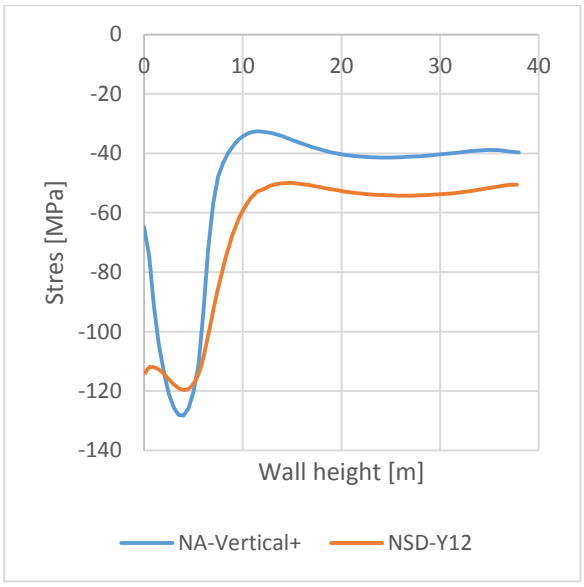

Y21 Vertical outside

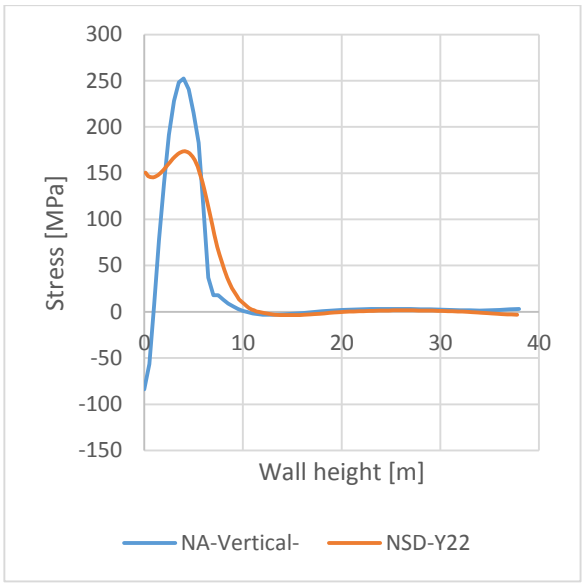

Y22 Vertical inside

8.14 Appendix N: Comparison non-linear shell forces for LC102, ftn = 0 MPa

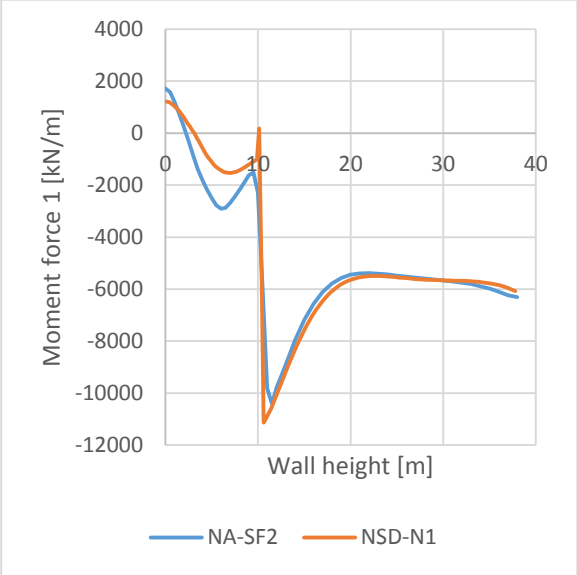

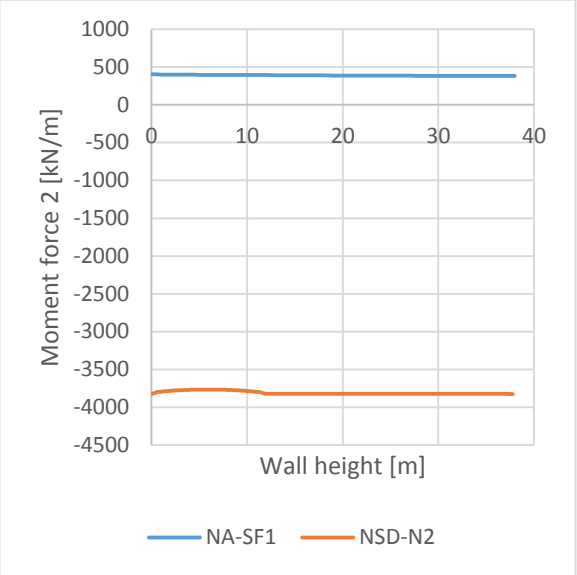

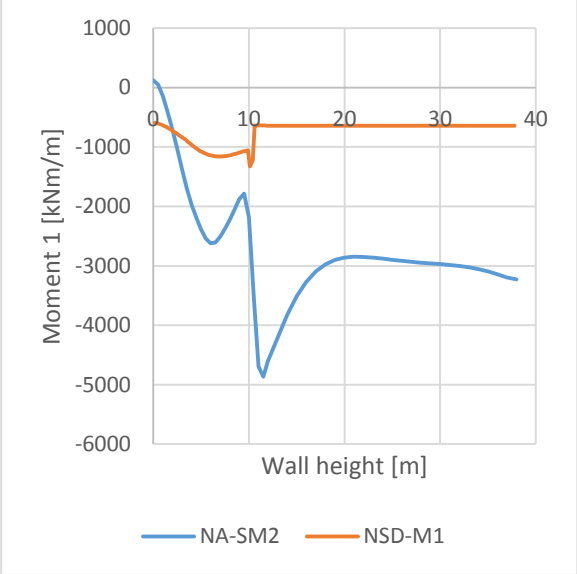

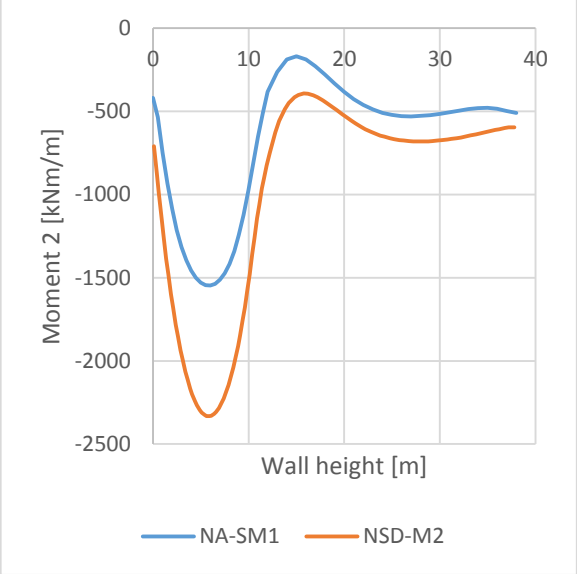

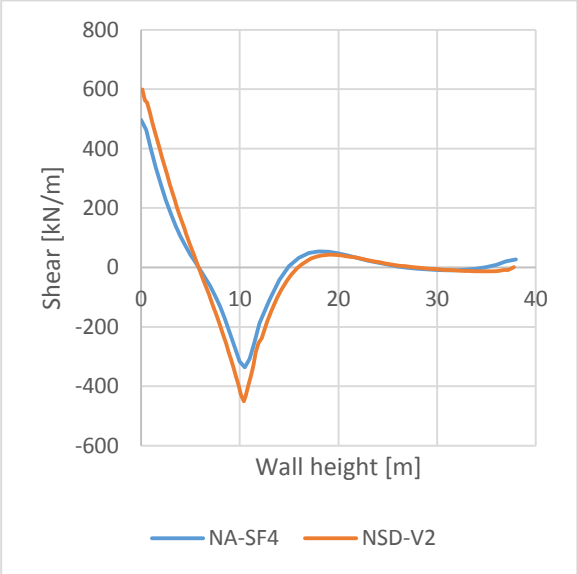

Comparison non-linear rebar stresses for LC102, ftn = 0 MPa

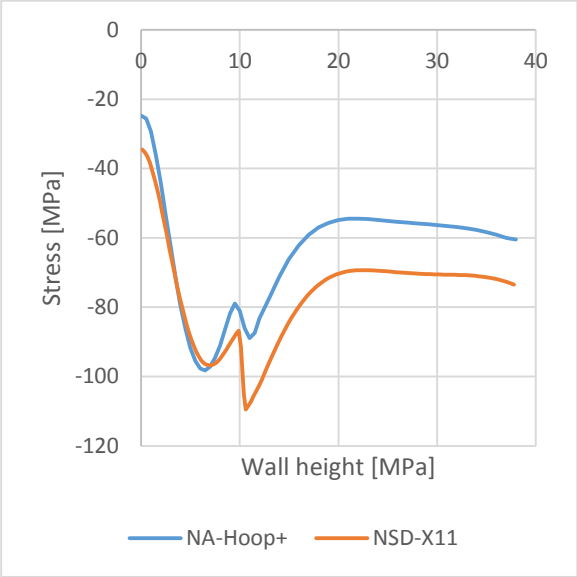

X11 Hoop outside

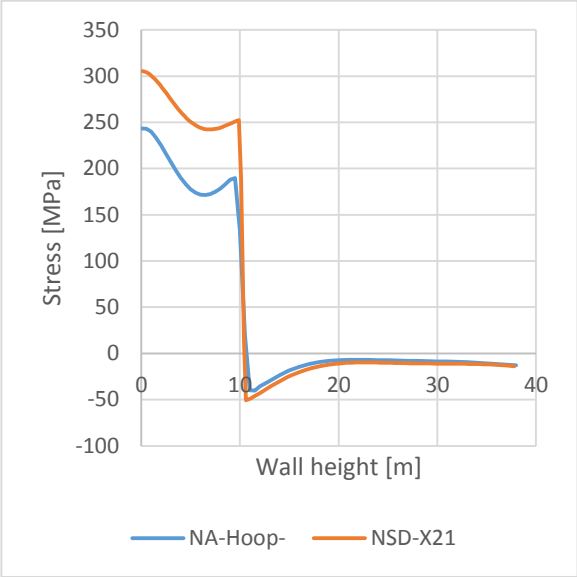

X21 Hoop inside

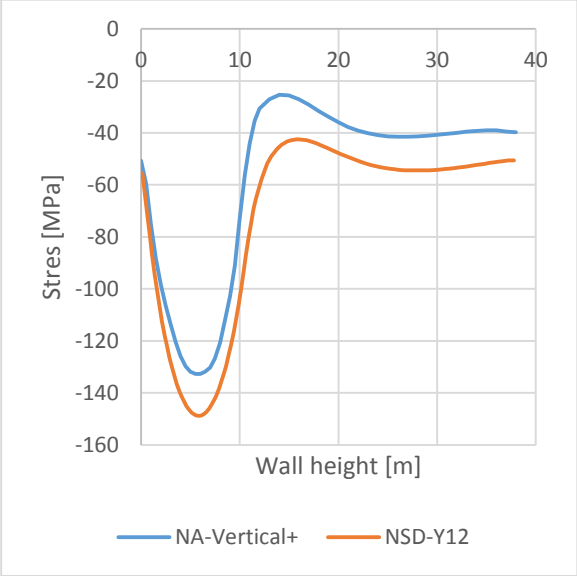

Y21 Vertical outside

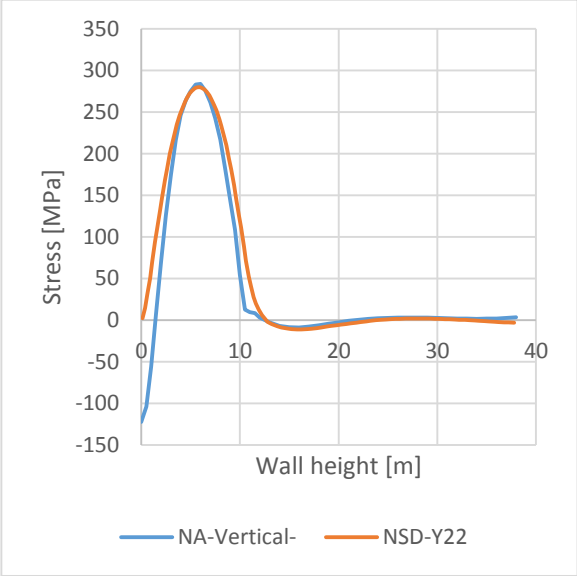

Y22 Vertical inside

8.15 Appendix N: Comparison of reinforcement for slab, ftn = 3 MPa

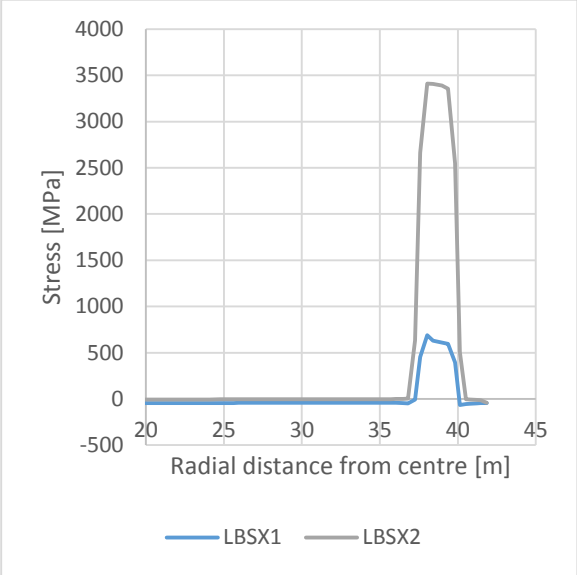

Load combination 101, linear stresses

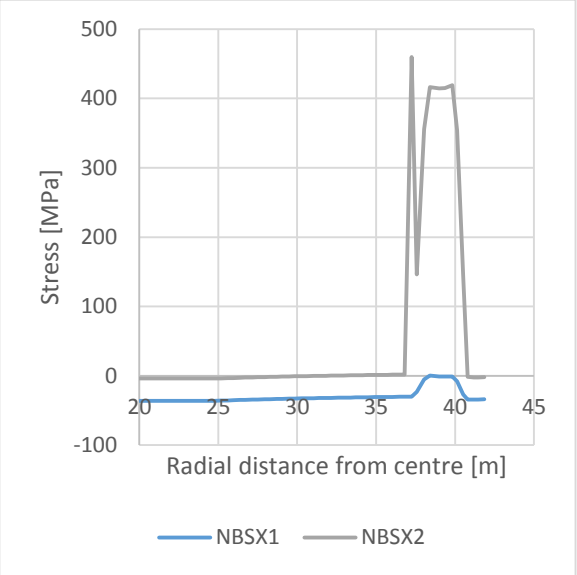

Load combination 101, non-linear stresses

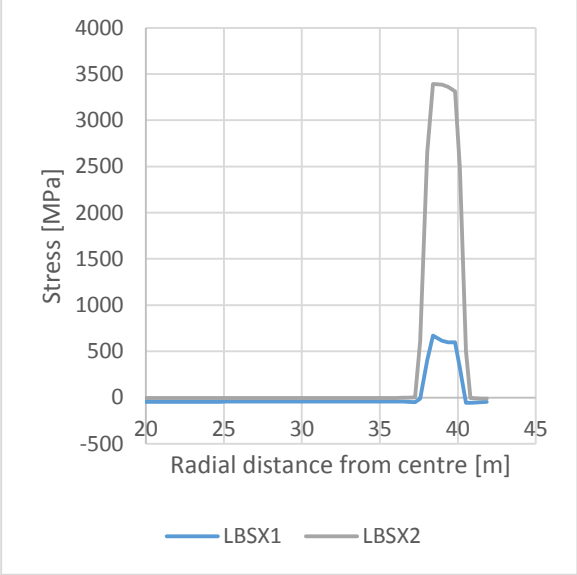

Load combination 102, linear stresses

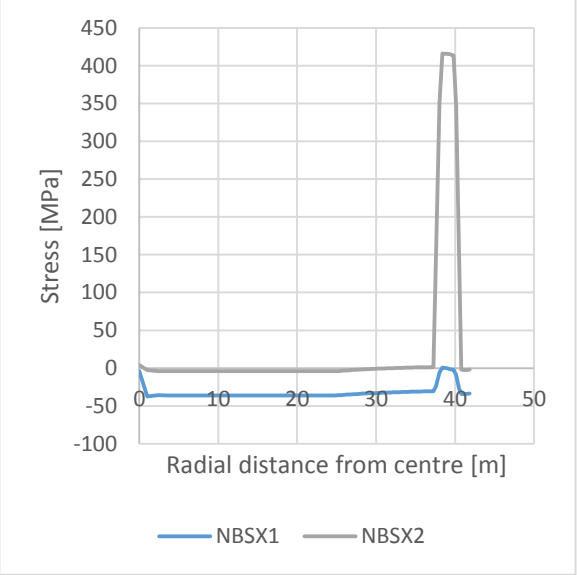

Load combination 102, non-linear stresses

8.16 Appendix O: Comparison of reinforcement for slab, ftn = 0 MPa

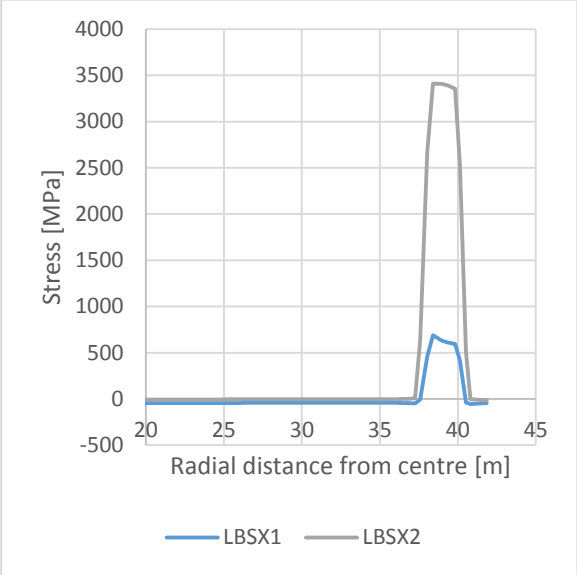

Load combination 101, linear stresses

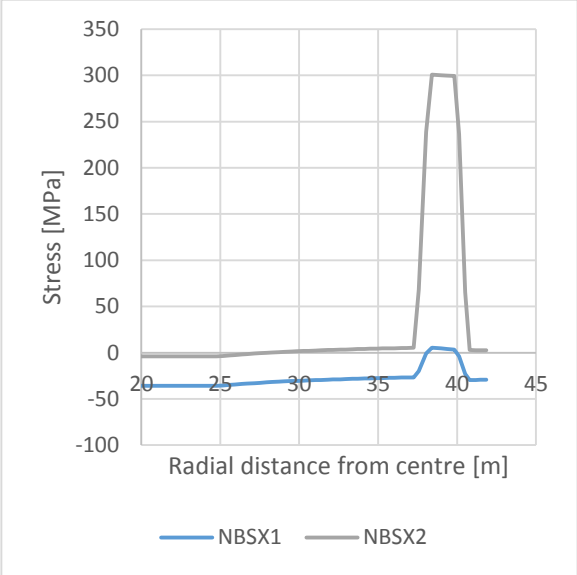

Load combination 101, non-linear stresses

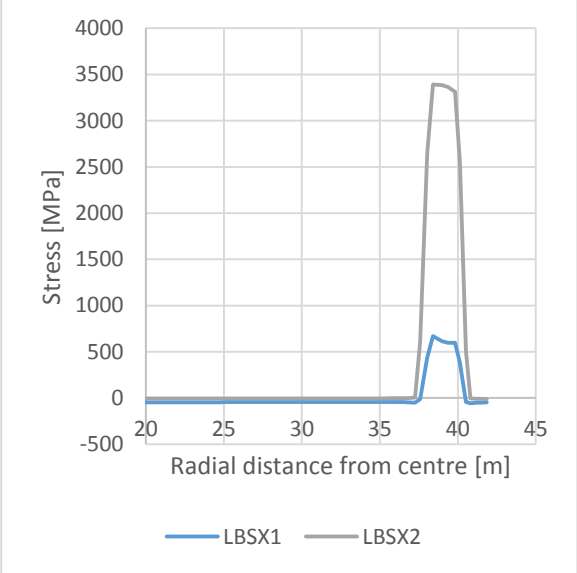

Load combination 102, linear stresses

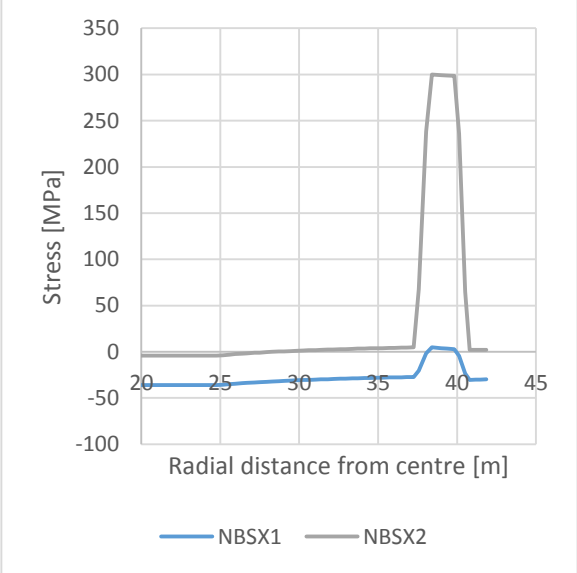

Load combination 102, non-linear stresses

8.17 Appendix P: ShellDesign input analysis file

```
HEADL  TEMPERATURE INVESTIGATION
HEADL  LNG TANK
% Analysis file:
RFILE FNM=R1 SUF=SIN
DECFI ND=ON
% ************************************************************************
% WALL (WALL) Section definitions:
SHSEC PA=WALL SE=1001 EL=12528 XF=1,0,0 XH=0,1,0  FS=1-480  HS=2-109       ET=VS
% 1,2,3 local axis definition
SHAXE PA=WALL XP=0,0,0 XA=0,1,0 AL=-90
% ************************************************************************
% BASE SLAB (BS) Section definitions:
SHSEC PA=BS SE=1001 EL=11343 XF=1,0,0 XH=0,1,0  FS=1-480  HS=1-70             ET=VS
% 1,2,3 local axis definition
SHAXE PA=BS  XC=0,0,0 XA=0,1,0 AL=-90
% ************************************************************************
% ROOF (RF) Section definitions:
%SHSEC PA=RF SE=1001 EL=21974 XF=1,0,0 XH=0,1,0  FS=1-480  HS=1-64          ET=VS
%% 1,2,3 local axis definition
%SHAXE PA=RF XC=0,40,0 XA=0,1,0 AL=-90
% ************************************************************************
% CREATE OLC-FILE
%OLCFI NF=LNG-TANK.OLC NAME=LNG-TANK VERS=1.0 DATE=03.04.14 RESP=BSN
% ************************************************************************
%% Material properties
%% Concrete properties
%CMPNS ID=1 GR=B65 FCN=45000 EPO=0.002293 EPU=0.003491 MFU=1 MFA=1  FTN=3572 FTA=3572
  CMPNS ID=1 GR=B65 FCN=45000 EPO=0.002293 EPU=0.003491 MFU=1 MFA=1 FTC=3000
CMPNS PRI=
%% Reinforcement properties
RMPNS ID=2      GR=460 MFU=1  MFA=1  EPU=0.005
RMPNS PRI=
%% Prestress properties
TEMAT ID=3      FSY=1400.E3 ESK=200.E6 MFU=1.0 MFA=1.0
TEMAT PRI=
```

```
% ***************************************************************************
% Load combinations:
BASCO ID=101  LF=1 OLC=1 LF=1 OLC=2 LF=1 OLC=4 LF=1 OLC=5 LF=1 OLC=6 LF=1 OLC=7 LF=1
OLC=8 LF=1 OLC=9 LF=1 OLC=10
BASCO ID=102  LF=1 OLC=1 LF=1 OLC=3 LF=1 OLC=4 LF=1 OLC=5 LF=1 OLC=6 LF=1 OLC=7 LF=1
OLC=8 LF=1 OLC=9 LF=1 OLC=11
% ***************************************************************************
%% Reinforcement types
%% Reinforcement identity for wall sections
RETYP ID=25000 MP=2  AR=3272E-6 OS=0.060
RETYP ID=25001 MP=2  AR=6544E-6 OS=0.085
RETYP ID=25002 MP=2  AR=6000E-6 OS=0.100
RETYP ID=25004 MP=2  AR=6000E-6 OS=0.050
RETYP ID=25005 MP=2  AR=6000E-6 OS=0.075
TETYP ID=26000 MP=3  AR=7000E-6 E0=5E-3     OS=0
TETYP ID=26001 MP=3  AR=4200E-6 E0=5E-3     OS=0
%% AR=phi*r^2*m/s=3.14*0.0125^2*1/0.15=3272E-6
%% AR=phi*r^2*m/s=3.14*0.0125^2*1/0.30=6544E-6
%% AR=Ap*M/S=4200E-6*1/0.6=7000E-6
%% AR=Ap*m/s=4200E-6*1/1  =4200E-6
CRWNS KT=1.5 CW=0.3E-3 C1=0.035 C2=0.050
% ***************************************************************************
%% Reinforcement location, wall section              (WALL)
%% Outer face
RELOC ID=X11          RT=25000       FA=1    AL=0    PA=WALL          %Hoop direction
RELOC ID=Y12          RT=25001       FA=1    AL=90   PA=WALL          %Vertical direction
%% Inner face
RELOC ID=X21          RT=25000       FA=2    AL=0    PA=WALL          %Hoop direction
RELOC ID=Y22          RT=25001       FA=2    AL=90   PA=WALL          %Vertical direction
TELOC ID=1            TT=26000       FA=0    AL=0    PA=WALL
TELOC ID=2            TT=26001       FA=0    AL=90   PA=WALL
% ***************************************************************************
%%Reinforcement location, base slab section (BS)
%% Outer face
RELOC ID=BSX1               RT=25002       FA=1    AL=0    PA=BS  %RP=XZ
RELOC ID=BSZ1               RT=25002       FA=1    AL=90   PA=BS  %RP=XZ
```

```
%% Inner face                    %
RELOC ID=BSX2                    RT=25002        FA=2    AL=0    PA=BS  %RP=XZ
RELOC ID=BSZ2                    RT=25002        FA=2    AL=90   PA=BS  %RP=XZ
%%Reinforcement location, roof section (RF)
%%Outer face
RELOC ID=RFX1                    RT=25004        FA=1    AL=0    PA=RF  %RP=XZ
RELOC ID=RFZ1                    RT=25005        FA=1    AL=90   PA=RF  %RP=XZ
%% Inner face                    %
RELOC ID=RFX2                    RT=25004        FA=2    AL=0    PA=RF  %RP=XZ
RELOC ID=RFZ2                    RT=25005        FA=2    AL=90   PA=RF  %RP=XZ
% ********************************************************************************
% Load cases to be verified before combined:
DECAS LS=ULS            BAS=101-102
% ********************************************************************************
% Order tables to be printed:
 TABLE TAB=DF FS=1
 TABLE UR=RS RL=ALL FS=1
 TABLE UR=CS FA=ALL FS=1
 TABLE TAB=DR FS=1
 TABLE TAB=DF FS=10
 TABLE UR=RS RL=ALL FS=10
 TABLE UR=CS FA=ALL FS=10
 TABLE TAB=DR FS=10
 TABLE UR=MAX FM= PA=WALL
 TABLE UR=MAX FM= PA=BS
 TABLE UR=MAX FM= PA=RF
% ********************************************************************************
% Order plot file to be created in FemView:
 FVFIL FN=WALL-L-B102-2 PA=WALL
 FVFIL FN=BS-L-B102-2   PA=BS
% Non-linear execution:
% NONLI TFI=T1.FEM NSR=10 NDT=0 URT=0 TYP=VST SPA=C:\"Program Files"\DNVS\"Sestra V8.6-
00"\Bin\Sestra.exe
% NONLI PRI=
% Execution mode:
 EXECD DM=V
```